VOLUME 33 SEPTEMBER 1955 NUMBER 9

Canadian Journal of Physics

Editor: G. M. VOLKOFF

Associate Editors:

L. G. ELLIOTT, *Atomic Energy of Canada, Ltd., Chalk River*
J. S. FOSTER, *McGill University*
G. HERZBERG, *National Research Council of Canada*
L. LEPRINCE-RINGUET, *Ecole Polytechnique, Paris*
R. W. PRINGLE, *University of Manitoba*
B. W. SARGENT, *Queen's University*
Sir FRANCIS SIMON, *Clarendon Laboratory, University of Oxford*
W. H. WATSON, *University of Toronto*

Published by THE NATIONAL RESEARCH COUNCIL
OTTAWA CANADA

CANADIAN JOURNAL OF PHYSICS

(*Formerly Section A, Canadian Journal of Research*)

Under the authority of the Chairman of the Committee of the Privy Council on Scientific and Industrial Research, the National Research Council issues THE CANADIAN JOURNAL OF PHYSICS and six other journals devoted to the publication, in English or French, of the results of original scientific research. Matters of general policy concerning these journals are the responsibility of a joint Editorial Board consisting of: members representing the National Research Council of Canada; the Editors of the Journals; and members representing the Royal Society of Canada and four other scientific societies.

EDITORIAL BOARD

Representatives of the National Research Council

A. N. Campbell, *University of Manitoba*
G. E. Hall, *University of Western Ontario*
E. G. D. Murray, *McGill University*
D. L. Thomson, *McGill University*
W. H. Watson (Chairman), *University of Toronto*

Editors of the Journals

D. L. Bailey, *University of Toronto*
T. W. M. Cameron, *Macdonald College*
J. B. Collip, *University of Western Ontario*
G. A. Ledingham, *National Research Council*
Léo Marion, *National Research Council*
R. G. E. Murray, *University of Western Ontario*
G. M. Volkoff, *University of British Columbia*

Representatives of Societies

D. L. Bailey, *University of Toronto*
Royal Society of Canada
T. W. M. Cameron, *Macdonald College*
Royal Society of Canada
J. B. Collip, *University of Western Ontario*
Canadian Physiological Society
R. G. E. Murray, *University of Western Ontario*
Canadian Society of Microbiologists
H. G. Thode, *McMaster University*
Chemical Institute of Canada
T. Thorvaldson, *University of Saskatchewan*
Royal Society of Canada
G. M. Volkoff, *University of British Columbia*
Royal Society of Canada; Canadian Association of Physicists

Ex officio

Léo Marion (Editor-in-Chief), *National Research Council*

Manuscripts for publication should be submitted to Dr. Léo Marion, Editor-in-Chief, Canadian Journal of Physics, National Research Council, Ottawa 2, Canada.
(For instructions on preparation of copy, see **Notes to Contributors** (inside back cover).)

Proof, correspondence concerning proof, and orders for reprints should be sent to the Manager, Editorial Office (Research Journals), Division of Administration, National Research Council, Ottawa 2, Canada.

Subscriptions, renewals, requests for single or back numbers, and all remittances should be sent to Division of Administration, National Research Council, Ottawa 2, Canada. Remittances should be made payable to the Receiver General of Canada, credit National Research Council.

The journals published, frequency of publication, and prices are:

Canadian Journal of Biochemistry and Physiology	Bimonthly	$3.00 a year
Canadian Journal of Botany	Bimonthly	$4.00 a year
Canadian Journal of Chemistry	Monthly	$5.00 a year
Canadian Journal of Microbiology*	Bimonthly	$3.00 a year
Canadian Journal of Physics	Monthly	$4.00 a year
Canadian Journal of Technology	Bimonthly	$3.00 a year
Canadian Journal of Zoology	Bimonthly	$3.00 a year

The price of single numbers of all journals is 75 cents.

*Volume 1 will combine three numbers published in 1954 with six published in 1955 and will be available at the regular annual subscription rate of $3.00.

Canadian Journal of Physics

Issued by THE NATIONAL RESEARCH COUNCIL OF CANADA

VOLUME 33 SEPTEMBER 1955 NUMBER 9

DIURNAL VARIATIONS IN THE NUMBER OF SHOWER METEORS DETECTED BY THE FORWARD-SCATTERING OF RADIO WAVES

PART I. THEORY[1]

BY C. O. HINES

ABSTRACT

Various observational factors affect the number of shower meteors which can be detected, in a given time interval, by the scattering of radio waves from the ionized meteor trails. The pertinent factors in the case of forward-scattering, where the transmitter and receiver are widely separated, are expressed approximately as functions of the position of the shower radiant. In combination, they provide an observational weight factor which may change appreciably as the radiant moves in the course of a day. The consequent diurnal variation in the occurrence of scattered signals may then be determined, and distinguished from variations due to random changes in the incidence rate of the meteors.

INTRODUCTION

A number of meteor swarms are encountered yearly by the earth, as it follows its course round the sun, and these give rise to a succession of meteor showers. The number of shower meteors incident on the earth may vary systematically as the earth passes through a swarm, and random fluctuations in the incidence rate will inevitably occur. The number incident above an observer's horizon will show a further variation, in this case diurnal, dependent upon the varying elevation of the shower radiant.

When the ionized meteor trails are detected by the (forward) scattering of radio waves transmitted from a distant station, their numbers are often found to vary appreciably throughout each day in a manner which cannot reasonably be attributed to any of the causes just mentioned. It seems likely, then, that the method of observation is itself responsible for a large part of the variation observed.

This possibility is investigated in the present paper, using a theory of forward-scattering developed by Eshleman (1). The treatment is approximate, and not justified if the transmission path is much shorter than 1000 km.; it is illustrated by contour charts for this path length, but is otherwise kept as general as possible. The charts are most simply applied only after a transformation of coordinates determined by the particular position and orientation of the path in question, but this stage of the work is given in outline only.

[1]*Manuscript received March 18, 1955.*
Contribution from the Radio Physics Laboratory of the Defence Research Board, Ottawa, Canada. The work was performed under project PCC No. D48-95-11-01.

The transformed chart appropriate to one path now in use, and a comparison with the corresponding observational data, will be included in a subsequent joint communication.

PRIMARY CONSIDERATIONS

The numeric count of shower meteors is governed basically by the number density in the meteor stream. Random fluctuations in this density may be severe, and may override much of the predictable variation introduced by observational factors. In calculating these factors then, it seemed reasonable to the writer to accept any approximation—even if only qualitatively justified—which would give a preliminary indication of the net observational effect. With this approach, it has been found useful to calculate many quantities at the mid-plane bisecting the transmitter–receiver axis, TR, and to apply the results as representative for other points. This approximation is justified when the TR axis is long enough, since the meteor horizons about T and R then overlap only in a narrow band near the mid-plane. (See Fig. 1.) There is, in fact, no overlap when TR exceeds about 2300 km.; but even for TR as short as 1600 km., the overlap extends only a third of the way from the mid-point M to T and to R. It is thought that the theory will be applicable even when the TR axis is as short as 1000 km., since, in practice, the antenna patterns will not cover the whole of the overlapping region. The effect of a typical antenna pattern will be illustrated in a later section.

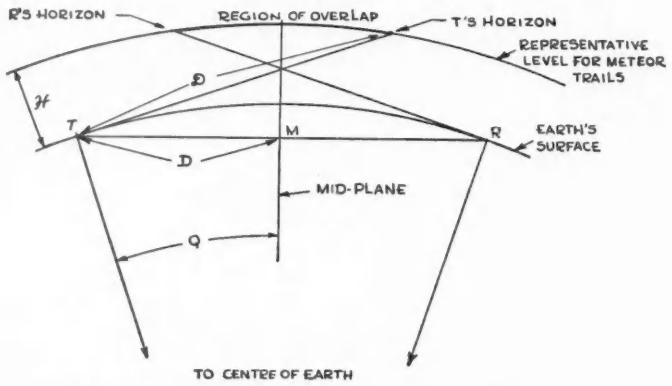

FIG. 1. Vertical section through the transmitter–receiver axis.

Forward-scattering from so-called underdense trails may be treated as a problem in Fresnel diffraction theory (1), and it is then evident that the principal Fresnel zone is potentially the most effective scattering region. Taken to an extreme, this fact suggests the following approximation: *meteor trails which contain the center point P of the associated Fresnel system within their lengths are potentially observable, and those that do not are not.* The points P are properly found as the points at which the meteor tracks become tangent to

one or other of the family of prolate spheroids about T and R as foci. These spheroids approximate to circular cylinders about TR as axis, near the mid-plane, and the condition for tangency to cylinders is much more easily obtained. If the shower radiant lies in a plane inclined at angle ψ to the vertical plane through TR, then the points at which the tracks become tangent to the cylinders lie in another plane through TR, this one inclined at angle ψ above the horizontal direction. (See Fig. 2, which represents projections on a plane normal to the plane depicted in Fig. 1, right-bisecting TR.) The dual role of ψ should be explicitly noted, for it may often lead to confusion: ψ measures the radiant position from a vertical plane, and the tangent points from a horizontal plane.

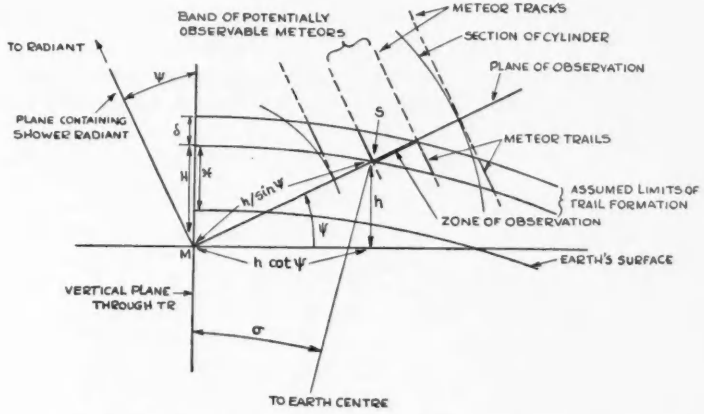

FIG. 2. Projection on the mid-plane bisecting the transmitter–receiver axis.

If the meteor trails are taken to extend between two levels, at heights $\mathscr{H}$ and $\mathscr{H}+\delta$ above a spherical earth of radius $\mathscr{R}(\gg \mathscr{H} \gg \delta)$, then the observationally relevant tangent points will comprise only a part of the inclined plane—that part which lies between heights $\mathscr{H}$ and $\mathscr{H}+\delta$, and which lies within the horizon circles about T and R. The slant breadth of this zone is given approximately by $\delta/\sin(\psi+\sigma)$, where σ is the angle subtended at the earth's center by the line MS, if S is the particular P point which lies in the mid-plane at the $\mathscr{H}$ level. The upper and lower sides of the zone approximate to straight lines near the mid-plane, parallel to the TR axis. The lower side lies at some height h above the horizontal plane through TR, given by

[1] $$h^2/\sin^2\psi + 2h\,\mathscr{R}\cos Q = \mathscr{R}^2\sin^2 Q + 2\mathscr{R}\mathscr{H} + \mathscr{H}^2,$$

where Q is half the angle subtended at the earth's center by TR; if the length of TR is $2D$, then

[2] $$\sin Q = D/\mathscr{R}.$$

In practice, writing

[3] $$\mathscr{H} + \mathscr{R} - \mathscr{R}\cos Q \equiv H,$$

[1] can be approximated successfully by

$$h = H(1 - H/2\,\mathscr{R}\cos Q\tan^2\psi) \tag{4}$$

for $\psi \gtrsim 20°$, and by

$$h = 2H/[1+(1 + 2H/\mathscr{R}\cos Q\sin^2\psi)^{\frac{1}{2}}] \tag{5}$$

for smaller ψ's, without significant error (3%).

The lower side of the observational zone is separated from the TR axis by a distance $h/\sin\psi$. It extends a distance d on either side of the mid-plane, determined by the horizon cutoff and hence by the relation

$$d = (\mathscr{D}^2 - h^2/\sin^2\psi)^{\frac{1}{2}} - D \tag{6}$$

where

$$\mathscr{D} \equiv [(\mathscr{R}+\mathscr{H})^2 - \mathscr{R}^2]^{\frac{1}{2}} \tag{7}$$

is the radius of a horizon circle at height $\mathscr{H}$. Equation [6] is illustrated by the plan view in Fig. 3, although the projections $\mathscr{D}'$ and $h\cot\psi$ appear there in place of $\mathscr{D}$ and $h/\sin\psi$.

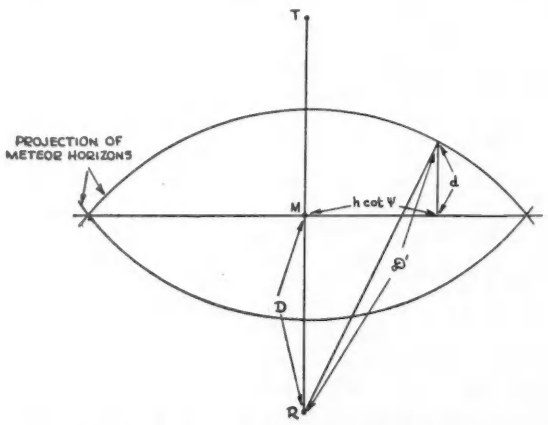

FIG. 3. Projection on the horizontal plane through the transmitter–receiver axis.

The area of the observational zone can now be determined approximately. Its projection on a plane normal to the meteor tracks is reduced by a factor $\sin\beta$, where β is the angle between the plane TSR and the radiant position. (β can be measured in a plane through TR, inclined at angle ψ to the vertical, from the TR axis as the $\beta = 0$ direction; together with ψ, it locates the radiant position. See Fig. 8.) The projected area is then given by

$$\mathscr{A} = 2\sin\beta\,[(\mathscr{D}^2 - h^2/\sin^2\psi)^{\frac{1}{2}} - D]\,\delta/\sin(\psi+\sigma). \tag{8}$$

The number of meteors whose trails are potentially observable, in the sense stated previously, will be proportional to this area, and so will have the functional form of the expression [8].

As introduced, δ is a constant. However, a meteor trail actually extends over an undefined distance with varying ionization density, and a weighted integration over δ should therefore be performed in principle. The form of the height variation of ionization is, however, effectively independent of the trail orientation (cf. Herlofson's development (3), or Kaiser's more recent summary (4), of the theory of trail formation). The integration would therefore produce no new functional dependence on β, ψ; it, and the factor δ, may be neglected in the subsequent development.

The height at which maximum ionization occurs does depend on χ, the zenith angle of the trail axis, but not very critically except when $\chi \to 90°$. The corresponding variation in the appropriate height $\mathscr{H}$ may therefore be ignored, and h may be determined from [1]–[5] with $\mathscr{H}$ constant.

SECONDARY CONSIDERATIONS

Not only must a meteor pass through the zone of observation for its trail to be observed and counted, but also the power scattered to the receiver must be sufficient to permit detection. The following functional dependence for the power scattered to R has been determined (1, 2):

$$[9] \qquad P_R \propto q^2 G_T G_R \sin^2\alpha / r_1 r_2 (r_1+r_2)(1-\cos^2\beta \sin^2\phi)$$

where q is the line density of ionization (assumed constant, but in practice at P), G_T and G_R are the transmitting and receiving antenna gains in the directions TP and RP respectively, r_1 and r_2 are the corresponding ranges, α is the angle between PR and the electric vector of the (plane polarized) wave incident on the trail at P, 2ϕ is the 'forward-scattering angle' TPR, and β is the angle between the trail and the plane TPR. This definition of β is the same as that given previously, when P lies in the mid-plane; it is approximately equivalent even at some distance from the mid-plane—so long as the cylindrical approximation is valid—and the distinction will be ignored.

If the receiving antenna accepts only a particular polarization component of the wave incident on it, then the $\sin^2\alpha$ factor in [9] should be replaced by $\cos^2\gamma$ to obtain the functional form of the power actually observed:

$$[10] \qquad P_0 \propto q^2 G_T G_R \cos^2\gamma / r_1 r_2 (r_1+r_2)(1-\cos^2\beta \sin^2\phi),$$

where γ is the angle between the electric vector of the wave incident on the trail and that component which is accepted by the receiving antenna. The modified formula will be adopted in this paper, on the assumption that the transmitting antenna propagates, and the receiving antenna accepts, only a horizontally polarized component.

The geometric factors in [10] are easily calculated for the point S. The distances r_1 and r_2 are identical then, and equal to

$$[11] \qquad r \equiv (D^2+h^2/\sin^2\psi)^{\frac{1}{2}},$$

while

$$[12] \qquad \sin\phi = D/r.$$

In a Cartesian system corresponding to the polar system defining the shower radiant (β, ψ), the zenith at T has direction cosines cos Q, 0, sin Q, and the

line TS has direction cosines proportional to h, $\pm h \cot \psi$, $-D$. (See Fig. 4; the $\pm$ alternative accounts for an observation on either side of the TR axis.)

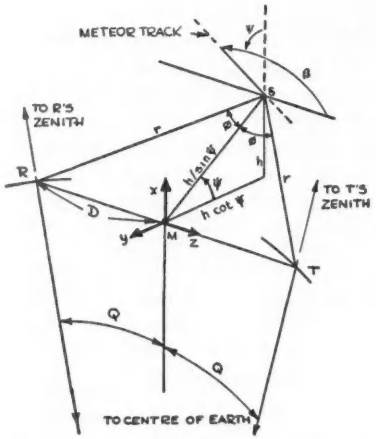

FIG. 4. Geometry of forward-scattering from a trail through S.

If the electric vector of the wave incident on the trail at S has direction cosines λ, μ, ν, then the condition for a horizontal polarization implies

[13] $$\lambda \cos Q + \nu \sin Q = 0$$

and the condition for a transverse wave implies

[14] $$\lambda h \pm \mu h \cot \psi - \nu D = 0.$$

Similar equations apply to the set λ', μ', ν' for the electric vector accepted by the receiver; Q and D need only be changed in sign. These relations, together with the implicit conditions $\lambda^2+\mu^2+\nu^2 = 1 = \lambda'^2+\mu'^2+\nu'^2$, can be combined to give

[15] $$|\cos \gamma| = |\lambda\lambda'+\mu\mu'+\nu\nu'| = \left|\frac{(D+h \tan Q)^2-h^2\cot^2\psi(1-\tan^2 Q)}{(D+h \tan Q)^2+h^2\cot^2\psi(1+\tan^2 Q)}\right|$$

$$\simeq |D^2-h^2\cot^2\psi|/(D^2+h^2\cot^2\psi),$$

where the approximation is justified over the relevant range 1000 km. $\lesssim 2D \lesssim$ 2300 km.

According to present theory of meteor trail formation (3, 4), the line density of ionization at each point along the trail is proportional to the initial mass m of the meteor and to cos χ. In the mid-plane, this second factor is equal to $\sin \beta \cos(\psi+\sigma)$. A further variation with zenith angle results from the varying height of maximum ionization, but such effects are small and will again be ignored.

The foregoing results may be combined to give the functional form of the observable amplitude:

[16] $$A_0 \propto P_0^{\frac{1}{2}} \propto mGf_0,$$

where the 'illumination factor' G is the geometric mean of G_T and G_R, and

[17] $$f_0 \equiv \frac{\sin\beta\cos(\psi+\sigma)|D^2-h^2\cot^2\psi|}{(D^2+h^2\cot^2\psi)r^{3/2}(1-\cos^2\beta\, D^2/r^2)^{\frac{1}{2}}}.$$

These relations apply, in the first instance, only to trails passing through S. Corresponding relations could be derived for other trails through the zone of observation, and they would not differ much from these if the zone were sufficiently small. For present purposes, then, [16] and [17] will be adopted as representative for all potentially observable meteor trails distinguished by the pair β, ψ.

If observations are confined to trails giving observed amplitudes equal to or exceeding some critical value A_c, then they will be confined to meteors with masses equal to or exceeding some critical mass

[18] $$m_c \propto A_c/Gf_0.$$

It is known empirically (5) that the number of meteors in a statistically large sample having masses equal to or exceeding any particular mass m_c is inversely proportional to m_c. (The relationship does not hold for all meteor showers, but it will be adopted here for want of anything better.) Accordingly, it is possible to detect only a fraction of the potentially observable trails passing through any part of the zone, and that fraction is proportional to Gf_0/A_c.

CONTOURS FOR CONSTANT GAIN

If variations in the illumination factor can be ignored, then the observed fraction of the potentially observable trails does not vary with position in the zone of observation. Instead, it depends only on the defining pair β, ψ, and has the functional form of f_0. Since the number of potentially observable trails has the functional form of $\mathscr{A}$ in [8], there is a net 'observability' factor

[19] $$f_0\mathscr{A} \propto F_0 \equiv \frac{\sin^2\beta\cot\psi[(\mathscr{D}^2-h^2/\sin^2\psi)^{\frac{1}{2}}-D]|D^2-h^2\cot^2\psi|}{r^{3/2}[1+h/(\mathscr{R}+\mathscr{H})\sin^2\psi][1-\cos^2\beta\, D^2/r^2]^{\frac{1}{2}}[D^2+h^2\cot^2\psi]}$$

with h given by [4] or [5] and r by [11]. In this, the approximation

[20] $$\cot(\psi+\sigma) \simeq \cot\psi/[1+h/(\mathscr{R}+\mathscr{H})\sin^2\psi]$$

has been adopted; no significant error results when $2D$ is in the relevant range.

A contour chart of F_0 is given in Fig. 5, for a transmission axis of length $2D$ = 1000 km., assuming $\mathscr{H}$ = 100 km. as a representative meteor height and taking the earth's radius $\mathscr{R}$ as 6370 km. This chart gives relative values, normalized to a possible maximum of 100, for the number of shower meteors counted per unit time when the radiant is in the β, ψ position, if the true flux density of meteors is constant. It will be seen that, as β and ψ change in the course of a day, there is ample scope for spurious observational changes in the numeric counts, beyond any random fluctuations in the true flux density.

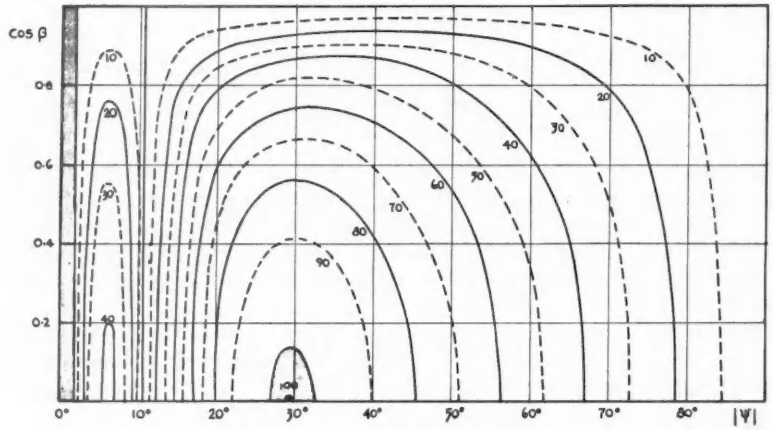

FIG. 5. Normalized contours of the observability factor F_0, for isotropic antenna gain.

A brief description of the zero contours may be useful. When $|\psi| > 90°$, $F_0 = 0$ because the shower radiant lies below the horizon and the trails are therefore formed in such positions that they cannot contain the center points of the corresponding Fresnel systems. At $|\psi| = 90°$, $\chi = 90°$; the zero in F_0 results from the vanishing ionization density implied in the theory of trail formation, though this itself involves an inherent approximation which is invalid when $\chi \to 90°$. When $|\psi| < 2°$, the radiant lies close to the vertical plane through TR, and the points of tangency lie well to the side of this plane; they lie, in fact, beyond the region of overlapping horizons, and hence the zero in F_0 (represented by the hatched area in the figure). At $|\psi| = 10.8°$, $F_0 = 0$ because $\cos\gamma = 0$ at the corresponding point S; this is not a true zero of F_0, since points P off the mid-plane will not lead to an exactly vanishing polarization factor, but a very low relative value of F_0 is certainly to be expected. (The region of overlapping horizons is not very broad, at this distance from the TR axis, so $\cos\gamma$ will approximate to zero throughout the relevant zone.) Finally, the decrease towards zero as $|90° - \beta| \to 90°$ results from two $\sin\beta$ factors; one is introduced by the projection which gives the number of potentially observable trails, the other by the $\cos\chi$ factor in the ionization density.

CONTOURS FOR A TYPICAL ANTENNA PATTERN

When anisotropies in the antenna patterns are appreciable, variations in the illumination factor G must be taken into account. This could be partially accomplished by evaluating G for each $S = S(\psi)$, and including it in [19] as a further factor. However, G may change appreciably within the relevant zone of observation, and it may actually limit the effective length of that zone. It therefore seems more appropriate to make an estimate of G as a function of distance from the mid-plane, at the height $\mathscr{H}$, and to integrate this value

along the length of the zone (at the distance $h \cot \psi$ to the side of the TR axis). This procedure would then provide the revised observability factor

$$[21] \quad F_0^* \equiv \int_{-d}^{d} G\, dz \frac{\sin^2\beta \cot \psi |D^2 - h^2 \cot^2 \psi|}{r^{3/2}[1 + h/(\mathscr{R} + \mathscr{H})\sin^2\psi][1 - \cos^2\beta\, D^2/r^2]^{\frac{1}{2}}[D^2 + h^2 \cot^2 \psi]}$$

with the length d given by [6] as before, and dz taken as an element of this length.

Fig. 6 illustrates an illumination function such as might be established by five-element Yagis as transmitting and receiving antennae. Only the main

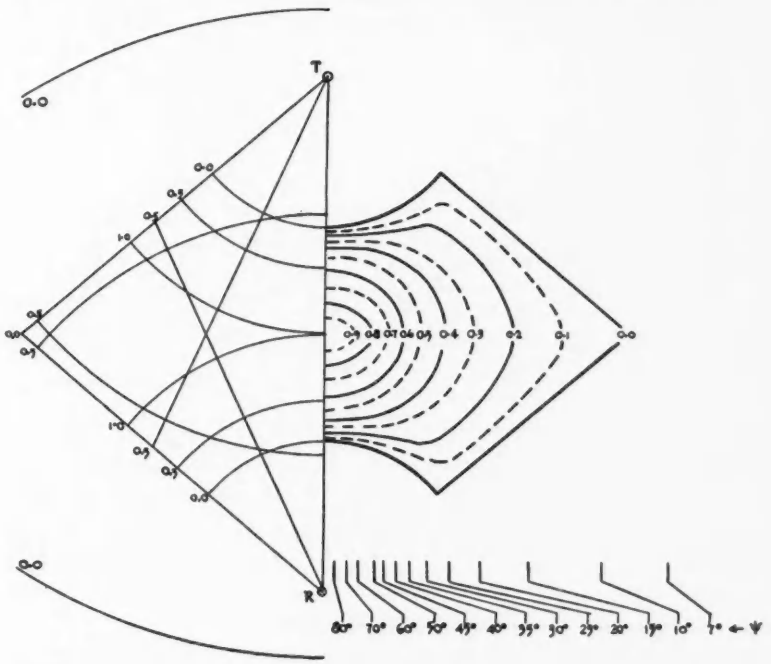

FIG. 6. Assumed antenna pattern construction lines, and contours of the corresponding illumination factor G, seen in projection on the horizontal plane through TR.

lobe of each is considered. It is taken to be beamed at the $\mathscr{H}$ level above the mid-point, to fall to zero power on the horizon and at an equal angle above the beam center, and to fall to zero power at 50° to either side of the axis. Half power is attained at half the angles to zero power, and a normalized value of unity at the center is employed. The construction lines are shown on the left of the diagram, and refer to the same $2D$, $\mathscr{H}$, and $\mathscr{R}$ values as before. The corresponding illumination factor is shown by contours on the right, and below that the projected positions of the observation zones (at $y = h \cot \psi$) are indicated for several ψ's. The increased importance of observa-

tion points P near the mid-plane is clear from this diagram. For comparison, the values of d, $G_S d$, and $\int G\, dz$ are tabulated after normalization to a maximum of unity (Table I). The contour chart of $F_0{}^*$ which corresponds to the assumed pattern is given in Fig. 7, after normalization to a maximum of 100.

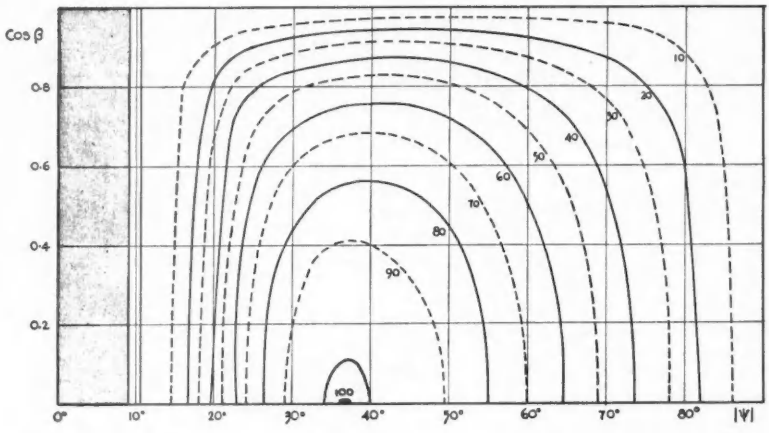

FIG. 7. Normalized contours of the observability factor $F_0{}^*$, for the illumination pattern of Fig. 6.

TABLE I

NORMALIZED EFFECTIVE LENGTHS OF THE ZONES OF OBSERVATION: d FOR ISOTROPIC ANTENNA GAIN; $G_S d$ AND $\int G dz$ FOR THE GAIN PATTERN OF FIG. 6

	7°	10°	15°	20°	25°	30°	35°	40°	45°	50°	60°	70°	80°	90°
d	0.64	0.78	0.88	0.93	0.96	0.97	0.98	0.98	0.99	0.99	0.99	1.00	1.00	1.00
$G_S d$	0.00	0.04	0.15	0.26	0.36	0.47	0.57	0.65	0.72	0.78	0.88	0.94	0.98	1.00
$\int G dz$	0.00	0.01	0.18	0.36	0.53	0.64	0.71	0.77	0.82	0.87	0.92	0.96	0.99	1.00

APPLICATION OF THE CONTOUR CHARTS

Shower radiants move with the stars in the course of a day, and introduce rather involved time variations in the related values of the β, ψ coordinates. When observations are to be made on a number of showers over a particular path, the related theoretical predictions can be obtained most conveniently after a change to celestial polar coordinates. The radiant paths would then appear as circles on the corresponding contour charts, and these paths would be traced at a uniform angular rate.

The transformation involves two parameters related to the mid-point of the TR axis, or to the point on the earth's surface directly above it. These parameters are the latitude l of the point, and the azimuth a of the TR axis (measured to the east from north, say). For clarity, choose the azimuth either of T or of R, such that a lies between 0° and 180°; measure β from the direction so chosen, and then measure $\psi > 0$ in the hemisphere away from the pole.

The related quantities

$$\begin{aligned} \tan t_0 &\equiv \tan a/\sin l, \\ \tan L &\equiv \tan l/\sin a, \\ \cos b &\equiv \cos a \cos l \end{aligned} \qquad [22]$$

are useful subsidiaries, and are constants of the path employed. The relations

$$\begin{aligned} \cos p &= \cos\beta \cos b + \sin\beta \sin b \sin(L-\psi), \\ \sin\tau &= \sin\beta \cos(L-\psi)/\sin p \end{aligned} \qquad [23]$$

may then be used to determine the polar distance p and the hour angle $t \equiv \tau + t_0$ (after lower transit), corresponding to the coordinates β, ψ. (See Fig. 8.)

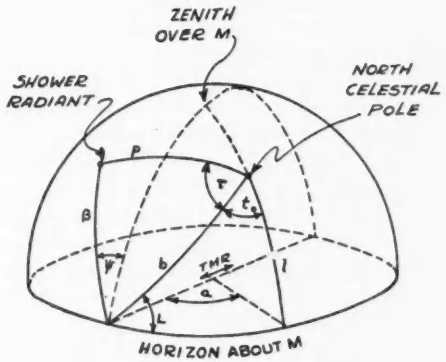

FIG. 8. The celestial hemisphere over M, and the pertinent angles of the coordinate transformation.

For some purposes—e.g., evaluating the effects of a finite shower radiant, or integrating to determine diurnal variations in random meteor counts—it is useful to plot the contour charts directly on a sphere.

ACKNOWLEDGMENTS

The author would like to acknowledge the helpful criticism of Dr. P. A. Forsyth and Dr. E. L. Vogan, whose present program of meteor observations provided the stimulus for the foregoing analysis.

REFERENCES

1. ESHLEMAN, V. R. Electronics Research Lab., Stanford University, Stanford, California, Tech. Rept. No. 49. July 15, 1952.
2. ESHLEMAN, V. R. and MANNING, L. A. Proc. Inst. Radio Engrs. 42: 530. 1954.
3. HERLOFSON, N. Repts. Progr. in Phys. 11: 444. 1946–47.
4. KAISER, T. R. Advances in Phys. 2: 495. 1953.
5. WATSON, F. G. Between the planets. The Blakiston Co., Philadelphia. 1941.

ON THE DETERMINATION OF ELECTROMECHANICAL COUPLING COEFFICIENTS IN A POLYRESONANT PIEZOELECTRIC VIBRATOR[1]

By E. A. G. Shaw

ABSTRACT

The well-known relationship between the electromechanical coupling coefficient and the separation (σ) of resonance and antiresonance frequencies requires modification where several significant modes occur within a small frequency interval. An expression is given for the "true" values of σ (i.e. those which would arise if each mode existed alone) in terms of the many moded system. The analysis neglects mechanical and electrical losses.

In the course of a recent study of the resonant vibrations of prepolarized barium titanate ceramic disks, it became necessary to determine the coefficients of electromechanical coupling in cases where several modes were separated by frequency intervals comparable with the differences between the frequencies of resonance and antiresonance of the individual modes. In such cases the characteristic variations of electrical impedance which occur in the resonance region are no longer related to the coupling coefficient in a simple manner. Indeed, in the most general case where there are many modes contained within a small frequency interval, each mode having a large coupling coefficient and large mechanical and electrical losses, the problem becomes highly intractable. The following treatment, however, while limited to loss-free systems, is capable of giving useful approximate values in many practical cases and has the merit of simplicity.

By way of introduction, we consider first a piezoelectric vibrator having only one normal mode with appreciable electromechanical coupling. In standard reference works (e.g. Cady (1)), it is shown that the electrical properties of such a resonator, neglecting losses, may be represented by the linear network of Fig. 1(*a*). (C_1 and L_1 arise from electrical coupling with the mechan-

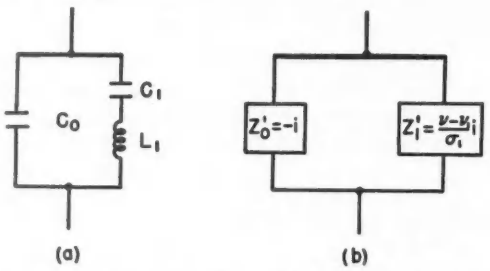

Fig. 1. Equivalent electrical networks of a single mode piezoelectric vibrator: (*a*) exact form; (*b*) idealized form with impedance linear in ν.

[1]*Manuscript received May 19, 1955.*
Contribution from the Division of Applied Physics, National Research Council, Ottawa, Canada. Issued as N.R.C. No. 3686.

ical resonator, while C_0 is the dielectric capacitance.) The network has zero impedance at the resonance frequency

[1] $$\nu_1 = 1/(2\pi\sqrt{L_1C_1})$$

and zero admittance at the antiresonance frequency

[2] $$\alpha_1 = \nu_1\sqrt{1+(C_1/C_0)}.$$

Hence,

[3] $$C_1/C_0 = (\alpha_1^2-\nu_1^2)/\nu_1^2 \simeq 2\sigma_1/\nu_1,$$

where $$\sigma_1 = \alpha_1-\nu_1 \ll \nu_1.$$

For the typical case of a longitudinally vibrating crystal, Mason (2) shows that the following relationship exists between σ_1/ν_1 and the coupling coefficient k_1:

[4] $$k_1^2 = \frac{\pi^2}{4}\frac{\sigma_1}{\nu_1}\left[1+\left(1-\frac{\pi^2}{4}\right)\frac{\sigma_1}{\nu_1}+\dots\right].$$

We now derive expressions for the impedances Z_0 and Z_1 of the two branches of the network 1(*a*) which have such a form that they may, with slight approximations, be made linear in ν. Combining [1] and [3] to eliminate C_1 and noting that $Z_0 = (2\pi i\nu C_0)^{-1}$, we have

$$Z_0 = -(2\pi iL_1/\nu)(\alpha_1^2-\nu_1^2)$$

[5] $$\simeq -4\pi iL_1\sigma_1.$$

Again,

$$Z_1 = 2\pi i\nu L_1+(2\pi i\nu C_1)^{-1}$$

$$= 2\pi i\nu_1 L_1\left[\left(1+\frac{\nu-\nu_1}{\nu_1}\right)-\left(1+\frac{\nu-\nu_1}{\nu_1}\right)^{-1}\right]$$

$$= 4\pi i(\nu-\nu_1)L_1\left[1-\frac{1}{2}\frac{\nu-\nu_1}{\nu_1}+\dots\right]$$

[6] $$\simeq 4\pi i(\nu-\nu_1)L_1.$$

The expressions [5] and [6] may be further simplified by expressing the approximate forms of Z_0 and Z_1 in units of $4\pi L_1\sigma_1 = (2\pi\nu_1C_0)^{-1}$. Then we have $Z_0' = -i$ and $Z_1' = i(\nu-\nu_1)/\sigma_1$ as shown in Fig. 1(*b*). The real network of 1(*a*) and the idealized network of 1(*b*) are approximately equivalent so long as $\nu \simeq \nu_1$; the divergences which occur at extremes of frequency will be considered later.

The network of Fig. 1 may now be generalized as shown in Fig. 2, which represents a resonator having n resonances lying within a restricted frequency interval. It is obvious that the frequencies of zero impedance are $\nu_1, \dots, \nu_n$, so that the resonance frequency of any one mode is not changed by the presence of the others. However, the frequencies of zero admittance $\alpha_1, \dots, \alpha_n$ are no longer equal to $(\nu_1+\sigma_1), \dots, (\nu_n+\sigma_n)$, as would be the case if each

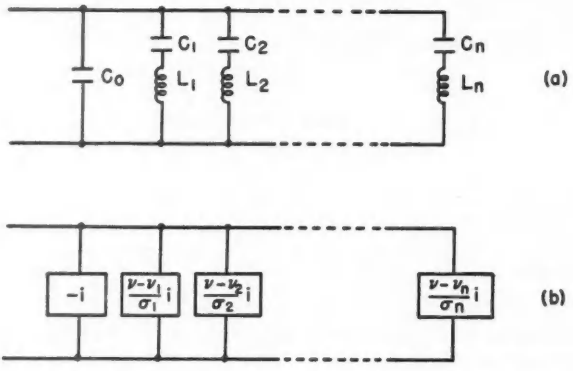

FIG. 2. Equivalent networks of a polyresonant vibrator: (*a*) exact form; (*b*) idealized form.

mode existed alone. Writing down the total admittance Y and setting it equal to zero, we have

$$[7]\quad Y = \left(-1+\frac{\sigma_1}{\nu-\nu_1}+\frac{\sigma_2}{\nu-\nu_2}+\ldots+\frac{\sigma_n}{\nu-\nu_n}\right)i$$

$$= \frac{-\prod_{r=1}^{n}(\nu-\nu_r)+\sigma_1(\nu-\nu_2)(\nu-\nu_3)\ldots(\nu-\nu_n)+\ldots+(\nu-\nu_1)(\nu-\nu_2)\ldots(\nu-\nu_{n-1})\sigma_n}{\prod_{r=1}^{n}(\nu-\nu_r)}\,i$$

$$= 0.$$

Thus, $\alpha_1, \ldots, \alpha_n$ are the roots of the numerator. Since the modes are numbered in an arbitrary fashion, it will be sufficient to obtain a result in one case only, viz. for σ_1. To this end, all frequencies are referred to ν_1, the transformed values being distinguished with primes. Thus $\nu' = \nu-\nu_1$, $\nu_1' = \nu_1-\nu_1 = 0$, $\alpha_1' = \alpha_1-\nu_1$, etc. Making these substitutions in the numerator of [7] and expanding with a view to obtaining an expression in descending powers of ν', we get

$$[8]\quad \prod_{r=1}^{n}(\nu'-\nu_r')-\sigma_1(\nu'-\nu_2')(\nu'-\nu_3')\ldots(\nu'-\nu_n')-\ldots$$
$$-(\nu'-\nu_1')(\nu'-\nu_2')\ldots(\nu'-\nu_{n-1}')\sigma_n$$
$$= (\nu')^n+\ldots\ldots\ldots\ldots+(-1)^n\nu_1'\nu_2'\ldots\nu_n'$$
$$-[\sigma_1(\nu')^{n-1}+\ldots+(-1)^{n-1}\sigma_1\nu_2'\nu_3'\ldots\nu_n']$$
$$-[\sigma_2(\nu')^{n-1}+\ldots+(-1)^{n-1}\nu_1'\sigma_2\nu_3'\ldots\nu_n']$$
$$\ldots\ldots\ldots\ldots\ldots\ldots\ldots\ldots\ldots$$
$$-[\sigma_n(\nu')^{n-1}+\ldots+(-1)^{n-1}\nu_1'\nu_2'\ldots\nu_{n-1}'\sigma_n].$$

This expression may be compared with the formal solution of [8]:

$$[9] \qquad \prod_{r=1}^{n} (\nu'-\alpha_r') = (\nu')^n + \ldots + (-1)^n \alpha_1' \alpha_2' \ldots \alpha_n' = 0.$$

It will be seen that, in both forms of the equation, the term in $(\nu')^n$ has a coefficient of unity; hence the constant terms in [8] and [9] must also be identical. Furthermore, since $\nu_1' = 0$ by definition, only the second line of [8] makes any contribution to the constant term. Hence,

$$\sigma_1 \nu_2' \nu_3' \ldots \nu_n' = \alpha_1' \alpha_2' \ldots \alpha_n'$$

or

$$[10] \qquad \sigma_1 = \frac{\alpha_1' \alpha_2' \ldots \alpha_n'}{\nu_2' \nu_3' \ldots \nu_n'} = \frac{(\alpha_1-\nu_1)(\alpha_2-\nu_1)\ldots(\alpha_n-\nu_1)}{(\nu_2-\nu_1)(\nu_3-\nu_1)\ldots(\nu_n-\nu_1)}.$$

In the same manner it may be shown that

$$[11] \qquad \sigma_m = \frac{(\alpha_1-\nu_m)(\alpha_2-\nu_m) \ldots\ldots\ldots\ldots\ldots\ldots\ldots\ldots (\alpha_n-\nu_m)}{(\nu_1-\nu_m)(\nu_2-\nu_m)\ldots(\nu_{m-1}-\nu_m)(\nu_{m+1}-\nu_m)(\nu_{m+2}-\nu_m)\ldots(\nu_n-\nu_m)}$$

where m takes successive values from 1 to n.

It will be noted that the right-hand side of [11] contains only observable quantities: the frequencies at which the network of 2(b) has zero impedance or zero admittance. Having thus obtained the values of σ_m the corresponding coupling coefficients, k_m, may then be deduced from [4]. However, the values so deduced are only accurate in so far as the network of 1(a) is accurately represented by 1(b). A comparison of the impedance of Z_1' of the idealized network 1(b) as a function of ν with the corresponding value $Z_1/4\pi L_1\sigma_1$ for the real network of 1(a) is made in Table I. It would appear that the diver-

TABLE I

	Impedance			
	$\nu = 0$	$\nu = \nu_1/2$	$\nu = 2\nu_1$	$\nu \to \infty$
Idealized network (Fig. 1(b)) $Z_1' = (i/\sigma_1)(\nu-\nu_1)$	$-i\nu_1/\sigma_1$	$-i\nu_1/2\sigma_1$	$+i\nu_1/\sigma_1$	$+i\nu/\sigma_1$
Real network (Fig. 1(a)) $\frac{Z_1}{4\pi L_1\sigma_1} = \frac{(i/\sigma_1)(\nu^2-\nu_1^2)}{2\nu}$	$-i\infty$	$-i3\nu_1/4\sigma_1$	$+i3\nu_1/4\sigma_1$	$+i\nu/2\sigma_1$

gence in impedance between the two networks leads to computed values of σ_m somewhat in excess of the exact values. Thus [11] provides excessive positive correction in respect of modes lying at frequencies very much greater than ν_m and inadequate negative correction in respect of those at frequencies very much less than ν_m. In most practical cases, however, only those modes lying close to ν_m are of much consequence, so that [11] gives σ_m with sufficient accuracy for most purposes.

It may be worth mentioning that values of σ_m calculated from [11] have been found to differ from $\alpha_m-\nu_m$ by as much as a factor of 3 in the case of the group of modes lying in the thickness resonance region of barium titanate disks.

It would be exceedingly difficult to extend [11] to take account of mechanical and electrical energy losses, but it is possible to estimate their importance by considering their effect on the electrical characteristics of a single mode resonator. Since this subject is discussed comprehensively in standard treatises (e.g. Cady (1)), only a few elementary results need be quoted here. While dielectric losses (those associated with C_0 in Fig. 1(*a*)) may appreciably affect the magnitude of the antiresonance impedance, the frequency of antiresonance is changed only to a negligible degree, even with such a lossy material as barium titanate ceramic. The mechanical losses, however, may modify appreciably both resonance and antiresonance frequencies, reducing the former and increasing the latter. Let a resistance $R_1 = 2\pi\nu_1 L_1 k_1$ ($k_1 = 1/"Q"$) be introduced in series with L_1 and C_1 in Fig. 1(*a*). Then it may be shown that, to the first order,

$$|Z_r/Z_0| = k_1\nu_1/2\sigma_1, \tag{12}$$

where Z_r is the magnitude of the impedance minimum and Z_0 is the dielectric impedance alone. Furthermore, it may be shown that the difference σ_1 between the frequencies of the impedance minimum and maximum is increased to the value σ_1^* where

$$\sigma_1^* = \sigma_1[1+(k_1^2\nu_1^2/2\sigma_1^2)+\ldots] \simeq \sigma_1[1+2|Z_r/Z_0|^2+\ldots]. \tag{13}$$

Thus, provided the impedance minimum is a small fraction of the dielectric impedance, losses do not appreciably affect determination of the electromechanical coupling coefficient of a singly resonant vibrator. Likewise, it may be inferred that [11] will give an accurate value of σ_m provided all of the modes lying close to σ_m have reasonably small impedance minima.

REFERENCES

1. CADY, W. G. Piezoelectricity. McGraw-Hill Book Company, Inc., New York. 1946. Chap. 14.
2. MASON, W. P. Piezoelectric crystals and their applications to ultrasonics. D. Van Nostrand Company, Inc., New York. 1950. p. 66.

THE EFFECT OF A RANDOM NOISE BACKGROUND UPON THE DETECTION OF A SINUSOIDAL SIGNAL[1]

By H. S. Heaps[2]

ABSTRACT

A sinusoidal signal is examined after reception upon a noise background of random phase and power distributed statistically according to a Rayleigh law. An expression is obtained for the probability distribution of the ratio of the power of the signal plus noise at any instant to the power of the noise which would be received at that instant in the absence of the signal. The corresponding result is given for the ratio of the averages over several observations. The equations contain as a parameter the ratio of the signal power to the mean noise power. When each observed value of the power is the average over a small time interval the formulae are applicable provided the noise and the signal have the same frequency. A similar analysis is presented to deal with the case in which the noise and the signal have different frequencies and in which each observation is the average over a small time interval. Comparison with the results of a previous paper, in which the signal was assumed to have a Rayleigh distribution in phase and power, indicates the effect of extreme fluctuation of an originally sinusoidal signal upon its resultant with a random noise background.

1. INTRODUCTION

A problem of frequent occurrence in connection with the propagation of acoustic or radio waves is the detection of an originally sinusoidal signal of the form $a\sin\omega t$ after it has travelled through an inhomogeneous medium and has been added to unwanted interference during the process of detection. It is sometimes of interest to detect only a portion of the resultant signal such as, for example, the part reflected from a particular inhomogeneity or, in the case of radio waves, the part reflected from the ionosphere.

If the receiver is situated sufficiently close to the source the signal upon reaching the receiver is essentially sinusoidal in character and has an envelope of constant amplitude $a(t) = a$ with respect to time. As the receiver is placed at greater distances from the source the signal travels through more inhomogeneities and its envelope $a(t)$ may differ significantly from that of a purely sinusoidal wave. For a receiver at a sufficient distance from the source the distortion of the signal may be such that its envelope contains no recognizable constant component and is best described statistically. Such a description may be necessary even if the inhomogeneities consist of quite small variations in the velocity of propagation and if the relative motions of the source, receiver, and elements of the medium are at low velocities. At any instant the sound reaching the receiver is the sum of waves which passed through the medium by paths of unequal travel time, and, if the travel times change by the order of a quarter wave period or more, a major change in the resultant wave will ensue (compare with Fig. 7 of Reference (12)).

At the receiver the required signal is added to a noise background of disturbances generated within the receiver or the medium. This noise background may include unwanted components of the generated signal or of previous

[1]*Manuscript received April 21, 1955.*
Contribution from the Naval Research Establishment, Dartmouth, Nova Scotia.
[2]*Department of Civil Engineering, Nova Scotia Technical College, Halifax, Nova Scotia.*

signals. Suppose that the noise background is slowly fluctuating in the sense that between two instants separated by a very small time interval the noise power remains unchanged while the phase increases by a periodic time factor. Suppose, however, that at two instants separated by a sufficiently large time interval the noise values may be related only statistically. At any instant both the signal and noise envelopes are specified by their amplitudes but the envelope of the signal plus the noise is dependent upon the amplitudes and the phase difference of the signal and the noise.

Throughout the present paper the signal and the noise at any instant are represented in the complex form $p^{\frac{1}{2}}\exp(i\theta)$ where p is real and is termed the power at that instant. It is assumed that at any instant all values of the phase θ are equally likely to occur. In the acoustical case it is known that noise due to reverberation from a large number of small random scatterers has a probability distribution of power according to a Rayleigh law (8, 13). Radio waves propagated through an inhomogeneous atmosphere and reflected from the ionosphere are found to contain a fluctuating component of power variation closely approximated by a Rayleigh law (3, 7, 9). Also, in the detection of radio waves, a Gaussian distribution holds for the amplitude of fluctuation noise due to thermal agitation or to shot effect within the receiver (6). In view of these results, and by virtue of the central limit theorem that the superposition of a large number of random amplitudes has a probability distribution according to a Gaussian law regardless of the form of the individual amplitude distributions (11, p. 48), it appears reasonable to suppose that the assumption of a noise background of power distributed according to a Rayleigh law is valid in many instances.

When the receiver is sufficiently distant from the source for the constant component of the received signal to be negligible the above considerations suggest that the power variation of the signal may also be supposed according to a Rayleigh law. The quantity detected by the receiver is then the sum of a Rayleigh distributed signal and a Rayleigh distributed noise. For this case the probability that, at any instant, the power of the received signal plus noise is a given multiple of the power of the noise alone has been obtained in an earlier paper (4), as has the corresponding result when the powers are averaged over several observations. The present paper considers the probability distribution of the ratio of the power at any instant of a sinusoidal signal plus a Rayleigh distributed noise background to the power of the noise which would be received at that instant in the absence of the signal. The formulae obtained are thus applicable in the case of a signal whose envelope exhibits negligible fluctuation. Comparison of the results with those of the earlier paper indicates the effect of extreme fluctuation of the signal upon its impression on a random noise background.

2. RATIO OF SIGNAL PLUS NOISE TO NOISE POWER FROM ONE OBSERVATION

For a noise of phase and power distributed according to a Rayleigh law the probability, at any instant, that the noise power p_n lies between p_n and p_n+dp_n with phase between θ and $\theta+d\theta$ in excess of the sinusoidal signal is

$$(1/2\pi\bar{p}_n)\exp(-p_n/\bar{p}_n)dp_n d\theta \qquad [1]$$

in terms of the mean noise power $\bar{p}_n$. The quantity $dp_n d\theta$ represents twice the area $p_n^{\frac{1}{2}} dp_n^{\frac{1}{2}} d\theta$ swept by the end point of the amplitude vector $p_n^{\frac{1}{2}} \exp(i\theta)$ as p_n and θ vary over the above ranges.

When a signal of constant power p is added to a noise of instantaneous power p_n the condition for the noise plus the signal to be of power q is that θ satisfies the equation

$$\cos\theta = (q-p-p_n)/2p^{\frac{1}{2}}p_n^{\frac{1}{2}}. \tag{2}$$

This equation has two solutions in θ if

$$|q^{\frac{1}{2}}-p^{\frac{1}{2}}| < p_n^{\frac{1}{2}} < |q^{\frac{1}{2}}+p^{\frac{1}{2}}| \tag{3}$$

and no solution otherwise. As q varies between q and $q+dq$ the end point of the vector $p_n^{\frac{1}{2}} \exp(i\theta)$, with θ determined by [2], ranges over an area of

$$[4p_n q-(p-p_n-q)^2]^{-\frac{1}{2}} dp_n dq. \tag{4}$$

Thus the probability that the signal plus noise power lies between q and $q+dq$ while the noise power lies between p_n and p_n+dp_n is

$$(1/\pi\bar{p}_n) \exp(-p_n/\bar{p}_n)[4pq-(p_n-p-q)^2]^{-\frac{1}{2}} dp_n dq. \tag{5}$$

The probability that the signal plus noise power lies between q and $q+dq$ is obtained by integration of [5] over the range of p_n restricted by the condition [3]. The substitution $p_n = p+q+2p^{\frac{1}{2}}q^{\frac{1}{2}} \cos\phi$ enables the integration to proceed over the range $0 < \phi < \pi$ and leads to the expression

$$(1/\bar{p}_n) \exp[-(p+q)/\bar{p}_n] I_0(2p^{\frac{1}{2}}q^{\frac{1}{2}}/\bar{p}_n) dq \tag{6}$$

in agreement with equations [3.10–11] of Rice (11) and equation [5] of Blake (1) which refer to the corresponding distribution of amplitude. The expression [6] refers to the distribution of power and is plotted as a function of q in Fig. 1 for $p/\bar{p}_n$ values of 0.1, 1, and 2. The broken curves are of the corre-

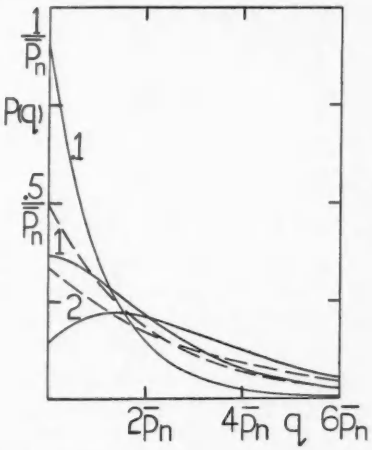

FIG. 1. Probability distribution $P(q)$ of power q of the signal of mean power $c\bar{p}_n$ plus noise of mean power $\bar{p}_n$. The continuous curves are for a sinusoidal signal (expression 6); the broken curves are for a Rayleigh signal (Reference 4). For each pair of curves the value of c is indicated. When $c = 0.1$ the two curves are indistinguishable.

sponding Rayleigh distributions for the case in which the signal is Rayleigh distributed of mean power p. The probability distribution of the phase of the resultant of a sinusoidal signal and a Rayleigh distributed noise has been investigated by Norton, Shultz, and Yarbrough (10).

Putting $q = kp_n$ and $dq = p_n dk$ in [5] the probability that the power of the signal plus noise lies between k and $k+dk$ times the power of the noise alone is $P(k)dk$ where

$$[7] \qquad P(k) = (1/\pi\bar{p}_n)\int \exp(-p_n/\bar{p}_n)[4kpp_n-(p_n-p-kp_n)^2]^{-\frac{1}{2}}p_n dp_n,$$

the integration being from $p/(1+k^{\frac{1}{2}})^2$ to $p/(1-k^{\frac{1}{2}})^2$. The substitution $p_n = p(1+k-2k^{\frac{1}{2}}\cos\phi)/(1-k)^2$ reduces [7] to the form

$$[8] \qquad P(k) = [p|1-k|^{-3}/\pi\bar{p}_n]\exp[-(1+k)(1-k)^{-2}p/\bar{p}_n]$$
$$\times\left[(1+k)\int_0^\pi \exp(a\cos\phi)d\phi - 2k^{\frac{1}{2}}\int_0^\pi \exp(a\cos\phi)\cos\phi\, d\phi\right]$$

where a denotes $2k^{\frac{1}{2}}(1-k)^{-2}p/\bar{p}_n$ and $|1-k|$ signifies the numerical value of $1-k$. The integrals appearing in [8] may be expressed in terms of the modified Bessel functions as $\pi I_0(a)$ and $\pi I_1(a)$ respectively (14, p. 181). Substitution into [8], with c denoting $p/\bar{p}_n$, then leads to

$$[9] \qquad P(k) = c|1-k|^{-3}\exp[-(1+k)(1-k)^{-2}c][(1+k)I_0(a)-2k^{\frac{1}{2}}I_1(a)].$$

For values of $c \ll 1$ the formula for $P(k)$ takes the form

$$[10] \qquad P(k) = c(1+k)|1-k|^{-3}$$

as for a Rayleigh distributed signal when $c \ll 1$ (4). For values of $c \gg 1$ the asymptotic form of [9] bears no resemblance to the corresponding expression

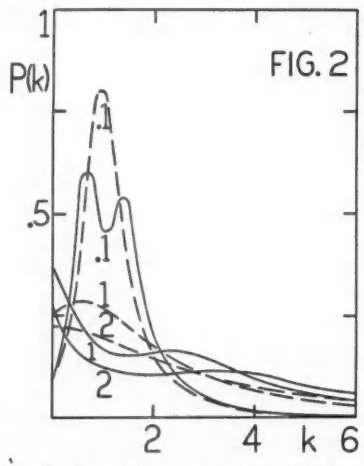

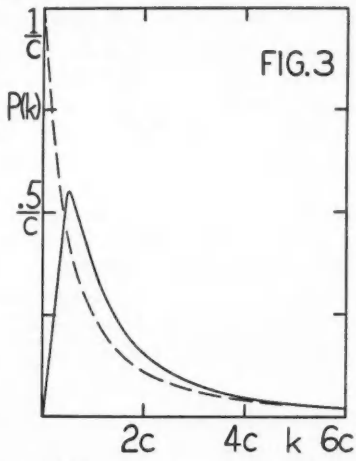

FIG. 2. Probability distribution of $P(k)$, the probability that, at any instant, the signal plus noise power is equal to k times the noise power (equation 9). The dotted curves refer to a Rayleigh signal. On each curve the value of c, the mean signal power/mean noise power, is indicated.

FIG. 3. Probability distribution of $P(k)$ when $c \gg 1$.

for a Rayleigh distributed signal. When $k = 1$, a becomes infinite and the asymptotic formulae for $I_0(a)$ and $I_1(a)$ (14, p. 203) reduce [9] to

$$[11] \qquad P(1) = (1/8)(1/\pi)^{\frac{1}{2}}c^{\frac{1}{2}}[\exp(-\tfrac{1}{4}c)][1+2/c].$$

The graphs of $P(k)$ for $c = 0.1$, 1, 2, and $\gg 1$ are drawn in Figs. 2 and 3, the dotted graphs being of the corresponding functions for the case of a Rayleigh distributed signal as calculated in Reference (4). The values of c are as indicated for each pair of curves. The most striking difference between the distributions for the sinusoidal and Rayleigh signals is a reduction of the maximum and, for $c = 0.1$ and 1, the occurrence of a minimum in the sinusoidal case.

3. RATIO FROM THE MEAN OF SEVERAL RANDOM OBSERVATIONS

Let the signal plus noise power be averaged over $r+1$ observations separated by sufficiently large time intervals for them to be independent although the mean characteristics of the signal and noise remain unchanged. Then the power of the signal plus noise averaged over the $r+1$ observations has a probability distribution dependent upon the value of r. Similarly the power of the noise alone averaged over the $r+1$ observations has a probability distribution dependent upon r. In this section the 'mean' noise power $\bar{p}_n$ refers to the average over a very long time while the 'average' noise power refers to the average of $r+1$ independent discrete samples.

By repeated application of equation [5] it follows that the probability that the sum of the noise powers lies between p_n and p_n+dp_n while the sum of the signal plus noise powers lies between q and $q+dq$ is

$$[12] \qquad dp_n dq(\pi\bar{p}_n)^{-r-1}\exp(-p_n/\bar{p}_n)\int\cdots\int[4py_1-(x_1-p-y_1)^2]^{-\frac{1}{2}}$$

$$\times[4p(y_2-y_1)-(x_2-x_1-p-y_2+y_1)^2]^{-\frac{1}{2}}\cdots[4p(q-y_r)-(p_n-x_r-p-q+y_r)^2]^{-\frac{1}{2}}$$
$$\times dx_1dy_1\ldots dx_rdy_r$$

where the integrations are over $0 < x_1 < x_2 < \ldots$ and $0 < y_1 < y_2 < \ldots$ subject to the condition that the expression within each square bracket of [12] remain positive. Repeated use of the identity

$$[13] \qquad \int_0^t\int_0^s[4mpy-(x-mp-y)^2]^{m-3/2}[4m(t-y)-(s-x-p-t+y)^2]^{-\frac{1}{2}}dxdy$$
$$= [\tfrac{1}{4}\pi m^{m-1}(m+1)^{-m}/(m-\tfrac{1}{2})p][4(m+1)pt-(s-mp-p-t)^2]^2,$$

proved by application of the Faltung theorem for the double Laplace transform to the functions $[4mpy-(x-mp-y)^2]^{m-3/2}$ and $[4m(t-y)-(s-x-p-t+y)^2]^{-\frac{1}{2}}$ (see Appendix), enables [12] to be written in the form

$$[14] \qquad (1/\pi)[r!/(2r)!](r+1)^{-r}p^{-r}\bar{p}^{-r-1}[4(r+1)pq-(p_n-rp-p-q)]^{r-\frac{1}{2}}.$$

Putting $q = kp_n$ and $dq = p_ndk$, the probability that the average signal plus noise power lies between k and $k+dk$ times the average noise power is $P_{r+1}(k)dk$, where

$$[15] \qquad P_{r+1}(k) = (1/\pi)[r!/(2r)!](r+1)^{-r}p^{-r}\bar{p}_n^{-r-1}$$
$$\times\int[4(r+1)kpp_n-(p_n-rp-p-kp_n)^2]^{r-\frac{1}{2}}p_n\exp(-p_n/\bar{p}_n)dp_n,$$

the integration being from $(1+k^{\frac{1}{2}})^{-2}(r+1)p$ to $(1-k^{\frac{1}{2}})^{-2}(r+1)p$. The substitution $p_n = (1-k)^{-2}(r+1)p(1+k-2k^{\frac{1}{2}}\cos\phi)$ transforms [15] to the form

$$[16] \quad P_{r+1}(k) = (1/\pi)[r!/(2r)!]2^{2r}k^r(r+1)^{r+1}(1-k)^{-2r-3}p^{r+1}\bar{p}_n^{-r-1} \times \exp[-(1+k)(1-k)^{-2}(r+1)p/\bar{p}_n]\left[(1+k)\int_0^\pi \exp(a\cos\phi)\sin^{2r}\phi\, d\phi - 2k^{\frac{1}{2}}\int_0^\pi \exp(a\cos\phi)\cos\phi\sin^{2r}\phi\, d\phi\right]$$

where a denotes $2k^{\frac{1}{2}}(1-k)^{-2}(r+1)p/\bar{p}_n$. The first integral in [16] has the value $\pi^{\frac{1}{2}}(\frac{1}{2}a)^{-r}\Gamma(r+\frac{1}{2})I_r(a)$ (14, p. 79). The second integral may be obtained as the derivative of the first with respect to a. Substitution into the formula for $P_{r+1}(k)$, with c denoting $p/\bar{p}_n$, leads to

$$[17] \quad P_r(k) = k^{\frac{1}{2}(r-1)}(1-k)^{-3}rc\exp[-(1+k)(1-k)^{-2}rc][(1+k)I_{r-1}(a) - 2k^{\frac{1}{2}}I_r(a)]$$

in which a is equal to $2k^{\frac{1}{2}}(1-k)^{-2}rc$.

For values of r between 0 and 11 and of a between 0 and 6 the values of $I_r(a) = (-i)^rJ_r(ia)$ may be obtained from Reference (5), pp. 232–233. For large values of a the asymptotic form of $I_r(a)$ (14, p. 203) may be applied in the form

$$[18] \quad I_r(a) = (2\pi a)^{-\frac{1}{2}}(\exp a)[1-(4r^2-1)/8a+(2r-1)(1+k)(1-k^{\frac{1}{2}})^{-2}/2a]$$

and leads to

$$[19] \quad P_r(k) = \tfrac{1}{2}(1/\pi)^{\frac{1}{2}}k^{(2r-3)/4}(1+k^{\frac{1}{2}})^{-2}r^{\frac{1}{2}}c^{\frac{1}{2}}\exp[-rc(1+k^{\frac{1}{2}})^{-2}] \times[1-(4r^2-1)/8a+(4r^2-1)(4r^2-9)/128a^2+(2r-1)(1+k)(1-k^{\frac{1}{2}})^{-2}/2a - (2r+1)(2r-1)(2r-3)(1+k)(1-k^{\frac{1}{2}})^{-2}/16a^2].$$

For calculation of $P_r(k)$ when $k = 1$ the form [19] must be used and reduces to

$$[20] \quad P_r(1) = (1/8)(1/\pi)^{\frac{1}{2}}r^{\frac{1}{2}}c^{\frac{1}{2}}[\exp(-\tfrac{1}{4}rc)][1+2(2r-1)/rc].$$

The quantity $P_r(k)dk$ is the probability that the power of the sum of a sinusoidal signal and a Rayleigh distributed noise background averaged over r random observations lies between k and $k+dk$ times the averaged noise power which would be obtained in the absence of the signal. The graphs of $P_r(k)$ for $c = 0.1$, 1, and $\gg 1$ are drawn in Figs. 4–6 for r values of 1, 2, and 3. The probability that the ratio of the averaged powers exceeds k is given by

$$[21] \quad Q_r(k) = \int_k^\infty P_r(k)dk.$$

Numerical integration of the integral appearing in equation [21] leads to values of $Q_r(k)$ as drawn in Figs. 7 and 8.

The median value of k with respect to $P_r(k)$ is the value of k at which $Q_r(k)$ is equal to $\frac{1}{2}$. For a Rayleigh signal the median value of k is equal to $c+1$ regardless of the number of observations averaged (4), but for a sinusoidal signal it is apparent from Figs. 7 and 8 that the median value depends upon the magnitude of r and decreases with increasing r. For a given value of c the value of k at which $Q_r(k)$ is independent of r is less than the median value.

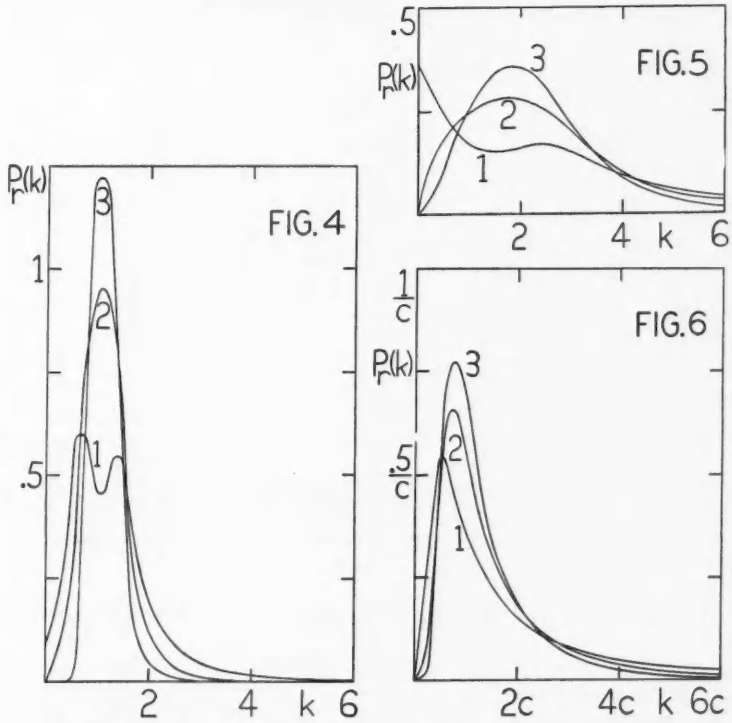

FIG. 4. Probability distribution of $P_r(k)$, the probability that the signal plus noise power averaged over r random samples is equal to k times the averaged noise power (equations 17, 19). On each curve the value of r is indicated. c, the mean signal power/mean noise power, is 0.1.

FIG. 5. Probability distribution of $P_r(k)$ when $c = 1$. The value of r is indicated on each curve.

FIG. 6. Probability distribution of $P_r(k)$ when $c \gg 1$. The value of r is indicated on each curve.

Equation [9] of Section 2 compares the signal plus noise power with the noise power at a single instant and may be used to compare the averages over a small time interval provided the signal and noise have the same frequency. If the signal and the noise are of different frequency let ωt denote the increase in phase difference between the noise and the signal during the time t and suppose that the noise power does not change significantly throughout this time. An attempt to extend the approach of Section 2 to compare the signal and noise power averaged over the time t with the power of the noise alone averaged over the time t replaces the expression [4] by a more complicated function, and a similar subsequent analysis does not appear to be feasible. However there are two instances in which the resulting equations are much simplified. The first is when $\omega t = 0$, in which case the analysis proceeds as in Section 2 with p, p_n, and q denoting averages over the time t; the second is when $\omega t \gg 1$, in which case the signal plus noise power averaged over the time

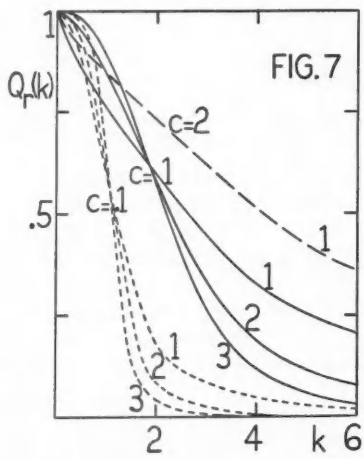

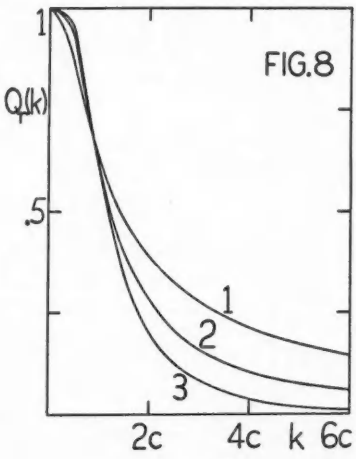

FIG. 7. Probability distribution of $Q_r(k)$, the probability that the signal plus noise power averaged over r random samples is at least k times the averaged noise power (equation 21). The value of r is indicated on each curve. c denotes the signal power/mean noise power.

FIG. 8. Probability distribution of $Q_r(k)$ when $c \gg 1$. The value of r is indicated on each curve.

t is given by $Q = p+p_n$ where p and p_n refer to averages over the interval t (4).

If $\omega t \gg 1$ then $p_n = Q-p$ and the condition that the average noise plus signal power lies between k and $k+dk$ times the average noise power is that p_n lies between $p_n = p/(k-1)$ and p_n+dp_n where $dp_n = -pdk/(k-1)^2$. The probability of this occurrence is $\bar{P}(k)dk$ where

$$\bar{P}(k) = c(k-1)^{-2}\exp[-c/(k-1)] \tag{22}$$

and k is necessarily greater than unity. The probability that the average noise plus signal power is greater than k times the average noise power is

$$\bar{Q}(k) = \int_k^\infty \bar{P}(k)dk = 1-\exp[-c/(k-1)]. \tag{23}$$

If the above interval averages are again averaged over a random set of r time intervals the condition that the ratio of the average noise plus signal power to the average noise power lies between k and $k+dk$ is that the sum of the noise powers lies between P_n and P_n+dP_n where $P_n = rp/(k-1)$ and $dP_n = -rpdk/(k-1)^2$. Now the probability that the sum of r interval averages of the noise power lies between P_n and P_n+dP_n is

$$[1/(r-1)!]\bar{p}_n^{-r}P_n^{r-1}\exp(-P_n/\bar{p}_n)dP_n, \tag{24}$$

and hence the probability that the ratio k lies between k and $k+dk$ is $\bar{P}_r(k)dk$ where

$$\bar{P}_r(k) = [1/(r-1)!](rc)^r(k-1)^{-r-1}\exp[-rc/(k-1)] \tag{25}$$

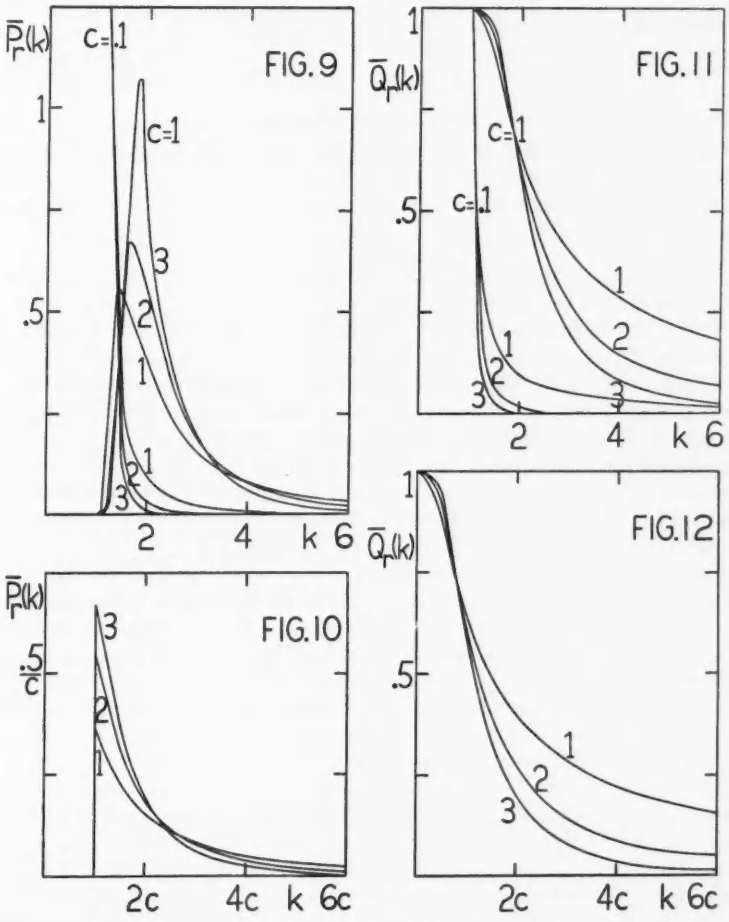

FIG. 9. Probability distribution of $\bar{P}_r(k)$ (equation 25) applying to the case $\omega t \gg 1$, drawn for comparison with Figs. 4 and 5. The value of r is indicated on each curve.

FIG. 10. Probability distribution of $\bar{P}_r(k)$ when $c \gg 1$, drawn for comparison with Fig. 6.

FIG. 11. Probability distribution of $\bar{Q}_r(k)$ (equation 26) applying to the case $\omega t \gg 1$, drawn for comparison with Fig. 7.

FIG. 12. Probability distribution of $\bar{Q}_r(k)$ when $c \gg 1$, drawn for comparison with Fig. 8.

and k is at least unity. The probability that the average noise plus signal power exceeds the average noise power by at least a factor k is

$$[26] \qquad \bar{Q}_r(k) = \int_k^\infty \bar{P}_r(k)dk$$

$$= 1-\exp[-rc/(k-1)]\sum_{n=0}^{r-1}(1/n!)[rc/(k-1)]^n,$$

which may also be expressed in the form

$$\bar{Q}_r(k) = \exp[-rc/(k-1)] \sum_{n=r}^{\infty} (1/n!)[rc/(k-1)]^n.$$

Graphs of $\bar{P}_r(k)$ and $\bar{Q}_r(k)$ are drawn in Figs. 9–12 for $c = 0.1$, 1, and $\gg 1$ and $r = 1, 2$, and 3. It is to be noted that $\bar{P}_r(k)$ and $\bar{Q}_r(k)$ depend upon the values of r in contrast to the case of a Rayleigh distributed signal in which $\bar{P}_r(k)$ and $\bar{Q}_r(k)$ are independent of the number r of intervals considered (4).

4. CONCLUDING REMARKS

Comparison of the results of this and of the earlier paper (4) enables an evaluation to be made of the effect of fluctuation of the signal envelope upon its impression on a random noise background. Consider, for example, the case of a sinusoidal pulsed signal emitted by an underwater source of sound, it being assumed that the initial rise of each pulse occupies less time than is required for a significant fluctuation in the noise power. Suppose that a receiver placed near the source receives a signal of essentially constant envelope and of power large compared to that of the noise background. Suppose also that as the receiver recedes from the source the received signal power decreases in relation to the noise.

Before arrival of the signal the receiver registers the noise background which, upon arrival of the signal, increases suddenly by a factor k. If the receiver is close to the source, the probability distribution of k is as shown in Fig. 6, and the effect of averaging the initial increase over several pulses is to concentrate the distribution to the neighborhood of $k = c$. If, on the other hand, the signal plus noise is averaged over a complete pulse of duration t such that $\omega t \gg 1$, then the ratio k has the distribution of Fig. 10, which is similar to that of Fig. 6 except that k values of less than unity do not occur.

If the receiver is sufficiently distant from the source for the mean noise background to have the power of the received signal, then the initial increase upon arrival of a signal has the distribution of Fig. 5. This differs significantly from the distribution of pulse averages shown in Fig. 9 in that the latter distributions indicate greater probability of k values between 1.5 and 2.5. For a detection system responsive to k values in excess of a threshold value between 1 and 2, Figs. 7 and 11 show that observation of pulse averages increases the probability of detection by about 10 to 20%. Comparison of Fig. 7 with Fig. 5 of Reference (4) shows that, with a threshold between 1 and 2, the probability of detection of the initial increase is approximately the same as for a Rayleigh signal. But comparison of Fig. 11 with Fig. 8 of Reference (4) shows that, with a similar threshold, the probability of detection of a sinusoidal signal by pulse averages may be 30% more than of one that is Rayleigh distributed.

If the mean noise power is 10 times the signal power, comparison of Figs. 7 and 11 shows that a detection system with a threshold in excess of approximately 1.2 detects fewer signals by pulse averages than by initial increases

caused by the arrival of a pulse. However, the detection probabilities are small in each case and differ by only a few per cent from the detection probabilities of a Rayleigh distributed signal.

ACKNOWLEDGMENTS

The author wishes to express his appreciation to the Defence Research Board of Canada for permission to publish this paper, which has arisen as part of an investigation under N.R.E. Project D12-38-03-03.

APPENDIX

The identity [13] may be proved as follows. Let I denote the expression

$$[27] \quad \int_0^t \int_0^s [4mpy-(x-mp-y)^2]^{m-3/2}[4m(t-y)-(s-x-p-t+y)^2]^{-\frac{1}{2}}dxdy.$$

By virtue of the Faltung theorem for the double Laplace transform I may also be written in the form

$$[28] \quad I = (2\pi i)^{-2}\int\int_{\gamma-i\infty}^{\gamma+i\infty} F_m(u,v)F_1(u,v)\exp(us+vt)dudv$$

where

$$[29] \quad F_m(u,v) = \int\int [4mpy-(x-mp-y)^2]^{m-3/2}\exp(-xu-yv)dxdy.$$

The range of integration in [29] includes all positive values of x and y for which $4mpy-(x-mp-y)^2 > 0$.

Putting $x = mp+y-2(mpy)^{\frac{1}{2}}\cos\theta$ equation [29] becomes

$$[30] \quad F_m(u,v) = \exp(-mpu)\int_0^\infty (4mpy)^{m-1}\exp(-uy-vy)dy \times\int_0^\pi \exp[(4mpy)^{\frac{1}{2}}u\cos\theta]\sin^{2m-2}\theta d\theta$$

$$= \pi^{\frac{1}{2}}\Gamma(m-\tfrac{1}{2})(4mp)^{m-1}(mpu^2)^{-\frac{1}{2}(m-1)}[\exp(-mpu)] \times\int_0^\infty y^{\frac{1}{2}(m-1)}I_{m-1}(4mpu^2y)^{\frac{1}{2}}\exp(-uy-vy)dy$$

by Reference (14), p. 79. The integral appearing in [30] is of a type listed in Reference (2), p. 197, and hence

$$[31] \quad F_m(u,v) = \pi^{\frac{1}{2}}\Gamma(m-\tfrac{1}{2})2^{2m-2}(mp)^{m-1}(u+v)^{-m}\exp[-mpuv/(u+v)].$$

Accordingly

$$[32] \quad I = (2\pi i)^{-2}\pi^{3/2}\Gamma(m-\tfrac{1}{2})2^{2m-2}(mp)^{m-1}\int_{\gamma-i\infty}^{\gamma+i\infty}\exp[(t-s-mp-p)v]dv \times\int_{\gamma-i\infty}^{\gamma+i\infty} u^{-m-1}\exp[(m+1)pv^2/u]\exp(su)du.$$

The second integral in [32] has the value (2, p. 245)

$$(2\pi i)[(m+1)pv^2]^{-m/2}s^{m/2}I_m[4(m+1)psv^2]^{\frac{1}{2}},$$

and so [32] may be written as

$$[33] \quad I = (2\pi i)^{-1}\pi^{3/2}\Gamma(m-\tfrac{1}{2})2^{2m-2}(mp)^{m-1}s^{m/2} \times \int_{\gamma-i\infty}^{\gamma+i\infty} v^{-m}I_m[4(m+1)psv^2]^{\frac{1}{2}}\exp[-4(m+1)psv^2]^{\frac{1}{2}}\exp(Tv)dv$$

with T denoting $t-s-mp-p+2[(m+1)ps]^{\frac{1}{2}}$. The last integral is equal to (2, p. 277)

$$[34] \quad [1/\Gamma(m+\tfrac{1}{2})]\pi^{-\frac{1}{2}}[16(m+1)ps]^{-m/2}\{[16(m+1)ps]^{\frac{1}{2}}T-T^2\}^{m-\frac{1}{2}}.$$

Substitution of [34] into [33], and replacement of T by its value in terms of s and t, finally leads to

$$[35] \quad I = [\tfrac{1}{4}\pi m^{m-1}(m+1)^{-m}/(m-\tfrac{1}{2})p][4(m+1)pt-(s-mp-p-t)^2]^2,$$

which completes the proof of equation [13].

REFERENCES

1. BLAKE, L. V. Proc. Inst. Radio Engrs. 38: 301. 1950.
2. ERDÉLYI, A., MAGNUS, W., OBERHETTINGER, F., and TRICOMI, F. G. Tables of integral transforms. Vol. I. McGraw-Hill Book Company, Inc., New York. 1954.
3. HARWOOD, J. Proc. Inst. Elec. Engrs. (London), Pt. IV, 101: 183. 1954.
4. HEAPS, H. S. Can. J. Phys. 33: 1. 1955.
5. JAHNKE, E. and EMDE, F. Tables of functions. 4th ed. Dover Publications, Inc., New York. 1945.
6. LANDON, V. D. Proc. Inst. Radio Engrs. 29: 50. 1941.
7. MCNICOL, R. W. E. Proc. Inst. Elec. Engrs. (London), Pt. III, 96: 517. 1949.
8. MARSHALL, J. S. and HITSCHFELD, W. Can. J. Phys. 31: 962. 1953.
9. MITRA, S. N. Proc. Inst. Elec. Engrs. (London), Pt. III, 96: 505. 1949.
10. NORTON, K. A., SHULTZ, E. L., and YARBROUGH, H. J. Appl. Phys. 23: 137. 1952.
11. RICE, S. O. Bell System Tech. J. 24: 46. 1945.
12. SHEEHY, M. J. J. Acoust. Soc. Amer. 22: 24. 1950.
13. WALLACE, P. R. Can. J. Phys. 31: 995. 1953.
14. WATSON, G. N. A treatise on the theory of Bessel functions. 2nd ed. Cambridge University Press, London. 1944.

INTERNATIONAL COMPARISONS OF THE CANADIAN PRIMARY RADIUM STANDARD[1]

By W. S. Michel and G. N. Whyte

ABSTRACT

The content in milligrams of radium element of the Canadian primary radium standard was measured relative to the certified weight of a primary standard of the United States by an ionization method. The problem of correcting for differences in the attenuation of the gamma radiation in the body of each source is important, since the standards differ greatly in shape; a method of making this correction is described. Other intercomparisons involving the Canadian standard are discussed, and a mean value for the content of the standard is derived from these comparisons. The agreement between this and the certified value is satisfactory.

I. INTRODUCTION

Measurements of the contents of radium sources, like measurements of mass and length, are based indirectly on a comparison with a national or international radium standard. In Canada all measurements of radium content, as well as the calibration of instruments for measuring gamma radiation, are based on the radium content of the Canadian primary radium standard, maintained in the laboratories of the National Research Council (and referred to hereafter as the NRC standard). An accurate knowledge of the value of this content is therefore of some importance.

The NRC standard differs in two important respects from most other national standards*: the glass tube containing the radium salt is much smaller than those of the other standards, with the result that the salt fills most of the tube rather than a small part of it; and the certified value of the content is based not on a direct weighing of the salt but simply on a comparison with the former international primary standard on the basis of the ionization produced by the gamma radiation. It has been established (5) that no account was taken in this comparison of any difference in the wall and salt absorption in the two sources. Comparisons of the NRC standard with other standards that permit a calculation of the radium content of the former are thus of considerable interest.

A welcome opportunity of this kind was provided by an interchange during the past few years of national radium standards for intercomparison purposes agreed on between the National Physical Laboratory (U.K.), the National Bureau of Standards (U.S.A.), and the National Research Council. Some of the results of these measurements have already been communicated in a joint statement by the three national laboratories to the Stockholm meeting of the Joint Commission on Standards, Units and Constants of Radioactivity. A joint statement on all the results obtained will be published elsewhere.

[1]*Manuscript received May 19, 1955.*
Contribution of the Division of Applied Physics, National Reseach Council, Ottawa, Ontario. Issued as N.R.C. No. 3697.

**The history of the national and international radium standards has recently been outlined by Davenport, Mann, McCraven, and Smith (2).*

This paper describes a recent comparison of the NRC standard and one of the standards of the National Bureau of Standards carried out in this laboratory, and summarizes the results of a number of other comparisons involving the NRC standard.

II. DETAILS OF THE NRC AND NBS STANDARDS

The Canadian primary radium standard is a glass tube containing very pure anhydrous radium chloride, stated by the supplier (Union Minière du Haut Katanga) to be free from thorium derivatives. It was acquired by the National Research Council in 1930 and subsequently certified by the Commission Internationale des Étalons de Radium to contain, in 1933, 24.24 mgm. of radium element. Standards measured at Paris and Vienna by the Commission are assigned Roman numerals: the NRC standard is number XIII.

The United States primary radium standard (NBS standard) measured here is one of two acquired by the United States in 1936 from a set of 20 prepared in 1934 by Professor Otto Hönigschmid. These standards were made up of carefully weighed amounts of highly purified anhydrous radium chloride. One of them is the present international standard in Paris, another is the present reserve standard in Vienna, and others have been acquired by the United Kingdom and Germany for use as national standards. The NBS standard used in this comparison was assigned the number 5440 by Hönigschmid. It was also compared with the former Paris and Vienna standards and received the number XV.

Particulars of the two standards are given in Table I, and they are also shown in Fig. 1(*c*) and (*d*). It should be noted that, while the two sources

TABLE I

PARTICULARS OF THE U.S. AND THE CANADIAN PRIMARY STANDARDS

	U.S. standard (NBS)	Canadian standard (NRC)
Identification or reference number	5440, XV	XIII
Radium content in mgm. element	20.45 [2] 20.38 [3]	24.24 [1]
Internal diameter, mm.	3 [4]	1.5 [5]
Wall thickness, mm.	0.27	0.25
Length, mm.	38.3	10.5 [5]
Nature of salt	Dark brown grains	Dark brown grains

[1]*Certified value from the comparison with the primary standards of 1912 in Paris and Vienna, 1933.*

[2]*Calculated from the weighed value determined by Hönigschmid on June 2, 1934; the relation 1 gm. $RaCl_2$ corresponds to 0.7612 gm. Ra was used.*

[3]*Certified value obtained by comparison with the primary standards of 1912 in Paris and Vienna, corrected to 1934.*

[4]*A more exact determination of the internal diameter of a portion of the tube was made as discussed below.*

[5]*As stated by Union Minière du Haut Katanga.*

contain about the same amount of salt, the glass tube of the NBS standard is larger in diameter and longer than that of the NRC standard. If the standards are held vertically, the length of the salt column is about one-twentieth of the total length for the NBS source, as against four-fifths of the length for the NRC one.

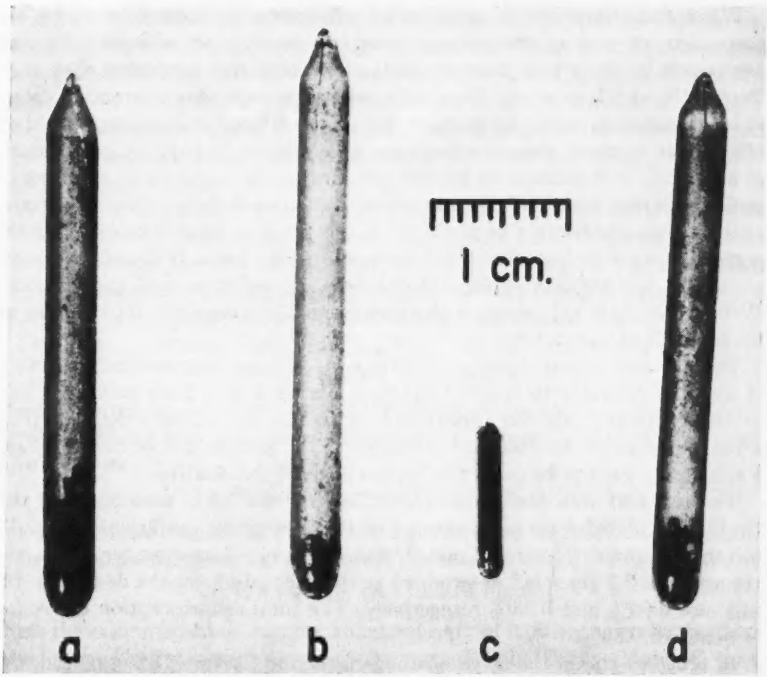

FIG. 1. Photograph of four national radium standards. (*a*) U.S. standard number XIV (NBS); (*b*) U.K. standard (NPL); (*c*) Canadian standard (NRC); (*d*) U.S. standard number XV (NBS). (Photograph by courtesy of the Journal of Research of the National Bureau of Standards.)

III. SELF-ABSORPTION CORRECTIONS

The masses of radium element in radium preparations in equilibrium may be compared by comparing the gamma radiation emitted by them, since the intensity of this radiation is proportional to the mass of radium element present. Correction must be made, however, for differences in self-absorption—attenuation of the gamma radiation in the radium-bearing material itself (salt absorption) and in the walls of the container (wall absorption)—if the sources differ physically. Before making the ionization comparison, it was necessary to consider this self-absorption correction.

Many of the old secondary standards are physically similar to each other and to the Hönigschmid standards. Even so, they may differ somewhat in grain size, in the relative amounts of free and occluded radon, and in grain position. Probably the differences in self-absorption due to these factors are minor; in any case, their effect has not been systematically investigated. The practice has been to assume, at least in comparisons involving physically similar sources of approximately the same content, that differences in self-absorption may be neglected.

When the assumption of equality of self-absorption cannot be made, the correction for each of the sources being compared must be known. Several workers have described their methods of making this correction (see, e.g., Perry (10) and Evans and Evans (3), who give numerous references). Since exact calculations cannot be made because of the difficulties in taking secondary effects into account, these methods are all empirical in part. In comparisons of standards it appears to be general practice to place sources in a horizontal position during measurement, care being taken to distribute the salt grains evenly along the bottom of the tube. However, it is difficult to calculate the correction for standards like the large ones in Fig. 1 in a horizontal position, since the salt consists of separated grains of uncertain size and position. Weiss (11) apparently made such corrections but gives little information on his methods of calculation.

For the comparison of the physically very different sources described here, it seemed preferable to conduct the measurements with both standards held vertically. In this position a mean density for the salt can be calculated from a measurement of the volume it occupies at the bottom end of the tube, and a salt correction can be computed on the basis of this density.

The salt and wall absorption corrections for the NRC standard held vertically, calculated from a knowledge of the absorption coefficients (9) valid for the National Research Council standard ionization chamber and using the value of 2.2 gm./cm.^{3} determined at this laboratory for the density of the salt, are 0.66% and 0.23% respectively. The total self-absorption correction is therefore 0.89%.

In order to obtain the corresponding correction for the NBS standard, one end of the standard was selected (all the ionization measurements were later made with this end down) and the salt shaken to the other end. The standard was then laid horizontal, immersed in Xylol, and viewed under a travelling microscope. Measurements of the internal diameter and wall thickness of the glass tube were made at intervals of 0.1 mm., starting from one end and working up to approximately the height that would be occupied by the salt in the vertical position (2.5 mm.). The wall correction for each zone was calculated using these measurements and the NRC linear absorption coefficient for soft glass of 8×10^{-3} mm^{-1}. A mean wall correction was then found by weighting the correction for each zone according to the volume of salt in the zone; the result was 0.21%. In a similar way the weighted mean salt absorption correction was found to be 1.23%, giving a total self-absorption correction of 1.44%, with an estimated error not exceeding 0.15%. This error is due mainly to the effects of refraction on the measurement of the inside dimensions of the tube. Incidentally, the density of the salt was found to be 2.2 gm./cm.^{3}, in exact agreement with that found for the NRC standard.

IV. CONTENT MEASUREMENT

The gamma-ray intensities from the two standards were compared on the NRC standard radium-measuring apparatus (9), which consists of a parallel-plate one-atmosphere ionization chamber with $\frac{1}{4}$ in. lead walls lined with

aluminum, and a modified Townsend balance circuit for measuring the ionization current. During measurement, each source was held vertically on a strip of thin cellulose adhesive tape mounted in a light aluminum frame. The frame fitted into a holder placed 60 to 80 cm. from the ionization chamber. The holder could be moved by means of a vernier adjustment so that the axes of the sources were at the same distance from the chamber during the determination of any one ratio.

A total of 10 measurements, at different distances, of the ionization ratio of the two sources were made by three observers. In half of the measurements one standard was measured first, in half the other. Due precautions were taken to compensate for possible drift of the apparatus. The procedure also included rotation of each standard through 180° between successive readings.

The mean gamma-ray ratio resulting from the measurements is

$$\text{NRC/NBS} = 1.192 \pm 0.0019,$$

where the uncertainty is the standard deviation of the mean of the measured ratios. Applying the absorption corrections calculated above, the content ratio becomes

$$\text{NRC/NBS} = 1.186 \pm 0.0024.$$

The weighed content of the NBS standard, corrected to 1933, is 20.46 mgm. of radium element. Based on this value, the content of the NRC standard is

$$20.46 \times 1.186 = 24.27 \pm 0.08 \text{ mgm.}.$$

where the estimated error includes an uncertainty of 0.03 mgm. in the weighed value of the NBS standard, based on the statement by Hönigschmid (4) that the total error in the weighed value of the *salt* could amount to 0.04 mgm.

V. OTHER COMPARISONS INVOLVING THE NRC STANDARD

Since its preparation in 1930, the NRC standard has been compared with other standards on a number of occasions. The results of several such comparisons will be summarized briefly.

(1) *Direct Comparison with the Former Paris Primary Radium Standard*

The original certification of the NRC standard in 1933 was made by a direct comparison with the former (1911) international primary standard in Paris, the sources being laid horizontally on top of a flat ionization chamber not unlike the National Research Council chamber. (A comparison was also made with the "1911" reserve standard in Vienna, but details of the measurement are not available.) As described by Mme. Curie (1), the Paris standard consisted of 16.75 mgm. of radium element in the form of the chloride filling a length of 32 mm. in a glass tube 0.9 mm. in inside diameter and 0.27 mm. in wall thickness. On the basis of these dimensions and the assumption that the absorption coefficients for the Paris chamber do not differ much from those for the NRC chamber, one can calculate values of 0.20% for the salt absorption and 0.24% for the wall absorption, a total of 0.44%. The corresponding corrections for the NRC standard, taking into account the fact that in the horizontal position the salt does not occupy the full cross-section of the tube,

are 0.56% and 0.23%, giving a total of 0.79%. The content of 24.24 mgm. originally deduced for the NRC primary neglecting self-absorption corrections should thus be increased by $0.79-0.44 = 0.35\%$. The result is 24.32 mgm.

(2) *Indirect Comparison with the United Kingdom Primary Radium Standard*

During 1951 a glass source belonging to NRC and containing about 25 mgm. of radium was measured at both the National Physical Laboratory (NPL) in the United Kingdom and the National Research Council (6). Since the content deduced at NPL was based on the content of the U.K. primary radium standard (NPL standard), and that deduced at NRC was based on the NRC standard, the measurements constituted an indirect comparison of these standards. The fact that the particular glass source used was similar in form to the NPL standard simplified the comparison with the latter, since the self-absorption in the two could be assumed to be the same. The value obtained at the National Physical Laboratory was 24.02 mgm. The value obtained at NRC, recalculated on the basis of more recent absorption coefficients, is 23.99 mgm. Taking the weighed content of the NPL standard to be correct, one may deduce that the certificate value of 24.24 mgm. for the NRC standard should be multiplied by a factor of 24.02/23.99, giving a value of 24.27 mgm.

(3) *Indirect Comparison with NBS Primary Standard*

In 1953 a platinum-enclosed secondary standard belonging to the National Bureau of Standards was compared at NRC with both the NBS and NRC standards (8). As in the previous case, this constituted an indirect comparison of the two standards. The absorption corrections were calculated in the manner described in Section III. The resulting content for the NRC standard was 24.17 mgm.

(4) *Direct Comparisons at the National Bureau of Standards*

Recently the primary standards of the United Kingdom, Canada, and the United States were intercompared by a number of methods at the National Bureau of Standards (2). Of the gamma-ray comparisons, that using the NBS standard electroscope lends itself most readily to analysis, since the same absorption corrections can be used as for the NRC chamber.

The NRC standard was measured against the NPL standard and the two NBS standards, the sources being held in a horizontal position to one side of the chamber. By applying self-absorption corrections to the ionization ratios obtained, one can calculate the content of the NRC standard on the basis of the weighed contents of the others. Such corrections were calculated by assuming the salt to be fine-grained and to lie uniformly along the tubes, estimating the volume occupied on the basis of a density of 2.2 gm./cm.^{2}, and determining the average absorption by graphical integration over the resulting segment-shaped cross-section. The assumption that the salt is fine-grained and uniform will certainly introduce some error, since the actual grains vary in size up to a few millimeters across and lie loosely along the bottom of the tube; but if one assumes the most extreme case—a single row of spherical

grains along the length of the tube—the resulting salt correction is only lower by enough to make a difference of less than 0.2% in the content. The correction calculated for this extreme condition is certainly low, so that it seems unlikely that the corrections calculated on the assumption of fine-grained uniform salt are in error by much more than 0.1%.

The content figures for the NRC standard deduced from the NBS measurements are presented in Table II, along with the other values obtained above. The mean value from all the ionization comparisons is 24.27 mgm. of radium element, with a standard deviation of about 0.1%.

TABLE II

VALUES OF THE RADIUM CONTENT OF THE NRC STANDARD DERIVED FROM IONIZATION COMPARISONS (AS OF 1933)

Compared with	At	Year	Derived content (mgm.)
International primary	Paris	1933	24.32
NPL standard (5432, indirect)	NPL & NRC	1951	24.27
NBS standard (XV, indirect)	NRC	1953	24.17
NBS standard (XV)	NRC	1953	24.27
NBS (XIV)	NBS	1954	24.29
NPL (5432)	NBS	1954	24.22
NBS (XV)	NBS	1954	24.33
			Mean = 24.27

(5) *Calorimetric Comparison at the National Bureau of Standards*

There exists one further measurement on the NRC standard. In the series of measurements at the National Bureau of Standards (2), the NRC source was compared with the NPL and NBS standards by a calorimetric method (7). The value derived from this work is 24.37 mgm., as of 1933.

VI. DISCUSSION

The mean value of 24.27 mgm. found for the radium content of the NRC standard from the ionization results in Table II differs by a little over 0.1% from the certified value of 24.24 mgm. Since the stated accuracy of the certified value is 0.2%, this agreement may be considered satisfactory.

The calorimetric value of 24.37 is 0.4% higher than the value obtained from ionization measurements, and although it depends on fairly large corrections for the growth of polonium and radium E in the sources compared, the discrepancy is not understood.

In any case, it is apparent that when one compares the NRC standard with a weighed standard by the ionization method and corrects for self-absorption with the aid of the NRC coefficients, one obtains a value for the content of the NRC standard that does not differ from the certificate value by more than about 0.3%. Conversely, if one deduces the content of another source from the certificate value of the NRC standard by this method, the result should be accurate to about 0.3%. This is the way in which the standard is used.

REFERENCES

1. CURIE, MME. P. J. phys. 2: 795. 1912.
2. DAVENPORT, T. I., MANN, W. B., MCCRAVEN, C. C., and SMITH, C. C. J. Research Natl. Bur. Standards, 53: 267. 1954.
3. EVANS, R. D. and EVANS, R. O. Revs. Mod. Phys. 20: 305. 1948.
4. HÖNIGSCHMID, O. Anz. Akad. Wiss. Wien, Math.-naturw. Kl. 82: 30. 1945.
5. JOLIOT-CURIE, MME. I. Personal communication.
6. KASTNER, J. and MORRISON, A. Natl. Research Council Can. Rept. No. PR-116. 1952.
7. MANN, W. B. J. Research Natl. Bur. Standards, 52: 177. 1954.
8. MICHEL, W. S. Natl. Research Council Can. Rept. No. PR-195. 1953.
9. MICHEL, W. S. Natl. Research Council Can. Rept. No. APR-271. 1955.
10. PERRY, W. E. Proc. Phys. Soc. (London), 57: 178. 1945.
11. WEISS, C. Z. Physik, 120: 652. 1943.

A METHOD FOR THE EVALUATION OF SOME LATTICE SUMS OCCURRING IN CALCULATIONS OF PHYSICAL PROPERTIES OF CRYSTALS. II[1]

By G. C. Benson and H. P. Schreiber[2]

ABSTRACT

The methods of a previous paper are applied to the evaluation of lattice sums of the form

$$\sum_{k,l}^{\infty}\sum_{m}^{\infty}{}_{-\infty} k^r l^s (k^2+l^2+m^2)^{-n} \qquad (r \text{ and } s \text{ positive integers}).$$

Useful transformations result when either r or s is even but not in general when both r and s are odd. A table of the function

$$\mathscr{S}_t(\infty) = \sum_{k,l}^{\infty} kl(k^2+l^2)^{-t/2}$$

for integral values of t from 5 to 30 is presented. This permits the extension of the method to the cases $r = 1$, $s = 1$ and $r = 1$, $s = 3$.

INTRODUCTION

In a previous paper (4) (henceforth referred to as I) a procedure was described by which certain types of lattice sums can be transformed into fairly rapidly converging series of known tabulated functions (exponential, modified Bessel, and Riemann ζ-functions, etc.). The application of this method to triple sums of the form

$$[1] \qquad T_n(r, s) = \sum_{k,l}^{\infty}\sum_{m}^{\infty}{}_{-\infty} k^r l^s (k^2+l^2+m^2)^{-n},$$

where r and s are positive integers, is considered in the present paper. Sums of this type occur in calculations of elastic properties (2) ($r = 2$, $s = 0$; $r = 2$, $s = 2$; $r = 4$, $s = 0$) and edge energies (3) ($r = 1$, $s = 1$) of crystals.

It is shown in the next section that when r and s are both odd, application of the methods of I to $T_n(r, s)$ gives rise to double sums which are not available as tabulated functions. The calculation of one of these, defined by

$$[2] \qquad \mathscr{S}_t(\infty) = \sum_{k,l}^{\infty} kl(k^2+l^2)^{-t/2},$$

is described in the third section and a table of values is presented there.

TREATMENT OF THE SUMS $T_n(r, s)$

It will be assumed that the values of r, s, and n in equation [1] are such that $T_n(r, s)$ is a convergent sum (i.e. $2n > r+s+3$). Application of the transformation described in I leads to the result

$$[3] \qquad T_n(r, s) = \frac{\sqrt{\pi}}{\Gamma(n)}\Bigg[\Gamma(n-\tfrac{1}{2})\, S_{n-\frac{1}{2}}(r, s) + 4\sum_{k,l,m}^{\infty} k^r l^s \left(\frac{m\pi}{\sqrt{(k^2+l^2)}}\right)^{n-\frac{1}{2}} K_{n-\frac{1}{2}}(2\pi m\sqrt{k^2+l^2})\Bigg]$$

[1]*Manuscript received May 17, 1955.*
Contribution from the Division of Pure Chemistry, National Research Council, Ottawa, Canada. Issued as N.R.C. No. 3703.
[2]*National Research Council of Canada Postdoctorate Fellow 1953—.*

where, in general,

$$[4] \qquad S_\nu(r, s) = \sum_{k,l}{}'_1^{\infty} k^r l^s (k^2+l^2)^{-\nu}.$$

Apart from $S_{n-\frac{1}{2}}(r, s)$, the terms of equation [3] are all similar to those encountered in the examples discussed in I, and the evaluation of $T_n(r, s)$ by means of this equation is dependent upon the possibility of evaluating these new double sums.

The functions $S_\nu(r, s)$ defined by equation [4] satisfy the symmetry relation

$$[5] \qquad S_\nu(r, s) = S_\nu(s, r)\,.$$

The power r can be lowered by the reduction formula

$$[6] \qquad S_\nu(r, s) = S_{\nu-1}(r-2, s) - S_\nu(r-2, s+2),$$

which after μ successive applications gives the relation

$$[7] \qquad S_\nu(r, s) = \sum_j^{\mu} (-1)^j\, {}^{\mu}C_j\, S_{\nu-\mu+j}(r-2\mu, s+2j).$$

In this equation, the quantities ${}^{\mu}C_j$ are the usual combinatorial coefficients.

For a further examination of $S_\nu(r, s)$ it is convenient to consider the following possibilities:

(i) one or both powers (r, s) even integers,

(ii) both powers (r, s) odd integers.

Case (i)

When at least one of the powers is even, no generality is lost by putting $r = 2p$, where p is an integer. This procedure is justified by the symmetry relation equation [5]. From equation [7] with $\mu = p$ it can be seen that

$$[8] \qquad S_\nu(2p, s) = \sum_j^{p} (-1)^j\, {}^{p}C_j\; S_{\nu-p+j}(0, s+2j).$$

This equation expresses $S_\nu(2p, s)$ as a sum of terms of the type

$$[9] \qquad S_\eta(0, q) = \sum_{k,l}{}'_1^{\infty} l^q (k^2+l^2)^{-\eta} = \sum_{k,l}{}'_1^{\infty} k^q (k^2+l^2)^{-\eta},$$

where q is an integer. These, when rewritten as

$$[10] \qquad S_\eta(0, q) = \frac{1}{2}\left[\sum_k{}'_1^{\infty} \sum_l{}'^{\infty}_{-\infty} k^q (k^2+l^2)^{-\eta} - \sum_k{}'_1^{\infty} k^{-(2\eta-q)} \right],$$

can be treated by the procedures of I.

It may also be noted that equation [8] with $s = 0$ gives

$$[11] \qquad S_\nu(2p, 0)[1-(-1)^p] = \sum_j^{p-1} (-1)^j\, {}^{p}C_j\, S_{\nu-p+j}(0, 2j)$$

which leads to a number of useful relations such as

$$[12] \qquad S_\nu(0, 2) = \tfrac{1}{2} S_{\nu-1}(0, 0),$$

$$S_\nu(0, 6) = \tfrac{1}{2}[S_{\nu-3}(0, 0) - 3S_{\nu-2}(0, 2) + 3S_{\nu-1}(0, 4)]$$

$$[13] \qquad = \tfrac{1}{4}[6S_{\nu-1}(0, 4) - S_{\nu-3}(0, 0)]\,.$$

Case (ii)

When both the powers r and s are odd, the reduction formula gives

$$S_r(2p+1, s) = \sum_j^p (-1)^j \, {}^pC_j \, S_{r-p+j}(1, s+2j). \tag{14}$$

Terms of the form $S_\eta(1, 2q+1)$ satisfy the relation

$$S_\eta(1, 2q+1)[1-(-1)^q] = \sum_j^{q-1} (-1)^j \, {}^qC_j \, S_{\eta-q+j}(1, 2j+1), \tag{15}$$

which is analogous to equation [11]. However they cannot be evaluated by application of the transformations described in I as can the sums $S_\eta(0, q)$.

In connection with some calculations of edge energies of alkali halide crystals (6), it was necessary to compute values of

$$S_{t/2}(1, 1) = \mathscr{S}_t(\infty) \tag{16}$$

for a number of integral values of t. The method of computation and a table of results are given in the next section. Assuming that $S_\eta(1, 1)$ is known as a function of η, $S_\eta(1, 3)$ can be obtained from

$$S_\eta(1, 3) = \tfrac{1}{2} S_{\eta-1}(1, 1) \tag{17}$$

but further extension of this process requires the evaluation of $S_\eta(1, 5)$, $S_\eta(1, 9)$, etc. Since there are no problems of physical significance giving rise to these higher sums, their evaluation does not appear to be worth while at this time.

EVALUATION OF THE SUM $\mathscr{S}_t(\infty)$

The function defined by equation [2] converges for $t > 4$. However for low values of t this convergence is very slow and it has not been possible to find a way of improving it.

A simple, direct method for estimating lattice sums of this type has been described by Misra (5) and Born and Huang (2). Essentially it depends on splitting the sum into two parts. The first, composed of contributions from lattice points lying within a certain radius R, is evaluated by direct summation. Contributions from points outside R are approximated by integration. This procedure was adopted in the present case but a square array defined by $k = 1, 2, \ldots, L$ and $l = 1, 2, \ldots, L$ was found to be more suitable than a circular one. The sum over the points of this array is denoted by

$$\mathscr{S}_t(L) = \sum_{k,l}^{L} kl(k^2+l^2)^{-t/2}. \tag{18}$$

An estimate of the contributions from the remaining points is given by the integral

$$\begin{aligned} \mathscr{I}_t(L) &= \int_{x=\frac{1}{2}}^{x=L+\frac{1}{2}} \int_{y=L+\frac{1}{2}}^{y=\infty} \frac{xy}{(x^2+y^2)^{t/2}} \, dxdy + \int_{x=L+\frac{1}{2}}^{x=\infty} \int_{y=\frac{1}{2}}^{y=\infty} \frac{xy}{(x^2+y^2)^{t/2}} \, dxdy \\ &= \frac{1}{(t-2)(t-4)} \left[\frac{2}{[(L+\frac{1}{2})^2+\frac{1}{4}]^{(t-4)/2}} - \frac{1}{2^{(t-4)/2}(L+\frac{1}{2})^{t-4}} \right]. \end{aligned} \tag{19}$$

The required sum $\mathscr{S}_t(\infty)$ is obtained from the equation

$$\mathscr{S}_t(\infty) = \lim_{L\to\infty} [\mathscr{S}_t(L) + \mathscr{I}_t(L)]. \tag{20}$$

The lowest value of t considered was 5. Table I shows the results obtained for $\mathscr{S}_5(L)$ and $\mathscr{I}_5(L)$ at a number of values of L. Up to $L = 20$, the sums

TABLE I

SUMMARY OF CALCULATIONS OF $\mathscr{S}_5(\infty)$

L	L^2, No. of terms in sum	$\mathscr{S}_5(L)$	$\mathscr{I}_5(L)$	$\mathscr{S}_5(L)+\mathscr{I}_5(L)$
10	100	0.3954144222	0.0409723649	0.4363867871
15	225	0.4085915330	0.0277817946	0.4363733276
20	400	0.4153568757	0.0210129854	0.4363698611
50	2500	0.4278340866	0.0085333016	0.4363673882
60	3600	0.4292443118	0.0071230023	0.4363673141
70	4900	0.4302545430	0.0061127325	0.4363672755
80	6400	0.4310138183	0.0053534354	0.4363672537
90	8100	0.4316053150	0.0047619252	0.4363672402
100	10000	0.4320791108	0.0042881209	0.4363672317
∞				0.43636718*

*Extrapolated value.

$\mathscr{S}_5(L)$ were evaluated with a desk calculating machine; above $L = 20$ it was necessary to have the sum programmed and evaluated on an electronic computer. It is interesting to note that the sum $\mathscr{S}_5(L)$ is still changing in the third significant figure after adding 10^4 terms. The extrapolation of $\mathscr{S}_5(L)+\mathscr{I}_5(L)$ to $L = \infty$ was accomplished graphically by plotting $\log_e\{[\mathscr{S}_5(L)+\mathscr{I}_5(L)]/C\}$ against the reciprocal of L. In this C is a constant approximately equal to $\mathscr{S}_5(\infty)$.

Other values of $\mathscr{S}_t(\infty)$ for integral t from 6 to 30 were calculated in a similar way but the limit L was reduced as t increased, since the convergence of the sum became more rapid. The final results are summarized in Table II. The

TABLE II

VALUES OF THE SUM $\mathscr{S}_t(\infty) = \sum_{k,l}^{\infty} kl(k^2+l^2)^{-t/2}$

t	$\mathscr{S}_t(\infty)$	t	$\mathscr{S}_t(\infty)$
5	4.3636718×10^{-1}	18	1.9552101×10^{-3}
6	1.9249534×10^{-1}	19	1.3819966×10^{-3}
7	1.1162796×10^{-1}	20	9.7697653×10^{-4}
8	7.1421138×10^{-2}	21	6.9071868×10^{-4}
9	4.7814603×10^{-2}	22	4.8836371×10^{-4}
10	3.2766933×10^{-2}	23	3.4530381×10^{-4}
11	2.2745505×10^{-2}	24	2.4415708×10^{-4}
12	1.5905826×10^{-2}	25	1.7264084×10^{-4}
13	1.1171254×10^{-2}	26	1.2207360×10^{-4}
14	7.8664535×10^{-3}	27	8.6318215×10^{-5}
15	5.5480988×10^{-3}	28	6.1035813×10^{-5}
16	3.9168060×10^{-3}	29	4.3158667×10^{-5}
17	2.7668234×10^{-3}	30	3.0517710×10^{-5}

graphical extrapolation was only required for the case $t = 5$. It was also possible eventually to dispense with the integration step; thus results for $t \geqslant 15$ are based on the direct summation of 100 terms (i.e. $L = 10$).

In the case of $t = 5$, the uncertainty in the graphical extrapolation is of the order of one unit in the eighth significant figure. For the sake of uniformity the results for $t \geqslant 6$ were rounded to eight significant figures with a possible error of ± 5 in the ninth digit. It is of interest that for high values of t the quantity $\log_e \mathscr{S}_t(\infty)$ is a nearly linear function of t with a limiting slope of $-\log_e \sqrt{2}$. This is useful in interpolating at non-integral values of t.

CONCLUSION

In the previous sections it has been shown that $T_n(r, s)$ can be reduced by the method of I to sums of known tabulated functions in all cases in which at least one of the powers r and s is even. When $r = 1$, $s = 1$ and $r = 1$, $s = 3$ the sum can also be handled by this method in conjunction with the table of the function $\mathscr{S}_t(\infty)$. In other cases where both r and s are odd, progress is hampered by the occurrence of certain double sums which cannot be reduced further and which have not been tabulated. It is easy to show that the above remarks also apply to sums similar to $T_n(r, s)$ but with $k+l+m$ restricted to odd or to even values.

Other sums similar to $T_n(r, s)$ but with the limits for k and l extending from $-\infty$ to $+\infty$ instead of from 1 to ∞ have been treated by Misra (5) and by Born and Bradburn (1). In this case the sum vanishes if either r or s is odd, thus

$$[21] \qquad \sum_{k,l,m}{}'_{-\infty}^{\infty} k^r l^s (k^2+l^2+m^2)^{-n} = 0 \qquad (r \text{ or } s \text{ odd}).$$

If both r and s are even the sum can be rewritten as

$$[22] \qquad \sum_{k,l,m}{}'_{-\infty}^{\infty} k^r l^s (k^2+l^2+m^2)^{-n} = 4T_n(r, s) \qquad (r \text{ and } s \text{ even})$$

and the right-hand side evaluated as already described.

ACKNOWLEDGMENT

The authors wish to express their indebtedness to Dr. J. F. Hart of the Applied Physics Branch, Division of Physics, National Research Council, for carrying out the evaluation of the sums $\mathscr{S}_t(L)$ on the FERUT at the Computation Centre, University of Toronto. They also would like to thank Dr. G. J. van der Maas of the Radio and Electrical Engineering Division, National Research Council, for several helpful discussions regarding the possibility of finding a suitable transform of the sum $\mathscr{S}_t(\infty)$.

REFERENCES

1. Born, M. and Bradburn, M. Proc. Cambridge Phil. Soc. 39: 104. 1942.
2. Born, M. and Huang, K. Dynamical theory of crystal lattices. Oxford University Press, London. 1954. Chap. 3 and Appendix III.
3. Born, M. and Stern, O. Sitzber. preuss. Akad. Wiss. Physik.-math. Kl. 48: 901. 1919.
4. van der Hoff, B. M. E. and Benson, G. C. Can. J. Phys. 31: 1087. 1953.
5. Misra, R. D. Proc. Cambridge Phil. Soc. 36: 173. 1940.
6. Schreiber, H. P. and Benson, G. C. Can. J. Phys. 33: 534. 1955.

EDGE ENERGIES OF ALKALI HALIDE CRYSTALS[1]

By H. P. Schreiber[2] and G. C. Benson

ABSTRACT

Theoretical calculations of the energies of <100> edges of sodium and potassium halide crystals are described. The present computations differ from those of previous workers by the inclusion of terms arising from van der Waals forces. It appears that these forces make a significant contribution to the edge energy.

I. INTRODUCTION

The heat of solution of a solid crystalline substance in a suitable solvent is a function of the particle size of the material. This dependence has been studied by several groups of workers (1, 6, 8) and used as an experimental method for determining the surface energy of solids. Even in the ideal case of perfectly shaped crystalline particles of a uniform size, the difference between the results for fine and coarse material measured in these experiments should not be exactly proportional to the difference in specific areas of the samples since it must contain other contributions which, if the crystals are not too small, can be associated with edges and corners. At present this variation from linearity is beyond the range of the experimental techniques employed but some estimate of its magnitude can be obtained from theoretical models.

Calculations of the edge energies of the alkali halides were made a number of years ago by Born and Stern (3) and by Lennard-Jones and Taylor (7). In these, the work necessary to form an edge was computed, assuming that the forces between ions could be represented as the sum of electrostatic and pure repulsive terms. More recently, Shuttleworth (13) has shown that van der Waals forces make a substantial contribution to the surface energies of the alkali halides. Although it is to be expected that this will also be true for the edge energy, verification of this point is of some interest.

In the next section the main features of the theoretical model for the calculation of the edge energies are summarized. The necessary lattice sums are evaluated in Section III, and the results for the <100> edge energies of some alkali halides are presented in Section IV.

II. DERIVATION OF THE EDGE ENERGY EXPRESSION

The usual classical Born–Mayer model (12) of an ionic crystal is assumed. At 0° K. and neglecting zero point motion, the crystal is represented as an array of positive and negative ions fixed at the sites of a space lattice and interacting according to additive central force laws.

In Fig. 1 an infinite crystal of the sodium chloride type, having nearest neighbor distance a_0, is represented schematically. An orthogonal Cartesian co-ordinate system is chosen to coincide with the principal crystalline axes.

[1]*Manuscript received May 17, 1955.*
Contribution from the Division of Pure Chemistry, National Research Council, Ottawa, Canada. Issued as N.R.C. No. 3702.
[2]*National Research Council of Canada Postdoctorate Fellow 1953—.*

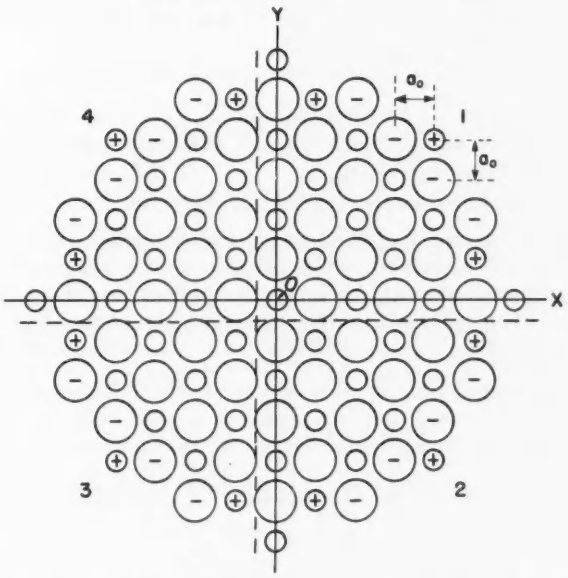

FIG. 1. The co-ordinate system. Diagram shows the XOY plane of an infinite sodium chloride type crystal with nearest neighbor distance a_0. The dashed lines indicate division of the crystal by the planes $x = -\frac{1}{2}a_0$ and $y = -\frac{1}{2}a_0$ to form four parts.

When the crystal is divided by the planes $x = -\frac{1}{2}a_0$ and $y = -\frac{1}{2}a_0$ (broken lines in Fig. 1) and the four parts infinitely separated, four <100> edges (perpendicular to the page in Fig. 1) are created.

If, following Born and Stern (3), the four parts are designated by the numbers 1, 2, 3, 4, the mean edge free energy per unit length is given by

[1] $$\bar{\kappa} = (U_{13}+U_{24})\,(4L)^{-1}$$

where U_{13} and U_{24} represent the energies of interaction between ions in diagonally opposite parts and L is the length of one of the edges. Stranski (14) has discussed the definition of the edge energy in unsymmetrical cases where U_{13} and U_{24} are not equal. However the formulation of Born and Stern is quite adequate in the present case, since U_{13} and U_{24} are equal, and thus the energy associated with unit length of any one of the four edges is

[2] $$\kappa = U_{13}(2L)^{-1}.$$

From a consideration of the periodicity occurring along the edge (i.e. in the Z-direction) it is evident that

[3] $$U_{13}L^{-1} = (U_{+}+U_{-})(2a_0)^{-1}$$

where U_{+} and U_{-} represent the interaction energy of all the ions in part 1 with those of part 3 which lie in the planes $Z = 0$ and $Z = a_0$ respectively.

The co-ordinates of an ion in part 1 are p_1a_0, p_2a_0, p_3a_0 where p_1, p_2, p_3 are integers such that

$$p_1 \geqslant 0,\ p_2 \geqslant 0,\ \text{and}\ -\infty \leqslant p_3 \leqslant \infty.$$

An ion of part 3 lying in the plane $Z = 0$ has co-ordinates $-q_1a_0$, $-q_2a_0$, 0 where q_1 and q_2 are integers satisfying the conditions $q_1 \geqslant 1$, $q_2 \geqslant 1$. The distance between these two ions is

$$[4] \qquad R(p_1, p_2, p_3, q_1, q_2) = a_0[(p_1+q_1)^2+(p_2+q_2)^2+p_3^2]^{\frac{1}{2}}.$$

The energy of interaction of two ions a distance R apart is represented by $\mathfrak{E}_{++}(R)$, $\mathfrak{E}_{--}(R)$, or $\mathfrak{E}_{+-}(R)$ according to the respective charges of the interacting ions. Assuming the origin to be at a positive site (as shown in Fig. 1),

$$[5] \qquad U_+ = \sum_{\substack{p_1+p_2+p_3 \text{ even} \\ q_1+q_2 \text{ even}}} \mathfrak{E}_{++}(R) + \sum_{\substack{p_1+p_2+p_3 \text{ odd} \\ q_1+q_2 \text{ odd}}} \mathfrak{E}_{--}(R) + \sum_{p_1+p_2+p_3+q_1+q_2 \text{ odd}} \mathfrak{E}_{+-}(R)$$

where the sums extend over all permitted values of the integers p_1, p_2, p_3, q_1, and q_2 consistent with the restriction listed below each summation sign. By shifting the origin to the negative ion at $(0, 0, a_0)$ it can be seen that

$$[6] \qquad U_- = \sum_{\substack{p_1+p_2+p_3 \text{ odd} \\ q_1+q_2 \text{ odd}}} \mathfrak{E}_{++}(R) + \sum_{\substack{p_1+p_2+p_3 \text{ even} \\ q_1+q_2 \text{ even}}} \mathfrak{E}_{--}(R) + \sum_{p_1+p_2+p_3+q_1+q_2 \text{ odd}} \mathfrak{E}_{+-}(R)$$

and hence

$$[7] \qquad \kappa = (2a_0)^{-1}\Bigg[\tfrac{1}{2}\sum_{p_1+p_2+p_3+q_1+q_2 \text{ even}} (\mathfrak{E}_{++}(R)+\mathfrak{E}_{--}(R)) + \sum_{p_1+p_2+p_3+q_1+q_2 \text{ odd}} \mathfrak{E}_{+-}(R)\Bigg].$$

These sums can be simplified by the substitutions

$$p_1+q_1 = k, \qquad p_2+q_2 = l, \qquad p_3 = m$$

where the k, l, and m must be integers such that $k \geqslant 1$, $l \geqslant 1$, and $-\infty \leqslant m \leqslant \infty$. The interionic distance R is then written as

$$[8] \qquad R(p_1, p_2, p_3, q_1, q_2) = r(k, l, m) = a_0[k^2+l^2+m^2]^{\frac{1}{2}}.$$

Since any fixed value of k can be made up from k pairs of values of p_1 and q_1' i.e. $(0, k)$, $(1, k-1)$, $\ldots$, $(k-1, 1)$ and similarly any fixed l from l pairs of values of p_2 and q_2, it is apparent that the edge energy can be written as

$$[9] \qquad \kappa = (2a_0)^{-1}\Bigg[\tfrac{1}{2}\sum_{\substack{k,\,l \\ k+l+m \text{ even}}}^{\infty}\sum_{m}^{\infty}{}_{-\infty} kl(\mathfrak{E}_{++}(r)+\mathfrak{E}_{--}(r)) + \sum_{\substack{k,\,l \\ k+l+m \text{ odd}}}^{\infty}\sum_{m}^{\infty}{}_{-\infty} kl\mathfrak{E}_{+-}(r)\Bigg]$$

Following Huggins and Mayer (5) the interaction $\mathfrak{E}_{ij}(r)$ between two ions of species i and j at distance r is taken to be

$$[10] \qquad \mathfrak{E}_{ij}(r) = Z_iZ_j\frac{e^2}{r} - \frac{c_{ij}}{r^6} - \frac{d_{ij}}{r^8} + bb_ib_jf_{ij}e^{-r/\rho}.$$

This is the sum of Coulombic, van der Waals attractive, and exponential repulsive terms, in which Z_i and Z_j are the valencies of the ions and e the electronic charge. For alkali halide crystals the van der Waals coefficients c_{ij} and d_{ij} have been tabulated by Mayer (9), the repulsive constants b, b_i, and ρ

by Huggins and Mayer (5), and excluding lithium salts, the Pauling factors* f_{++}, f_{--}, f_{+-} are 1.25, 0.75, and 1.00 respectively.

After the expression for the $\mathfrak{E}_{ij}(r)$ is substituted, equation [9] becomes

$$[11]\quad \kappa = (2a_0^{-1})\Big[\frac{e^2}{a_0}B_1 - \frac{1}{a_0^6}\Big(c_{+-}D_6' + \Big(\frac{c_{++}+c_{--}}{2}\Big)D_6''\Big) - \frac{1}{a_0^8}\Big(d_{+-}D_8' + \Big(\frac{d_{++}+d_{--}}{2}\Big)D_8''\Big) + b\Big(\frac{1.25b_+^2+0.75b_-^2}{2}\exp\Big(\frac{-\sqrt{2}a_0}{\rho}\Big) + 2b_+b_-\exp\Big(\frac{-\sqrt{3}a_0}{\rho}\Big)\Big)\Big],$$

repulsive terms arising from the interactions of ions farther apart than third neighbors having been neglected. The symbols B_1 and D_6', etc., are defined by the equations

$$[12]\quad B_1 = \sum_{k,\,l}^{\infty}{}_1 \sum_{m}^{\infty}{}_{-\infty} (-1)^{k+l+m} kl(k^2+l^2+m^2)^{-\frac{1}{2}},$$

$$[13]\quad D_{2n}' = \sum_{\substack{k,\,l \\ k+l+m\ \text{odd}}}^{\infty}{}_1 \sum_{m}^{\infty}{}_{-\infty} kl(k^2+l^2+m^2)^{-n},$$

$$[14]\quad D_{2n}'' = \sum_{\substack{k,\,l \\ k+l+m\ \text{even}}}^{\infty}{}_1 \sum_{m}^{\infty}{}_{-\infty} kl(k^2+l^2+m^2)^{-n}.$$

Although the sums D_{2n}' and D_{2n}'' are convergent only for $n > 5/2$, a uniform approach to the evaluation of these sums and of B_1 is obtained by expressing the latter in a formal way as

$$[15]\quad B_1 = D_1'' - D_1'.$$

III. EVALUATION OF THE SUMS B_1, D_6', D_6'', D_8', AND D_8''

Application of the transformations described by van der Hoff and Benson (4) and Benson and Schreiber (2) to the sums D_{2n}' and D_{2n}'' leads to the results

$$[16]\quad D_{2n}' = \frac{2\sqrt{\pi}}{\Gamma(n)}\Big[\tfrac{1}{4}\Gamma(n-\tfrac{1}{2})\mathcal{S}_{2n-1}(\infty) + \sum_{\substack{k,\,l \\ k+l\ \text{odd}}}^{\infty}{}_1 \sum_{m}^{\infty}{}_1 kl\Big(\frac{\pi m}{2\sqrt{(k^2+l^2)}}\Big)^{n-\frac{1}{2}} K_{n-\frac{1}{2}}(\pi m\sqrt{k^2+l^2}) + \sum_{\substack{k,\,l \\ k+l\ \text{even}}}^{\infty}{}_1 \sum_{m}^{\infty}{}_1 (-1)^m kl\Big(\frac{\pi m}{2\sqrt{(k^2+l^2)}}\Big)^{n-\frac{1}{2}} K_{n-\frac{1}{2}}(\pi m\sqrt{k^2+l^2})\Big]$$

and

$$[17]\quad D_{2n}'' = \frac{2\sqrt{\pi}}{\Gamma(n)}\Big[\tfrac{1}{4}\Gamma(n-\tfrac{1}{2})\mathcal{S}_{2n-1}(\infty) + \sum_{\substack{k,\,l \\ k+l\ \text{even}}}^{\infty}{}_1 \sum_{m}^{\infty}{}_1 kl\Big(\frac{\pi m}{2\sqrt{(k^2+l^2)}}\Big)^{n-\frac{1}{2}} K_{n-\frac{1}{2}}(\pi m\sqrt{k^2+l^2}) + \sum_{\substack{k,\,l \\ k+l\ \text{odd}}}^{\infty}{}_1 \sum_{m}^{\infty}{}_1 (-1)^m kl\Big(\frac{\pi m}{2\sqrt{(k^2+l^2)}}\Big)^{n-\frac{1}{2}} K_{n-\frac{1}{2}}(\pi m\sqrt{k^2+l^2})\Big]$$

These are usually denoted by c_{++}, c_{--}, and c_{+-}. The present notation has been adopted to avoid confusion with the van der Waals constants.

where the function

$$[18] \qquad \mathscr{S}_t(\infty) = \sum_{k,\,l}^{\infty} kl(k^2+l^2)^{-t/2}$$

has been tabulated for a number of integral values of t in Reference (2).

After subtracting equation [16] from equation [17] and putting $n = \frac{1}{2}$, the equation

$$[19] \qquad B_1 = 4\sum_{k,\,l}^{\infty}\sum_{m\ \text{odd}}^{\infty}(-1)^{k+l}kl\,K_0(\pi m\sqrt{k^2+l^2})$$

is obtained. Essentially this same result has been given by Born and Stern (3) but their method of derivation differs from that outlined above.

When n is an integer the modified Bessel functions in equations [16] and [17] are of half integral order and can be expressed in terms of exponentials. The formulae for D_{2n}' and D_{2n}'' then become

$$[20] \quad D_{2n}' = \frac{\pi}{2^{n-1}(n-1)!}\left[\frac{(2n-2)!}{2^n(n-1)!}\mathscr{S}_{2n-1}(\infty) + \pi^{n-1}\left(\sum_{\substack{k,\,l\\ k+l\ \text{odd}}}^{\infty}\sum_{m}^{\infty}T_n + \sum_{\substack{k,\,l\\ k+l\ \text{even}}}^{\infty}\sum_{m}^{\infty}(-1)^m T_n\right)\right]$$

and

$$[21] \quad D_{2n}'' = \frac{\pi}{2^{n-1}(n-1)!}\left[\frac{(2n-2)!}{2^n(n-1)!}\mathscr{S}_{2n-1}(\infty) + \pi^{n-1}\left(\sum_{\substack{k,\,l\\ k+l\ \text{even}}}^{\infty}\sum_{m}^{\infty}T_n + \sum_{\substack{k,\,l\\ k+l\ \text{odd}}}^{\infty}\sum_{m}^{\infty}(-1)^m T_n\right)\right]$$

where

$$[22] \quad T_n = \frac{klm^{n-1}}{(k^2+l^2)^{n/2}}\exp(-\pi m\sqrt{k^2+l^2})\sum_{\nu}^{n-1}\frac{(n-1+\nu)!}{\nu!(n-1-\nu)!}\frac{1}{(2\pi m\sqrt{(k^2+l^2)})^{\nu}}.$$

Numerical computation of the lattice sums B_1, D_6', D_6'', D_8', and D_8'' using these equations yields the values*

$$B_1 = 0.021822_6,$$
$$D_6' = 0.230288_2, \qquad D_6'' = 0.285893_0,$$
$$D_8' = 0.0368379_6, \qquad D_8'' = 0.0748789_9.$$

IV. RESULTS OF CALCULATIONS FOR SODIUM AND POTASSIUM HALIDE CRYSTALS

The contributions of the various terms of equation [11] to the <100> edge energies of the sodium and potassium halides are displayed in Table I. For consistency in these calculations, the electronic charge was taken to be 4.77×10^{-10} e.s.u. since this was the value employed in establishing the potential constants (see References 5 and 9); furthermore values of a_0 calculated from the potential constants by Shuttleworth (13) were used rather than experimental lattice spacings.

*Less accurate values which have been published by other authors are: $B_1 = 0.02186$, Born and Stern (3); $D_6' = 0.0365$ and $D_8'' = 0.0745$, Lennard-Jones and Taylor (7).

TABLE I

CONTRIBUTION OF THE DIFFERENT FORCES TO THE EDGE ENERGY OF AN UNDISTORTED <100> EDGE OF SOME ALKALI HALIDE CRYSTALS

Energies in 10^{-6} erg cm.$^{-1}$	NaF	NaCl	NaBr	NaI	KF	KCl	KBr	KI
Electrostatic	4.734	3.212	2.857	2.434	3.522	2.592	2.348	2.048
Dipole–dipole	−0.550	−0.756	−0.813	−0.895	−0.571	−0.594	−0.608	−0.644
Dipole–quadrupole	−0.027	−0.047	−0.052	−0.061	−0.019	−0.025	−0.027	−0.033
Repulsive	0.750	0.441	0.409	0.388	0.343	0.140	0.123	0.116
Total κ	4.91	2.85	2.40	1.87	3.27	2.11	1.84	1.49
Born and Stern	5.08	3.42	3.05	2.60	3.82	2.75	2.50	2.18
Lennard-Jones and Taylor	5.13	3.97			3.95	3.06		

V. CONCLUSION

For comparison, edge energies calculated from the formula derived by Born and Stern* (3) and the results of Lennard-Jones and Taylor (7) are shown in the last two lines of Table I. Although different forms of repulsive potential have been used in the three calculations, the main difference between the present results and the other two sets can be attributed to the lowering effect of the van der Waals terms. The contributions from these forces to the total edge energy vary progressively from 12 to 50% for the sodium halides and from 18 to 45% for the potassium salts. In general, van der Waals forces play only a minor role in the lattice energy, but a significant contribution to the surface energy has been noted by Shuttleworth (13). The relative contributions of van der Waals forces to the lattice, surface, and edge energies of sodium chloride are illustrated in Table II.

TABLE II

COMPARISON OF THE RELATIVE CONTRIBUTIONS OF DIFFERENT FORCES TO THE LATTICE ENERGY, {100} SURFACE ENERGY, AND <100> EDGE ENERGY OF SODIUM CHLORIDE

	Lattice energy, kcal. mol.$^{-1}$	{100} surface energy, erg cm.$^{-2}$	<100> edge energy, 10^{-6} erg cm.$^{-1}$
Electrostatic	207.2	345.6	3.212
Dipole–dipole	5.7	79.6	−0.756
Dipole–quadrupole	0.7	8.6	−0.047
Repulsive	−29.0	−245.3	0.441
Zero point	− 1.7		
Total	183	189	2.85
% Contribution of van der Waals terms	3.5	46	28

Born and Stern give two alternate formulae; one in terms of lattice parameter, the other in terms of density. The numerical factor in the latter is incorrect. The values of the edge energy which Lennard-Jones and Taylor attribute to Born and Stern are calculated from this erroneous equation. It should also be noted that in computing the last two lines of Table I, experimentally determined interionic distances were used, which differ slightly from Shuttleworth's values of a_0. The effect of this difference on the edge energy is slight.

Finally, it should be noted that along with previous authors it has been assumed inherently in the derivation of equation [11] that the ions of the newly formed edge are unpolarized and remain fixed at the regular lattice sites. The problem of calculating the equilibrium configuration of the ions near a crystal edge is a very difficult one and is complicated by the fact that as yet no really comprehensive treatment has been given for the distortion at the surface of the crystal. Some calculations by Molière, Rathje, and Stranski (10) indicate a tendency for ion pair formation in the crystal surfaces and edges of some alkali halides. However Patterson (11) has shown that these configurations in the surface are unstable when the effect of van der Waals forces is considered. Since polarization and distortion effects undoubtedly occur in the vicinity of the edges of real crystals, the values in Table I must be considered as first approximations to the edge energy.

REFERENCES

1. Benson, G. C. and Benson, G. W. Can. J. Chem. 33: 232. 1955.
2. Benson, G. C. and Schreiber, H. P. Can. J. Phys. 33: 529. 1955.
3. Born, M. and Stern, O. Sitzber. preuss. Akad. Wiss. Physik.-math. Kl. 48: 901. 1919.
4. van der Hoff, B. M. E. and Benson, G. C. Can. J. Phys. 31: 1087. 1953.
5. Huggins, M. L. and Mayer, J. E. J. Chem. Phys. 1: 643. 1933.
6. Jura, G. and Garland, C. W. J. Am. Chem. Soc. 74: 6033. 1952.
7. Lennard-Jones, J. E. and Taylor, P. A. Proc. Roy. Soc. (London), A, 109: 476. 1925.
8. Lipsett, S. G., Johnson, F. M. G., and Maass, O. J. Am. Chem. Soc. 49: 925. 1927.
9. Mayer, J. E. J. Chem. Phys. 1: 270. 1933.
10. Molière, K., Rathje, W., and Stranski, I. N. Discussions Faraday Soc. No. 5: 21. 1949.
11. Patterson, D. Trans. Faraday Soc. 48: 877. 1952.
12. Seitz, F. Modern theory of solids. McGraw-Hill Book Company, Inc., New York. 1940. Chap. 2.
13. Shuttleworth, R. Proc. Phys. Soc. (London), A, 62: 167. 1949.
14. Stranski, I. N. Z. Krist. 105: 287. 1944.

THE FISSION YIELDS OF ISOTOPES OF XENON AND KRYPTON IN THE NEUTRON FISSION OF U^{235} AND U^{238} [1]

By R. K. Wanless and H. G. Thode

ABSTRACT

Several uranium samples have been irradiated under various conditions in the Chalk River N.R.X. reactor and in the Los Alamos fast reactor. The fission gases, xenon and krypton, have been extracted from the irradiated material and the relative isotopic abundances determined mass spectrometrically. Fine structure in the mass – fission yield curve has been found in both the xenon and krypton mass ranges for $U^{235} + n$ and $U^{238} + n$ fission. It is observed that this fine structure shifts to lower masses, as predicted, for neutron fission of U^{238}. The proportions of U^{235} and U^{238} fission that have occurred in the irradiated samples have been estimated from the percentage change in fine structure.

INTRODUCTION

Early mass spectrometric determinations of the relative fission yields of the stable and long-lived isotopes of krypton and xenon (10, 13), produced in the thermal neutron fission of U^{235}, established the fact that the yields of Xe^{132} and Xe^{134} fell considerably above the smooth curve drawn through the adjacent xenon isotope yields. Glendenin (6) has postulated a chain branching mechanism to explain this "fine structure" in the fission yield curve. He suggested that primary fission fragments formed with 51 and 83 neutrons (one neutron in excess of a closed shell) would have sufficient excitation to emit the loosely bound 51st or 83rd neutron rather than achieve stability by undergoing β decay. This mechanism provided only a qualitative explanation of the observed yields in $U^{235} + n$ fission. Wiles *et al.* (15, 16) suggested that better quantitative agreement between predicted and observed yields could be obtained if a primary fission preference for nuclei with 82 neutrons was assumed in addition to the Glendenin chain branching mechanism.

Recently Pappas (11) has extended the "neutron boil-off" mechanism to include neutron emission by primary fission fragments with one, three, five, or seven neutrons in excess of a closed shell. By also taking into account a primary fission preference for 82-neutron nuclei, first suggested by Wiles, and tentatively assigning the 1.52-sec. delayed neutron activity to Sb^{135}, Pappas obtained a reasonably accurate quantitative explanation of the observed $U^{235} + n$ fission yields.

The "neutron boil-off" mechanism, as modified by Pappas, can be used to predict fine structure effects for other fissioning nuclei. The fission yields of the xenon and krypton isotopes in neutron fission of U^{238} are reported in this paper and compared with the yields predicted by Pappas.

In the earlier investigations of the relative yields of the xenon and krypton isotopes in $U^{235} + n$ fission, small variations in the abundances of the isotopes were often observed, depending on the irradiation conditions, position in nuclear reactor, etc., of the normal uranium samples. In particular, the high

[1]*Manuscript received May 9, 1955.*
Contribution from Hamilton College, McMaster University, Hamilton, Ontario.

yield at mass 134 was found to vary by a significant amount, the lowest yield being obtained when the samples were irradiated in regions of higher neutron flux, and greater neutron energies. Since the energy distribution of pile neutrons was such that some $U^{238} + n$ fission occurred, it was felt that the variation in the 134 mass yield found from sample to sample was due primarily to the different proportions of U^{238} and U^{235} neutron fission which had occurred. Although the mass–yield curve for U^{238} fission is known to parallel that for U^{235} fission fairly well in this mass range, the fine structure or abnormal yield at mass 134 was not expected to be the same for the two nuclei. In order to investigate these variations further and to obtain a satisfactory comparison between the relative fission yields for U^{235} and U^{238} fission, samples of natural uranium and samples of uranium depleted in U^{235} were irradiated in the thermal column of the N.R.X. pile and in the Los Alamos fast reactor respectively. The xenon and krypton gases extracted from these samples gave the isotope fission patterns for the strictly thermal neutron fission of U^{235} and for the fission of U^{238} (average neutron energy 0.5 Mev.).

Also in the course of this study, samples of natural uranium were irradiated under widely different conditions. For these samples, it was possible to estimate the proportion of U^{235} and U^{238} fission which had occurred by a comparison of the xenon isotope fission pattern of the natural uranium with those obtained for U^{235} (thermal neutrons) and U^{238} fission alone.

It is realized, of course, that the fission isotope patterns obtained for U^{235} will to some extent depend on the energy distribution of the neutrons during irradiation since symmetric fission increases as the energy of the neutrons increases from thermal energies to 14 Mev. (12). Also, fission yields will depend on neutron flux where nuclides with high neutron capture cross sections are involved. Therefore, any variations in yields due to these factors will be superimposed on effects due to varying proportions of U^{235} and U^{238} fission. Results indicate that although the varying proportions of U^{238} fission produce by far the greater effect on the fission yields in the xenon range, there is some indication that the distribution of fission products for U^{235} varies significantly as we go from a thermal distribution of neutrons to neutrons having an average energy of 0.5 Mev.

EXPERIMENTAL

(i) *Irradiation of Samples*

In order to more fully investigate the small variations in fission yields observed in the early work, old samples of fission product xenon and krypton were repurified. These samples, from uranium irradiated under widely differing conditions, were carefully compared by analyzing each sample on the mass spectrometer under identical operating conditions.

The irradiation data for the new samples used in this work are summarized in Table I. Irradiation 1 was normal uranium metal irradiated in the thermal column of the N.R.X. reactor at Chalk River. In this position the neutron energy distribution should be entirely thermal and hence no U^{238} fission would be expected. Irradiation 2 was normal uranium metal sheathed in cadmium

TABLE I

IRRADIATION DATA

Irradiation number	Description	Reactor	Approximate neutron flux,* n./cm.²/sec.	Approximate integrated neutron flux, n./cm.²
1	Normal uranium metal	N.R.X., Chalk River	5.0×10^{10} (thermal column)	2.9×10^{17}
2	Normal uranium metal sheathed in cadmium	N.R.X., Chalk River	1.5×10^{13}	1.5×10^{19}
3	Normal uranium metal	Fast reactor, Los Alamos	1.0×10^{12}	5.6×10^{18}
4	UO_3 depleted in U^{235}	Fast reactor, Los Alamos	1.0×10^{12}	1.7×10^{19}

**Flux values for the Chalk River irradiations are the estimated thermal neutron fluxes. Los Alamos irradiations were carried out in a fast neutron flux with average energy of 0.5 Mev.*

1/16 in. thick and irradiated in a high flux position in the N.R.X. reactor. Since cadmium absorbs most thermal neutrons and since there is an appreciable fraction of high energy neutrons at this irradiation position, considerable U^{238} fission would be expected in this sample. Irradiation 3 was normal uranium metal irradiated in the fast reactor at Los Alamos where the number of thermal neutrons is negligible. This sample should therefore show even more U^{238} fission than sample 2. Irradiation 4 was UO_3 depleted 30 to 50 times in U^{235} and was irradiated in the Los Alamos fast reactor. This sample should contain a negligible contribution of U^{235} fission. Duplicate samples were irradiated in each case to provide checks on the extraction, purification, and mass spectrometer analysis of the rare gas fission products.

(ii) *Preparation of Rare Gas Samples*

The apparatus used in this laboratory for the extraction and purification of fission product gases from irradiated uranium metal has been described by Arrol, Chackett, and Epstein (1). The method consists of dissolving the uranium in a saturated solution of cupric potassium chloride, drying the released gases with solid potassium hydroxide and magnesium perchlorate, and finally, purifying with calcium vapor. This procedure was followed exactly for samples 1, 2, and 3. In the case of sample 4 a slight modification was required since this sample was in the form of finely powdered UO_3. The UO_3 was dissolved in concentrated sulphuric acid rather than the cupric potassium chloride solution used for the uranium metal samples. The subsequent handling of the released gases was the same as described in Reference (1).

(iii) *Mass Spectrometry*

All gas samples were analyzed on a 180° direction focusing mass spectrometer. Magnetic scanning was employed throughout to focus ions of 1500 v. energy. An Applied Physics Corporation vibrating reed electrometer was used to amplify the ion currents which were recorded on a Leeds and Northrup Speedomax strip chart recorder. Typical isotope patterns of fission product krypton and xenon are shown in Figs. 1 and 2 respectively. At least 10 double spectrograms were recorded and averaged for each analysis.

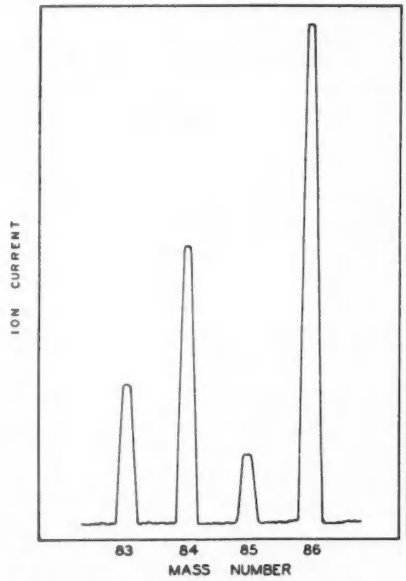

FIG. 1. Mass spectrogram of fission product krypton.

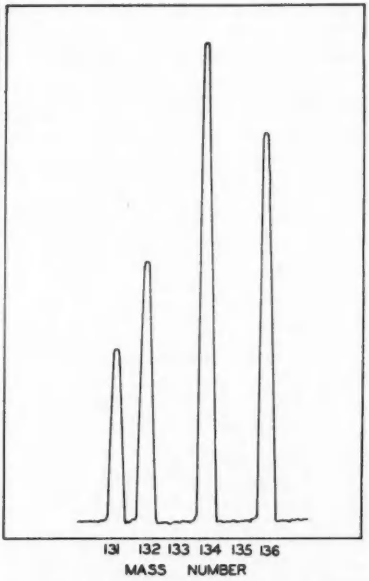

FIG. 2. Mass spectrogram of fission product xenon.

Care was taken to ensure that there were no residuals in the mass spectrometer before samples were admitted, and each sample was checked for impurities in the neighborhood of the krypton and xenon mass ranges. To remove any condensable impurities that might have been present in the samples a liquid air trap was employed between the sample input line and the mass spectrometer. The isotope ratios obtained for the xenon and krypton isotopes were reproducible to better than $\pm 0.5\%$.

RESULTS AND DISCUSSION

(i) *Xenon Isotope Fission Yields*

The mass spectrometer measurements of fission product isotope abundances only give relative fission yields for the isotopes of the element being studied. These yields must be normalized in some manner before they can be compared with yield data for other elements or with yields for the same element for a different fissioning nucleus. We have assigned the value 3.00%* to the fission yield of Xe^{131} in $U^{235} + n$ fission (thermal column irradiations).

The fission yield data for the old fission product samples which were reanalyzed are given in Table II (normalized at 3.00% for Xe^{131}). The approxi-

*Recently reported independent determinations of the yield of the 131 mass chain are: Katcoff and Rubinson—2.97% based on an absolute determination of the yield of Xe^{133} (8) and the relative yields of Xe^{133} and Xe^{131} reported by Macnamara et al. (10), and Wiles et al. (16). Yaffe et al.—3.21% based on an absolute determination of the yield of Ba^{140} (17) and on the relative yields of Ba^{140} and I^{131} (2).

TABLE II

FISSION YIELDS OF XENON ISOTOPES UNDER DIFFERING IRRADIATION CONDITIONS

Sample	Approximate neutron flux, n./cm.²/sec.	Approximate integrated neutron flux, n./cm.²	% Fission yield			
			Xe^{131}	Xe^{132}	Xe^{134}	Xe^{136*}
A	5.0×10^{12}	2.0×10^{18}	3.00†	4.47	8.19	7.96
B	6.0×10^{12}	4.3×10^{17}	3.00	4.49	8.09	7.25
C	3.6×10^{12}	4.6×10^{17}	3.00	4.50	8.19	7.19
D	3.0×10^{12}	9.1×10^{18}	3.00	4.56	8.33	7.42
E	2.6×10^{12}	3.2×10^{17}	3.00	4.50	8.25	7.47
F	2.6×10^{12}	1.1×10^{17}	3.00	4.50	8.12	7.06
G	2.1×10^{12}	4.3×10^{17}	3.00	4.49	8.16	7.08
H	1.8×10^{12}	4.4×10^{17}	3.00	4.52	8.26	7.35
I	7.5×10^{11}	4.5×10^{18}	3.00	4.51	8.22	7.14
J‡	6.0×10^{11}	8.3×10^{17}	3.00	4.50	8.17	6.99
K‡	6.0×10^{11}	8.3×10^{17}	3.00	4.49	8.05	6.88

**The yields of Xe^{136} have not been corrected for neutron capture in Xe^{135}.*

†Normalization point.

‡Samples J and K were irradiated at Oak Ridge. The remaining samples were irradiated in the N.R.X. reactor at Chalk River in different positions.

mate neutron fluxes at which these samples were irradiated are also shown. The large variation in the yield of Xe^{136} in these samples is the result of varying amounts of neutron capture in Xe^{135}. (The amount of capture is dependent on the length of irradiation as well as the neutron flux.) As can be seen from Table II, there are smaller, but still significant, variations in the yields of Xe^{134} and some indication of variations in the yields of Xe^{132}. These latter two effects are not the result of any known or suspected neutron capture process. Since some of these samples were irradiated in positions in which a fairly high flux of fast neutrons is present, the variations in the yield of Xe^{134} (and Xe^{132} if there is a real effect at this mass) may be due to a considerable contribution of $U^{238} + n$ fission in some of the samples.

The fission product isotope abundance data for the new irradiations are given in Table III. The deviations shown in this table are the "standard deviations" of the mass spectrometer measurements. As stated previously, irradiation 1 should represent 100% $U^{235} + n$ fission and irradiation 4 100% $U^{238} + n$ fission. Irradiations 2 and 3 were carried out under conditions in which appreciable contributions of both U^{235} and U^{238} fission would be expected with the larger contribution of U^{238} fission expected in irradiation 3. It can be seen from Table III that an increase in the amount of U^{238} fission results mainly in a decrease in the relative yield of Xe^{134} accompanied by an increase in the relative yields of Xe^{131} and Xe^{132}. In all these later irradiations variations in the Xe^{136} yield due to neutron capture in Xe^{135} are small because of the low flux of thermal neutrons. The Xe^{136} yield correction for this process is 0.7% for the thermal column irradiation and negligible in other cases. The Xe^{136} yield data in Table III for the different irradiations are therefore comparable and free from neutron capture effects.

To obtain a comparison between the results of the new irradiations and the data given in Table II, the yield data for the four new irradiations have been

TABLE III

MASS SPECTROMETER ABUNDANCES OF FISSION PRODUCT XENON

Irradiation	Sample		Atom per cent			
			Xe^{131}	Xe^{132}	Xe^{134}	Xe^{136*}
1	Thermal column	1	13.43±.05	20.10±.05	36.78±.04	29.69±.08
		2	13.41±.04	20.03±.05	36.81±.05	29.75±.07
		3	13.34±.13	19.98±.13	36.89±.14	29.79±.20
		Average	13.39	20.04	36.83	29.74
2	Cd shielded	(1)	13.67±.07	20.67±.07	36.21±.08	29.45±.06
		(2)	13.71±.03	20.36±.04	36.14±.07	29.79±.06
		Average	13.69	20.51	36.18	29.62
3	Los Alamos Normal U	#1	13.72±.08	21.81±.09	34.25±.09	30.22±.09
		#2	13.72±.06	21.74±.05	34.20±.05	30.34±.05
		Average	13.72	21.77	34.23	30.28
4	Depleted UO_3	#1	15.39±.14	22.96±.12	32.71±.18	28.94±.09
		#2	16.06±.11	23.15±.13	32.16±.09	28.63±.13
		Average	15.72	23.05	32.44	28.79

**The Xe^{136} yield for the thermal column samples should be decreased by 0.7% to correct for neutron capture in Xe^{135}. This correction should be negligible for the other samples.*

TABLE IV

FISSION PRODUCT XENON ABUNDANCE DATA NORMALIZED AT MASS 131

Irradiation	Sample	Relative abundance			
		Xe^{131}	Xe^{132}	Xe^{134}	Xe^{136}
1	Thermal column (U^{235} fission)	3.00	4.49	8.25	6.62*
2	Cadmium shielded normal uranium	3.00	4.49	7.93	6.49
3	Los Alamos normal uranium	3.00	4.76	7.48	6.84
4	Los Alamos depleted uranium (U^{238} fission)	3.00	4.40	6.19	5.49

**The yield of Xe^{136} in the thermal column sample has been corrected for neutron capture in Xe^{135}.*

normalized to 3.00 at mass 131 in Table IV. It is obvious that the results for the 11 samples in Table II resemble very closely those for the thermal column irradiations, indicating that the amount of U^{238} fission in the former samples is not large.

The data in Table IV should not be interpreted as an indication that the absolute fission yield of Xe^{131} is 3.00% in both U^{235} and U^{238} fission. No highly accurate radiochemical yield measurements have been reported for neutron fission of U^{238} in the xenon mass range.* Therefore it is not possible to normalize the relative xenon fission yield data obtained for U^{238} fission (depleted uranium

**Keller, Steinberg, and Glendenin have recently reported a yield of 4.7±0.7% for Te^{132} (9).*

irradiations). Although a comparison of the actual yields of the xenon isotopes in the U^{235} and U^{238} fission samples is not possible, several conclusions can be drawn from the relative yield data.

The fission product xenon abundance data for the new irradiations are plotted in Fig. 3. The right-hand ordinate scale in this figure gives the fission yields for the thermal column irradiations (U^{235} fission). The curve in Fig. 3

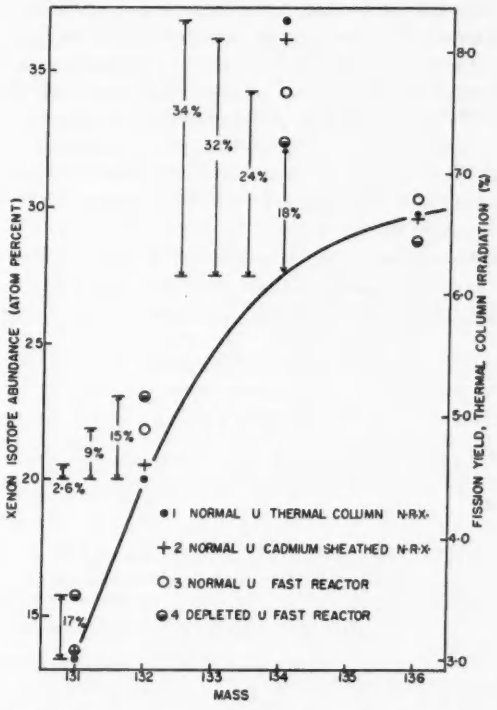

FIG. 3. Fission product xenon isotope abundance variations.

indicates the approximate position of the smooth radiochemical fission yield curve for U^{235} fission (4). Since radiochemical studies (4) indicate that the smooth yield curve for U^{238} fission parallels that for U^{235} fission in the xenon mass range, the curve in Fig. 3 should also represent the position of the U^{238} smooth curve compared to the experimental points for the Los Alamos depleted uranium irradiation. Therefore, when the relative yields of the xenon isotopes are plotted as atom per cent in Fig. 3, it is possible to measure the magnitude of fine structure effects from one smooth curve. In this manner the variation of fine structure can be studied without the necessity of knowing absolute fission yield data for the different irradiations.

The amount of fine structure (i.e. the percentage increase of the observed

yield over the smooth curve value) observed in each of the four different irradiations is indicated on Fig. 3. It is obvious that the fine structure at mass 134 decreases in going from U^{235} to U^{238} fission (thermal column irradiation to Los Alamos depleted uranium irradiation). At the same time, fine structure appears at masses 132 and 131 in U^{238} fission which was not evident in U^{235} fission.

In order to interpret the results of the cadmium sheathed and Los Alamos normal uranium irradiations, it was first assumed that these samples contained contributions of both U^{235} fission xenon (with the abundances observed for the thermal column irradiations) and U^{238} fission xenon (with the abundances observed for irradiation number 4). This assumption, of course, will only be completely valid if the relative yields of the xenon isotopes in $U^{235} + n$ fission do not change when the neutron energy is altered. With this assumption it is possible to calculate the contribution of fission xenon from U^{238} fission in irradiations 2 and 3 as follows:

Let Y_m^{235} = observed abundance mass m in U^{235} fission (irradiation 1),

Y_m^{238} = observed abundance mass m in U^{238} fission (irradiation 4),

Y_m^{x} = observed abundance mass m in irradiation 2 or 3.

If a is the fractional contribution of xenon from U^{238} fission in irradiation 2 or 3, then

$$Y_m^{x} = (1-a)\,Y_m^{235} + a\,Y_m^{238}.$$

The values of a found by substituting the abundance values from Table III in this equation are given in Table V. The contributions of xenon from U^{238}

TABLE V

CALCULATED CONTRIBUTION OF XENON FROM U^{238} FISSION TO THE OBSERVED ABUNDANCES IN IRRADIATIONS 2 AND 3

Calculated from mass	Fractional contribution of xenon from U^{238} fission	
	Irradiation 2	Irradiation 3
131	.13	.14
132	.16	.58
134	.15	.59
136	.13	−.57
	Average .14	

fission calculated from the different xenon isotope abundances for irradiation 2 agree very well. The calculations indicate that for the cadmium sheathed irradiation 14% of the fission product xenon resulted from U^{238} fission. However, the calculated U^{238} fission contributions for irradiation 3 from the different xenon isotope abundances do not agree with each other. This disagreement is almost certainly due to the fact that the U^{235} fission yields at high neutron energies are not the same as those observed with thermal neutrons.

The samples for irradiation number 2 were normal uranium sheathed in cadmium and were irradiated in the N.R.X. reactor at Chalk River. The

cadmium sheath on these samples would absorb all thermal neutrons but the absorption of neutrons with energies greater than ~ 1 ev. would be small. Since there is a considerable epithermal neutron flux at the position in the N.R.X. reactor at which these samples were irradiated in addition to the flux of fast "fission spectrum" neutrons, the majority of the U^{235} fission in these samples would be produced by epithermal neutrons and not by the fast neutrons. Therefore the effective neutron energy for the U^{235} fission contribution in irradiation 2 was probably not very high. For this reason the U^{235} fission contribution in irradiation 2 would be expected to produce fission xenon with essentially the same isotope abundance as observed in thermal neutron fission of U^{235}. In this case, therefore, the assumption made in calculating the U^{238} fission contribution is valid and the good agreement shown in Table V, column 2, would be expected.

The samples used in irradiation 3 were normal uranium and were irradiated in the fast reactor at Los Alamos. In this reactor the neutron energy distribution is essentially the fission neutron spectrum and therefore the U^{235} fission in these samples will be produced by high energy neutrons. Therefore the assumption made in calculating the U^{238} fission contribution for this irradiation (Table V, column 3) will not be valid unless the U^{235} fission yields do not change with relatively large changes in neutron energy. Since it is known (12) that the fission yields do vary when the neutron energy is changed by a large amount, the disagreement in Table V, column 3, is not surprising.

There is good agreement between the calculated U^{238} fission contributions for irradiation 3 at masses 132 and 134. Also the difference between the U^{235} and U^{238} yields is greatest at mass 134, and thus less likely to be greatly altered by neutron energy changes. For these reasons, it is reasonable to assume that the contribution of fission xenon from U^{238} fission is about 59% for irradiation 3 and that the discrepancies at mass 131 and 136 in Table V, column 3, are the result of the variation with neutron energy of the xenon yields from U^{235} fission.

It should be noted that the 14% and 59% contributions of fission xenon from U^{238} fission in irradiations 2 and 3 respectively do not necessarily indicate that U^{238} fission accounted for 14% and 59% of the fission in these samples. The latter is only true if the absolute fission yield of the stable xenon isotopes is the same in both U^{235} and U^{238} fission. Actually radiochemical yield studies (4) indicate that the smooth yield curves for U^{235} and U^{238} fission are quite close together in the mass range 131–136. Therefore the total yield of xenon in each type of fission is probably nearly the same. On this basis it can be said that for the cadmium sheathed irradiation approximately 15% of the fission was $U^{238} + n$ fission. The corresponding figure for the normal uranium irradiated at Los Alamos is about 60%. Furthermore it can be seen from Fig. 3 that, if the total yield of xenon is the same for U^{235} and U^{238} fission, the fission yield of Xe^{131} in U^{238} fission (depleted uranium irradiation 4) is approximately 3.50% compared to 3.00% for the same isotope in U^{235} fission.

The "neutron boil-off" mechanism suggested by Glendenin and elaborated by Pappas to explain the fine structure observed in $U^{235} + n$ fission would predict a higher yield at mass 131 and 132 in U^{238} fission than in U^{235} fission. This

is in agreement with the results given in Table III. A quantitative comparison between the predicted and experimental yields is given in Table VI where the

TABLE VI

PREDICTED AND OBSERVED FINE STRUCTURE EFFECTS IN XENON FISSION YIELDS

Mass	U^{235}		U^{238}	
	Predicted	Observed	Predicted	Observed
131	3.00*	3.00*	3.50*	3.50*
132	4.65	4.49	5.10	5.04
134	7.74	8.21	7.31	7.01
136	6.50	6.48	6.63	6.24

**Normalization point.*

predicted yields have been calculated following the method adopted by Pappas (11). In this table the U^{238} results have been arbitrarily normalized at 3.50% for Xe^{131}. It can be seen that the quantitative agreement is quite good. However, it should be noted that the predicted fine structure is too low for U^{235} fission and too high for U^{238} fission. Recently (5) it has been found that the discrepancy between the predicted and experimental yields is much larger in the case of U^{233} fission. This indicates that while the mechanism developed by Pappas offers a reasonably accurate explanation of the observed fine structure in the xenon range in U^{235} and U^{238} fission (Table VI), it must be further modified before it will completely explain all available experimental data.

(ii) *Krypton Isotope Fission Yields*

Table VII contains the krypton isotope abundance data for the irradiations listed in Table I. In normalizing the krypton results a value of 5.05 was

TABLE VII

MASS SPECTROMETER ABUNDANCES OF FISSION PRODUCT KRYPTON

Irradiation	Sample		Atom per cent			
			Kr^{83}	Kr^{84}	Kr^{85*}	Kr^{86}
1	Thermal column	1	14.16±.06	26.32±.13	7.50±.05	52.02±.13
		2	14.07±.06	26.10±.14	7.55±.06	52.28±.07
		3	14.07±.07	25.38±.14	7.72±.15	52.83±.25
		Average	14.10	25.93	7.59	52.38
2	Cd sheathed	(1)	14.22±.01	27.09±.05	7.31±.06	51.38±.09
		(2)	14.04±.13	26.77±.07	7.67±.09	51.52±.16
		Average	14.13	26.93	7.49	51.45
3	Los Alamos Normal uranium	#1	15.08±.30	28.52±.11	6.93±.20	49.47±.28
		#2	14.85±.38	27.62±.42	6.56±.24	50.97±.42
		Average	14.97	28.07	6.74	50.22
4	Depleted UO_3	#2	14.50±.60	30.50±1.40	5.50±.50	49.50±1.10

**Kr^{85} corrected assuming $T_{\frac{1}{2}} = 10.27$ years.*

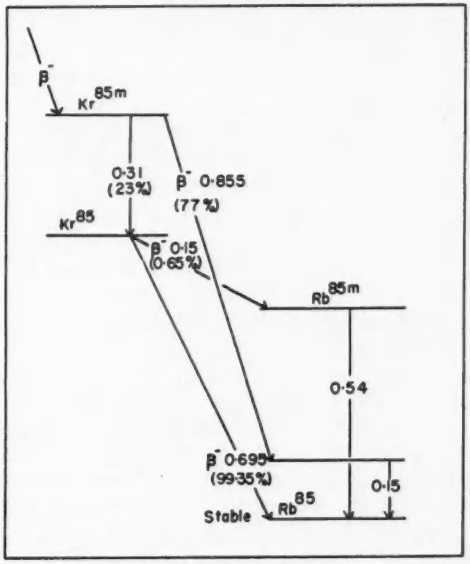

FIG. 4. Kr^{85} decay scheme (7).

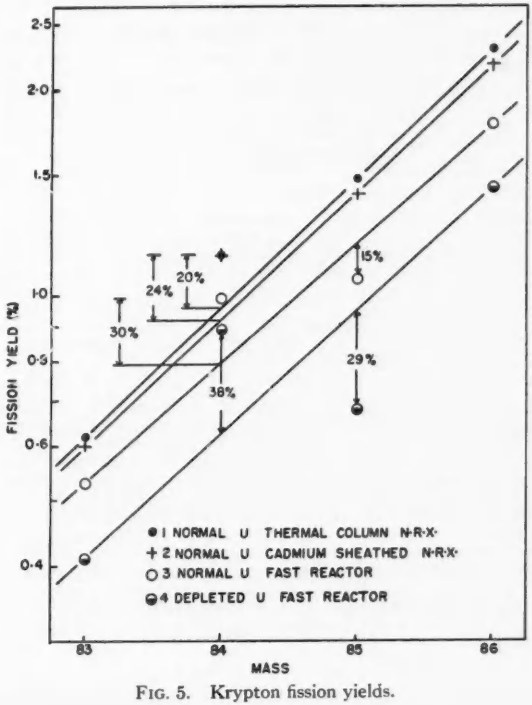

FIG. 5. Krypton fission yields.

employed for the ratio of fission product xenon to fission product krypton in U^{235} fission (1). Since there is a discrepancy between reported values of this ratio (1, 13), a precise determination is at present under way in this laboratory. The normalization employed however will not alter the conclusions drawn here.

The krypton isotope abundances for irradiation 1 ($U^{235} + n$ fission) have been normalized at 0.62% for mass 83. The krypton isotope at mass 85 has two isomeric states (Fig. 4), a long-lived one with a half-life of 10.27 years (14) and a short-lived one with a 4.4-hour half-life (7). Since the shorter-lived isomer will have completely decayed before the fission gases were extracted from the uranium samples, the mass spectrometer results will indicate only the yield of the 10.27-year isomer. All Kr^{85} yields have been corrected for the decay of the long-lived isomer up to the time of analysis. In order to compare the fission yields at this mass, the Kr^{85} yield for irradiation 1 has been arbitrarily placed on the smooth curve (see Fig. 5) and the yields for the other samples have been increased proportionately. This corresponds to a branching ratio for the decay of Kr^{85} of 0.29. The value of this branching ratio measured directly from β decay data is 0.28 (3). The assumption that the mass 85 yield falls on the smooth curve for U^{235} fission (sample 1) would therefore appear to be justified. The 85 mass chain yields for the other samples have been adjusted assuming that the branching ratio remains constant as the fissioning nucleus is changed from U^{235} to U^{238}. This latter procedure is justified since, on the basis of Glendenin's charge distribution theory, the primary yield of Kr^{85} and Kr^{85m} is negligible in both cases (6).

There is a decided shift of the light mass peak of the fission yield curve between U^{235} and U^{238} fission (4). In Fig. 5 the depleted UO_3 yields (irradiation 4) have been displaced at mass 86 by 0.86% (see Table VIII) to correspond to the above-mentioned shift. The Los Alamos normal uranium results (irradiation 3) have been adjusted at mass 86 in accordance with a 60%

TABLE VIII

KRYPTON FISSION YIELDS

Irradiation	Sample	% Fission yield			
		Kr^{83}	Kr^{84}	Kr^{85*}	Kr^{86}
1	Thermal column	0.62	1.14	1.48	2.30
2	Cd sheathed	0.60	1.14	1.41	2.18
3	Los Alamos normal uranium	0.53	0.99	1.06	1.78
4	Los Alamos depleted uranium	0.42	0.89	0.68	1.44

**The mass 85 chain has been corrected for the decay of the 4.4-hour isomer of Kr^{85} by arbitrarily placing the mass 85 yield on the smooth mass–yield curve for sample 1 ($U^{235} + n$ fission). This corresponds to a branching ratio for the decay of Kr^{85} of 0.29. The value of this branching ratio measured directly from β decay data is 0.28 (3). The assumption that the mass 85 yield falls on the smooth curve for U^{235} fission (sample 1) would therefore appear to be justified. The 85 mass chain yields for the other samples have been adjusted assuming that the branching ratio remains constant as the fissioning nucleus is changed from U^{235} to U^{238}. This latter procedure is justified since the primary yield of mass 85 is negligible in both cases.*

$U^{238} + n$ fission in this sample (as indicated from the xenon data). Finally, the cadmium sheathed results (irradiation 2) have been incorporated in Fig. 5 by adjusting the mass 86 yield to correspond to 15% $U^{238} + n$ fission as determined from the xenon results. It is now possible to draw four roughly parallel smooth curves from which the percentage variations may be calculated. Again if fine structure is defined as the percentage variation from the respective smooth curves, these results indicate large fine structure shifts at masses 84 and 85.

It will be noted that at mass 84 the fission yields are all higher than the corresponding smooth curve values while at mass 85 the opposite is found to be the case. The fine structure shift in going from $U^{235} + n$ fission to $U^{238} + n$ fission amounts to $38-20 = 18\%$ at mass 84 and 29% at mass 85 (see Fig. 5).

The fine structures determined for the Los Alamos normal uranium and the Chalk River cadmium sheathed irradiations, 3 and 2 respectively, fall in the intermediate range and indicate $10/18 = 56\%$ and $4/18 = 22\%$ $U^{238} + n$ fission respectively when calculated from the mass 84 fission yields. However, when calculated from the yield values at mass 85, the corresponding $U^{238} + n$ fission contributions indicated are 52% and 0%. The $U^{238} + n$ contribution indicated for the Los Alamos normal uranium sample is in good agreement with the value found in the xenon range (60%). In the case of the cadmium sheathed sample the 22% $U^{238} + n$ fission contribution indicated at mass 84 agrees with that found in the xenon range at mass 134, but does not agree at mass 85. This latter discrepancy may be due to the difficulty experienced in measuring the small peak recorded at mass 85 (see Fig. 1).

The occurrence of fine structure in the krypton mass range has now been definitely established for the first time. This fine structure changes in going from $U^{235} + n$ to $U^{238} + n$ fission. Specifically, the yield at mass 84 increases while the yield at mass 85 decreases for U^{238} fission compared to the values obtained for U^{235} thermal neutron fission. The fission yields predicted by the method of Pappas have been calculated and no agreement has been found with the experimentally determined yields.

Since the observed fine structure does not appear to be the result of a Glendenin type "neutron boil-off" from primary fission fragments with 51, 53, 55, and 57 neutrons, some other explanation must be found for the observed fine structure. It is suggested that a delayed neutron emitter in the 85 mass chain produces the observed fine structure at masses 84 and 85. The tentative assignment of such an activity to As^{85} (the actual neutron emission occurring after the β-decay of As^{85}) is possible on the basis of nuclear systematics. Since the cumulative yield of As^{85} would be expected to be higher for U^{238} fission than for U^{235} fission on the basis of Glendenin's charge distribution theory (6, 11), the fine structure resulting from delayed neutron emission by As^{85} would be more pronounced in U^{238} fission. This is in qualitative agreement* with the experimental results (Fig. 5).

**It has been shown that a reasonable quantitative explanation of the observed fine structure in the krypton region can be obtained not only for U^{235} and U^{238} fission but also for U^{233} and Pu^{239} fission and for the spontaneous fission of U^{238} by assigning the 0.43 sec. delayed neutron activity to As^{85} (W. H. Fleming, Ph.D. thesis, McMaster University, 1954).*

ACKNOWLEDGMENTS

This work has been made possible through the financial assistance of the National Research Council of Canada. The authors wish to thank Atomic Energy of Canada Limited both for financial aid and for arranging the irradiation of uranium samples at Chalk River and at United States Atomic Energy Commission Establishments. Also, we wish to thank W. H. Fleming for assistance with several analyses and in the preparation of the manuscript.

REFERENCES

1. ARROL, W. J., CHACKETT, K. F., and EPSTEIN, S. Can. J. Research, B, 27: 757. 1949.
2. BARTHOLOMEW, R. M., BROWN, F., HAWKINGS, R. C., MERRITT, W. F., and YAFFE, L. Can. J. Chem. 31: 120. 1953.
3. BERGSTROM, I. M. Siegbahn commemorative volume. Uppsala. 1951. p. 355.
4. CORYELL, C. D. and SUGARMAN, N. Radiochemical studies: the fission products. McGraw-Hill Book Company, Inc., New York. 1951.
5. FLEMING, W., TOMLINSON, R. H., and THODE, H. G. Can. J. Phys. 32: 522. 1954.
6. GLENDENIN, L. E. Mass. Inst. Technol. Nuclear Science Lab. Tech. Rept. No. 35. 1949.
7. HOLLANDER, J. M., PERLMAN, I., and SEABORG, G. T. Revs. Mod. Phys. 25: 469. 1953.
8. KATCOFF, S. and RUBINSON, W. Phys. Rev. 91: 1458. 1953.
9. KELLER, R. N., STEINBERG, E. P., and GLENDENIN, L. E. Phys. Rev. 94: 969. 1954.
10. MACNAMARA, J., COLLINS, C. B. and THODE, H. G. Phys. Rev. 78: 129. 1950.
11. PAPPAS, A. C. Mass. Inst. Technol. Nuclear Science Lab. Tech. Rept. No. 63. 1953.
12. SPENCE, R. W. Brookhaven Conf. Rept. BNL-C-9. 1949.
13. THODE, H. G. and GRAHAM, R. L. Can. J. Research, A, 25: 1. 1947.
14. WANLESS, R. K. and THODE, H. G. Can. J. Phys. 31: 517. 1953.
15. WILES, D. R. M. Sc. Thesis, McMaster University, Hamilton, Ont. 1950.
16. WILES, D. R., SMITH, B. W., HORSLEY, R., and THODE, H. G. Can. J. Phys. 31: 419. 1953.
17. YAFFE, L., THODE, H. G., MERRITT, W. F., HAWKINGS, R. C., BROWN, F., and BARTHOLOMEW, R. M. Can. J. Chem. 32: 1017. 1954.

THE PROTON COMPONENT OF COSMIC RAYS AT AIRCRAFT ALTITUDES[1]

By K. W. Ogilvie[2]

ABSTRACT

Experiments with a heavy particle selector installed in an aircraft show that the proton intensity in the energy range 230 to 480 Mev. has a variation with height which is exponential, with absorption length 128±10 gm./cm.^{2} The latitude effect between $\lambda = 40°$N. and $\lambda = 56°$N. is in general agreement with that found for fast (up to 5 Mev.) neutrons. Some information has been obtained on the variation of the average specific yield for primary energies below 5 Bev.

INTRODUCTION

The altitude and latitude dependence of the nucleonic component of the cosmic radiation have been studied (13) using neutron counters carried in aircraft. The present experiments supplement this work in the region between geomagnetic latitudes 56° and 40°, and between ground level and 25,000 ft., by using a 'heavy particle detector' that records the passage of protons of energy between 230 and 480 Mev.

APPARATUS

The apparatus, Fig. 1, consists of a Cerenkov counter of large area, 16 in. × 16 in., containing water, placed in a Geiger counter telescope. Passage of

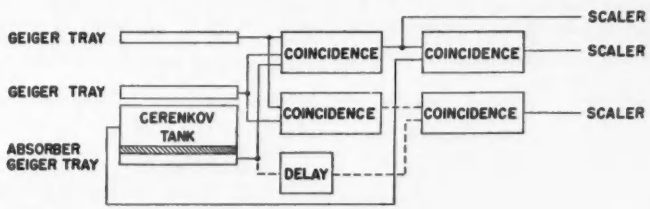

FIG. 1. Block diagram of apparatus. Anticoincidences between the outputs of the top two coincidence circuits denote heavy particles; anticoincidence circuit not shown.

a particle through the telescope, without a corresponding count in the Cerenkov counter, indicates that the particle was travelling at a velocity below the Cerenkov threshold. This quantity is $V_c = c/n$, where c is the velocity of light in free space and n is the refractive index of the substance used as the Cerenkov radiator. Deurden and Hyams (2) have shown that absorbers can be placed in the Geiger telescope in such a way that all the particles with mass less than a certain figure (μ mesons) that penetrate them are travelling faster than V_c, and that in this condition the apparatus counts particles with greater

[1]*Manuscript received June 17, 1955.*
Contribution from the Division of Pure Physics, National Research Council, Ottawa, Canada. Issued as N.R.C. No. 3707.
[2]*National Research Laboratories Postdoctorate Fellow.*

mass (protons) in an appropriate energy range, by means of recording anti-coincidences between the Geiger telescope and the Cerenkov counter. A relativistic particle must travel through the tank for a distance less than 20% of its depth to be recorded. A more complete description of the apparatus will be contained in a paper to be published shortly. With the present apparatus with an absorber of 3.7 cm. Pb, sensitivity to protons is obtained in the energy range 230 to 480 Mev., in which region the intensity at sea level is 3.03×10^{-5} particles/cm.^{2}/steradian/sec. (6).

RESULTS

The Altitude Dependence of the Intensity of Protons

The apparatus, mounted in two racks, was installed in a 'North Star' aircraft of the Central Experimental and Proving Establishment, R.C.A.F., Rockcliffe. The aircraft was then flown at 5000-ft. levels up to and including 25,000 ft. for periods ranging from three hours at 5000 ft. to one hour at 25,000 ft. Altitude was determined by the pilot's altimeter, which was set at 29.92 in. on the ground before each flight, and checked by a similar instrument mounted close to the apparatus. These altimeters are related to the N.A.C.A. standard atmosphere, which was used in the reduction from altitude to pressure in gm./cm.^{2} (7), and fluctuations in altitude were less than 100 ft. at 25,000 ft. The flights followed courses closely parallel to geographic latitude 45° 30′, which at this longitude is roughly parallel to geomagnetic latitude 57° and, in any case, is close to the knee of the latitude effect. The courses followed at the different levels during flight 1 are shown in Fig. 2. The results obtained for the 'heavy particle' rate are set out in Table I, and those for the 'hard component' in Table II.

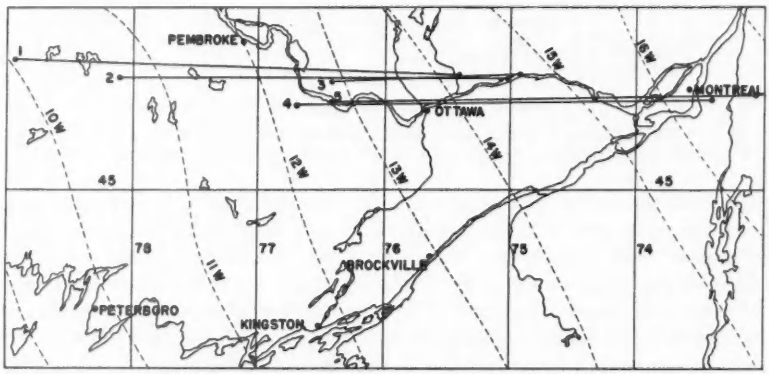

FIG. 2. Courses for constant altitude run 1.

Fig. 3 shows these data plotted on a semilog scale, together with the best-fit straight line for the data of Table I. This gives the value 128 ± 12 gm./cm.^{2} for the absorption length of the particles observed, which are to a good approxi-

TABLE I

VARIATION OF ANTICOINCIDENCE COUNTING RATE WITH ALTITUDE

Altitude, ft.	Flight and date				Weighted mean
	1 17/3/55	2 24/3/55	3 25/3/55	4 28/3/55	
25,000	8832±150			7500±200	8160±150
20,000	3800±100			3400±100	3600±70
15,000	2160±100		1500±80	2010±60	1890±60
10,000	576±20	546±20			560±20
5,000	272±20		175±12		194±15
Sea level					516±0.5

N.B.—All errors statistical.

TABLE II

VARIATION OF TRIPLE COINCIDENCE COUNTING RATE WITH ALTITUDE

Altitude, ft.	Flight and date				Mean
	1 17/3/55	2 24/3/55	3 25/3/55	4 28/3/55	
25,000	136800			137500	137200
20,000	90000			92700	91300
15,000	59400		54300	60500	58070
10,000	38900	38400			38650
5,000	26600		26500		26500
Sea level					19300

Examination of the records of the neutron recording pile at Ottawa for the period 9 to 31 March, 1955, disclose an intensity increase of 3½% on the 13 which had decayed to 1½% by the 17 March. Small fluctuations of the order of 1% persisted through the period of the experiments.

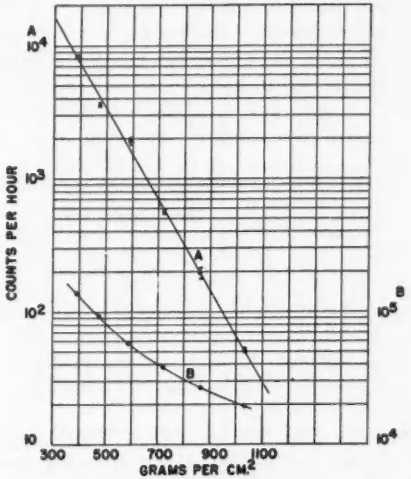

FIG. 3. A. Altitude variation of proton rate. B. Altitude variation of triple coincidence rate.

mation only protons. The good straight line obtained for the proton rate variation is inconsistent with a significant proportion of the anticoincidence counts being due to slow μ-mesons, taking into account the much smaller increase of the μ-meson rate with altitude. Some proton counts could be due to deuterons, since the altitude variation of the deuteron intensity is likely to be similar to that of protons, but the proportion is thought to be less than 10%. The lower mass limit of particles to which the apparatus is sensitive is approximately 550 electron masses, so that π-mesons cannot be detected.

As may be seen from Fig. 1, an accidental triple coincidence in the telescope will be recorded as a proton, if unaccompanied by a cancelling pulse from the Cerenkov counter. This point has been investigated in connection with other experiments with an identical apparatus at sea level. The total rate of triple coincidences is given by the expression

$$N_c = N+3N_1N_2N_3T^2+2N_{12}N_3T+2N_{13}N_2T+2N_{23}N_1T,$$

where N is the number of real triple coincidences, N_r the counting rate in the rth counter, and N_{rs} the actual coincidence rate between counters r and s. With the present value of the resolving time, $T = 2$ μsec., the contribution of the second term may be neglected; the last two terms involve the traversal of the tank by relativistic particles, and thus need not be considered. The third term then remains, and must however represent a large overestimate of the actual number of spurious protons. This is because many of the particles adding to the term $2N_{12}N_3T$, by their traversals of counter trays 2 and 3, also go through enough of the tank to be detected and give rise to a cancelling pulse. The term $2N_{12}N_3T$ was measured during the experiments, using the circuit shown dotted in Fig. 1, and remained throughout at about 10% of the total; no correction has been applied for this effect.

In order to convert the counting rates to absolute intensities it is necessary to evaluate the solid angle of the apparatus using the triple rate at sea level and the known hard component intensity. The values given in Table III have

TABLE III

PRESSURE VARIATIONS OF THE ABSOLUTE INTENSITIES (IN PARTICLES/CM.^{2}/SEC./STERADIAN)

Pressure	Proton intensity	Hard component intensity (7.6 cm.)	Hard component intensity (10.4 cm.) (9)
383	$508\pm10\times10^{-5}$	6.12×10^{-2}	5.2×10^{-2}
475	244 ± 5	4.07	3.8
583	117.5 ± 4	2.59	2.7
710	34.8 ± 1.2	1.72	1.8
860	10.2 ± 0.8	1.18	
1030	3.2 ± 0.3	0.86 (assumed)	

been obtained in this way, and have also been corrected for the loss of particles from the lower end of the energy interval due to the lengthening of the path through the absorber by scattering. This correction, amounting to 19 ± 5%, is evaluated in the following way. The lateral distribution about the pro-

jection on the lower counter tray of their point of entry to the absorber may be calculated for protons of various energies.

Assuming their paths to be initially vertical, there will be, for each energy, numbers of protons unable to penetrate the absorber, namely those for which the deflection due to scattering is greater than x, given by

$$x^2 = (0.907R)^2 - d^2,$$

where d is the absorber thickness, here 3.7 cm.

The factor $0.907 = T/R$ is given by Koenig (3), where T is the straight track in an absorber corresponding to an actual path of length R followed by the particle. At 270 Mev., for example, 40% of the protons will not penetrate to the lower counter, while at 320 Mev. only 6½% will fail to be recorded. In order to work out the correction the shape of the spectrum must be known, and it is by taking the spectrum of Mylroi and Wilson that we arrive at the value given above. It must be emphasized that the corrections affect the absolute values of the proton intensity only, and have an effect on the slope of the proton curve that is less than the experimental error. The values shown in column four of Table III were obtained by Neher in airplane flights at latitude 53° N. geomagnetic.

Discussion

Simpson (12) finds for the exponential absorption length of the neutron producing radiation in the atmosphere at geomagnetic latitude 53° the value

$$L = 153 \pm 2 \text{ gm./cm.}^2$$

The detector used by Simpson was a BF_3 proportional counter surrounded by paraffin, with a cadmium shield, and responded to neutrons with energies between 0.4 ev. and about 5 Mev. The atmospheric absorption of high energy 'N rays' is exponential with an absorption length of about 125 gm. cm.^{2} (10).

Our result, corresponding to a mean energy of about 400 Mev., because of the loss of low energy particles by scattering, agrees well with the latter value. Rossi (11), using the production spectrum of protons at 50 gm./cm.^{2} measured by Camerini *et al.* (1), finds the following expression for the intensity of protons of energy E at depth x gm./cm.^{2}

$$J^P(E, x) = \frac{Ae^{-x/L}}{K(E)} \frac{E_m - E}{(50+E_m)(50+E)},$$

where E is defined by the relation

$R(E_m) = R(E) + x$, $R(E)$ being the range of a proton of energy E.

Thus

$$\exp\left(\frac{-(x_2-x_1)}{L}\right) = \frac{J^P(E, x_1)}{J^P(E, x_2)}\left[\frac{E_{m_2}-E}{E_{m_1}-E}\frac{50+E_{m_1}}{50+E_{m_2}}\right].$$

Working out the bracketed expression, Y, with $E = 400$ Mev., and $x_2 = 1030$ gm./cm.^{2}, we arrive at the factors given in Table IV. The quantities in column three are plotted in Fig. 4 and yield a value of $L = 122 \pm 12$ gm./cm.^{2}

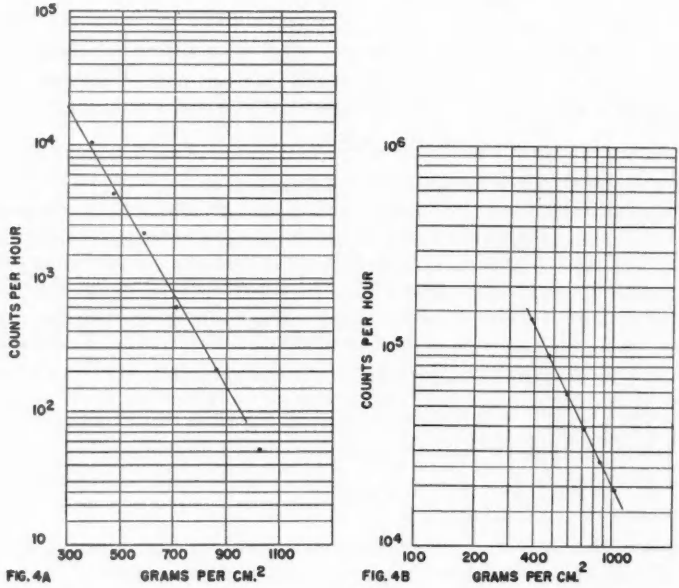

FIG. 4. A. Altitude variation of proton intensity. B. Altitude variation of triple coincidence rate.

TABLE IV

CORRECTED PROTON RATE

x, gm./cm.²	Y	$J^p(E, x_1)$
383	1.26	10280
475	1.18	4200
583	1.12	2140
710	1.07	600
860	1.03	200.5
1030	1.00	51.6

The Latitude Effect

A flight was undertaken by the same aircraft, carrying the same apparatus, from Ottawa along a line joining Ottawa to Nassau, and terminating at Miami. The results set out below in Table V show that this course follows longitude 76° W. which corresponds closely to a constant geomagnetic longitude. The altitude chosen was 20,000 ft. (= 475 gm./cm.²), a compromise between counting rate and convenience, as the aircraft employed was unpressurized. The reduction from geographic to geomagnetic latitude was made using the curves of McNish (5). The statistical errors are seen in Table V to be approximately ±2%, the counting intervals being approximately 25 min. in duration.

TABLE V

RESULTS OF LATITUDE VARIATION EXPERIMENT

Mean geographic position		Mean geomagnetic latitude	Counting rate of protons per hour	Triple coincidence rate per hour
Latitude	Longitude			
		Going south		
43° 50′ N.	76° 4′ W.	55° 30′	4180±80	90,500±400
42° 13′	76° 2′	53° 53′	4305±80	91,600±400
40° 15′	76° 9′	51° 55′	3980±80	90,400±400
38° 18′	76° 29′	49° 58′	3900±80	90,700±400
36° 7′	76° 40′	47° 47′	3690±80	88,300±400
34° 2′	76° 50′	45° 42′	3900±80	89,200±400
32° 12′	76° 44′	43° 52′	3520±80	86,500±400
30° 35′	76° 44′	42° 15′	3710±80	87,000±400
29° 6′	76° 50′	40° 46′	3140±80	83,000±400
27° 40′	76° 43′	39° 20′	2945±80	83,000±400
		Going north		
33° 42′	77° 0′	45° 22′	3790±80	87,000±400
36° 5′	76° 45′	47° 45′	3940±80	88,400±400
37° 20′	76° 30′	49° 0′	4000±80	88,400±400
40° 9′	76° 28′	51° 49′	4160±80	—
42° 5′	76° 20′	53° 45′	4340±80	89,500±400
44° 14′	75° 57′	55° 54′	4470±80	89,500±400

The aircraft position was obtained at frequent intervals, and the mean counting rate for each counting interval plotted at the position corresponding to the center of that interval.

We must now consider the possible influence of the longitude effect. In the region of longitude 95°–110° W., and at geomagnetic latitude 41°, $[\partial I/\partial\phi]_\lambda = -1\%$ per degree (12), at atmospheric depth 448 gm./cm.², for neutrons. Reference to the table shows that error due to longitude variation during the flight is less than the statistical errors. We can compare the slope of the curves and the magnitude of the effects for neutrons and protons, but not the intensities, by assuming that the variation of the longitude effect with latitude is the same in the region of longitude 76° W. as in the region of 116° W. In Fig. 5 our results are plotted together with those of Simpson (12), curve B, for fast neutrons at 448 gm./cm.² (23,000 ft.) and longitude 116° W. Correspondence is close, but our results suggest a knee at higher latitudes than the neutron results. The accuracy is hardly high enough to settle this, however. Table V also contains details of the triple coincidence rates recorded at the same time as the proton counts. These are plotted in Fig. 6. A knee can be observed in this curve at $\lambda = 53°$, and the observed intensity difference found between $\lambda = 54°$ and $\lambda = 39°$ is 8.3±2%. The total absorber in the telescope was 3.7 cm. of lead, 20 cm. of water, and the counter walls.

The Average Specific Yield

Below about 200 gm./cm.² in the atmosphere, protons in our present energy range observed at depth x gm./cm.² are produced close to this depth. Thus a measurement of the vertical proton flux amounts to a measurement of the proton production rate at the same depth. The total production rate at depth x

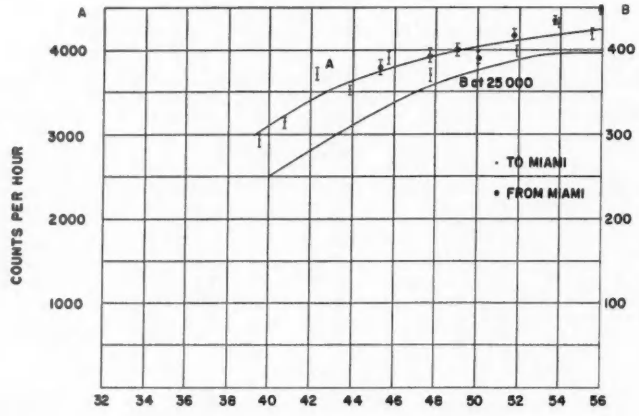

FIG. 5.

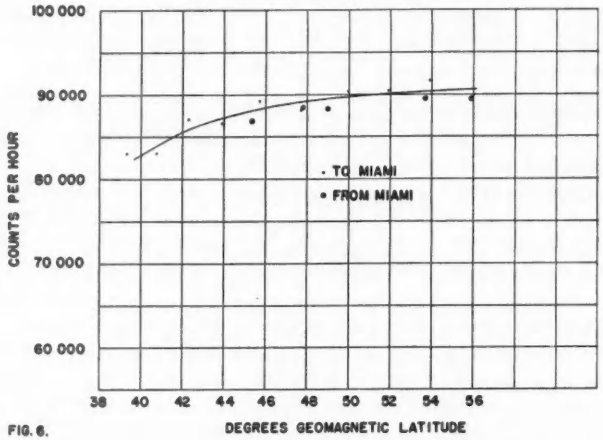

FIG. 6.

FIG. 5. A. Latitude variation of proton intensity. B. Neutron curve due to Simpson.
FIG. 6. Latitude variation of triple coincidence rate.

and latitude λ, due to primaries arriving into unit solid angle in a vertical direction, is given, (14), by the expression

$$R_s(\lambda, x) = -\int_{N_T(\lambda)}^{\infty} \sum_A S_A(N, x)\, f_A(N)[dF_T/dN]\, dN,$$

where dF_T/dN is the total differential flux of primary particles per unit solid angle having momentum to charge ratio equal to N, $f_A(N)$ is the fraction of primaries having atomic weight A, and $S_A(N, x)$ is the specific yield. This latter quantity is, in our case, the production rate of protons in our energy range, due to a unit vertical flux of primary particles of atomic weight A and

momentum to charge ratio N. The average specific yield is then given by the relation

$$S(N, x) = \sum_A S_A(N, x) f_A(N)$$

so that

$$S(N, x) = dR_v(\lambda, x)/dF_T(N).$$

The quantity R_v may be equated to the counting rate of our apparatus, corrected to absolute intensity. The latter procedure entails errors of less than 20%, and the Gross transformation need not be applied to our results, contrary to the procedure adopted by Treiman (14), since a telescope is used here. In the case of exponential variation of the counting rate with altitude, the Gross transformation reduces to multiplication by a factor $[1+x/L]/2\pi$, where L is a function of λ. Between 55° and 20° latitude, L varies from 125 to 135 gm./cm.^{2} (4). We can obtain the vertical cutoff values of momentum to charge ratio, $N(\lambda)$, for the values of λ at which our observations were made, from the results of Neher (8), and the corresponding quantities $F_T(N)$ from the spectrum of Winckler (15). Following Treiman, we plot the vertical proton production rate at 475 gm./cm.^{2} against the vertical primary flux, Fig. 7. On differentiating

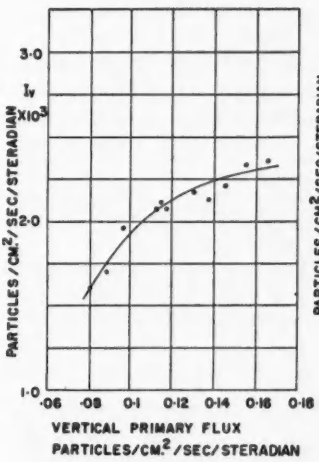

FIG. 7. Vertical intensity of protons plotted against vertical primary flux.

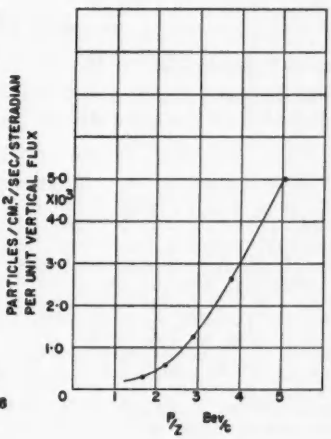

FIG. 8. Yield of particles in our energy range as a function of P/Z.

the smooth curve shown, we obtain the relation between the average specific yield and the momentum to charge ratio, Fig. 8. It will be seen that observations were not carried out sufficiently close to the equator to show any levelling off of the yield curve, which is still rising steeply at a primary particle (proton) momentum of 5 Bev./c. A primary proton can just penetrate 475 gm./cm.^{2} of

air when its momentum is 2.1 Bev./c, so that a primary proton can be detected by our apparatus when it has a momentum of 2.8 Bev./c. Neglecting the possibility of a primary particle arriving at our level by travelling a large portion of the range as a neutron, the yield at $P/Z = 2.8$ Bev./c should be

$$Y(P/Z = 2.8) = e^{-475/L_i},$$

where L_i is the interaction length of such a proton. This follows from the fact that any interaction suffered will cause a loss of energy and so eliminate the particle from our counting rate. The relation leads to a value $L_i = 71$ gm./cm.^{2}, this being regarded more as a check upon the accuracy of the absolute intensities deduced from the counting rates, rather than as a determination of the interaction length of high energy protons.

Conclusions

From the foregoing we may conclude that the altitude dependence of 400 Mev. protons is exponential with an absorption length of 122 ± 12 gm./cm.^{2}, taking into account the modification of the spectrum with height. The latitude effect for such protons shows a similar variation to that of fast neutrons between $\lambda = 56°$ and $\lambda = 40°$ geomagnetic, and the amount of the effect is 28.4%, but there is some evidence that the knee of the latitude effect is above $\lambda = 54°$.

ACKNOWLEDGMENT

The author would like to thank the R.C.A.F., Air Material Command, Rockcliffe, for their generous and expert assistance, and especially F/Lt. J. Henry, the pilot of the aircraft, and Dr. D. C. Rose for assistance and discussion.

REFERENCES

1. Camerini, U., Fowler, P. H., Lock, W. O., and Muirhead, H. Phil. Mag. 41: 413. 1950.
2. Deurden, T. and Hyams, B. D. Phil. Mag. 43: 717. 1952.
3. Koenig, H. P. Phys. Rev. 69: 590. 1946.
4. McMahon, A. J., Rossi, B., and Burditt, W. F. Phys. Rev. 80: 157. 1950.
5. McNish, A. G. Terrestrial Magnetism and Atm. Elect. 41: 37. 1936.
6. Mylroi, M. G. and Wilson, J. G. Proc. Phys. Soc. (London), A, 64: 404. 1951.
7. N. A. C. A. Rept. No. 538. 1935.
8. Neher, H. V. Phys. Rev. 78: 674. 1950.
9. Neher, H. V. Progress in cosmic ray physics. North-Holland Pub. Co., Amsterdam. 1952. p. 284.
10. Puppi, G. and Dellaporta, N. Progress in cosmic ray physics. North-Holland Pub. Co., Amsterdam. 1952. p. 356.
11. Rossi, B. High energy particles. Prentice-Hall, Inc., New York. 1952. p. 486.
12. Simpson, J. A. Phys. Rev. 83: 1175. 1951.
13. Simpson, J. A., Fonger, W., and Treiman, S. B. Phys. Rev. 90: 934. 1953.
14. Treiman, S. B. Phys. Rev. 86: 917. 1952.
15. Winckler, J. R., Stix, T., Dwight, K., and Sabin, R. Phys. Rev. 79: 656. 1950.

FIELD EQUATIONS FROM PARTICLE EQUATIONS[1]

By W. J. Archibald

ABSTRACT

A simple point of view is developed which shows how various types of field equations may be obtained from the relativistic Hamiltonian of a particle.

The energy in the various fields (electromagnetic, meson, etc.) is concentrated in small regions of space and as these concentrated bundles of energy are moving rapidly, they appear as particles to an observer. Sometimes these bundles of energy have zero inertial mass (photons) and sometimes they do not (mesons). This suggests that there must be some simple connection between field equations and the equations of motion of a particle. Of course, the quantization of the field equations explains satisfactorily the existence of the "photons in the field". What is attempted here is to show that, without resorting to field quantization, field equations and particle equations are intimately related.

ELECTROMAGNETIC FIELD

As a simple example consider Maxwell's equations for the electromagnetic field in empty space. It is sufficient to take

$$\nabla \times \mathbf{E} = -\dot{\mathbf{H}}/c, \qquad \nabla \times \mathbf{H} = \dot{\mathbf{E}}/c, \tag{1}$$

since $\nabla \cdot \mathbf{E} = \nabla \cdot \mathbf{H} = 0$ follow from these if they are imposed as conditions at $t = 0$. From [1], the equation for $\mathbf{F} = \mathbf{E} + i\mathbf{H}$ is

$$\dot{\mathbf{F}}/c = -i\nabla \times \mathbf{F}. \tag{2}$$

On multiplying by $i\hbar$ this may be written

$$\mathfrak{H}\mathbf{F} = ic\mathbf{p} \times \mathbf{F}, \tag{3}$$

where $\mathfrak{H} \rightarrow i\hbar\partial/\partial t$ and $\mathbf{p} \rightarrow -i\hbar\nabla$. Equation [3] can be written in matrix form as

$$\mathfrak{H} \begin{vmatrix} F_x \\ F_y \\ F_z \end{vmatrix} = ic \begin{vmatrix} 0 & -p_z & p_y \\ p_z & 0 & -p_x \\ -p_y & p_x & 0 \end{vmatrix} \begin{vmatrix} F_x \\ F_y \\ F_z \end{vmatrix}. \tag{4}$$

If only the operator part of [4] is retained, it becomes

$$\mathfrak{H} = c\boldsymbol{\tau} \cdot \mathbf{p}, \tag{5}$$

where

$$\tau_x = \begin{vmatrix} 0 & 0 & 0 \\ 0 & 0 & -i \\ 0 & i & 0 \end{vmatrix}, \qquad \tau_y = \begin{vmatrix} 0 & 0 & i \\ 0 & 0 & 0 \\ -i & 0 & 0 \end{vmatrix}, \qquad \tau_z = \begin{vmatrix} 0 & -i & 0 \\ i & 0 & 0 \\ 0 & 0 & 0 \end{vmatrix}. \tag{6}$$

Equation [5] looks like the Dirac operator for a particle of zero rest mass, and

[1]*Manuscript received May 20, 1955.*
Contribution from the Department of Physics, Dalhousie University, Halifax, Nova Scotia.

the well-behaved solutions of [4] would certainly be consistent with physically significant solutions of [1].

If [5] is accepted as the Hamiltonian operator for a particle, then certain properties of this particle follow immediately: e.g. the operator $M_z+\hbar\tau_z$, where $M_z = xp_y-yp_x$, commutes with $\mathfrak{H}$ so that it is a constant of the motion. Thus $\hbar\tau_z$ is the operator associated with the z component of the particle's spin, and this operator has the eigenvalues $\hbar$, 0, and $-\hbar$. In confirmation of this picture it is easy to show that $\boldsymbol{\tau}\times\boldsymbol{\tau} = i\boldsymbol{\tau}$, which must be true if $\hbar\tau$ is to be a spin operator. Furthermore, $|\psi|^2 = |F_x|^2+|F_y|^2+|F_z|^2 = E^2+H^2$. Thus the probability of finding the particle in a volume of given size is greatest in those regions where the classical field energy density is greatest. In summary, this particle has unit spin and is most likely to be found where the fields are strongest.

MESON FIELD

For the second example the process is reversed: we start from the equation for a particle and arrive at the equations for a field. The relativistic energy equation for a free particle of rest mass m_0 and energy E may be written as

$$(im_0c)^2 = (iE/c)^2+p_x^2+p_y^2+p_z^2,$$

or

$$[7] \qquad (im_0c)^2 = p_0^2+p_1^2+p_2^2+p_3^2 = P^2,$$

where obvious abbreviations have been introduced. The four p's are the components of a 4-vector of constant length. To set up the quantum mechanical equation for a particle Dirac used a symbolic 4-vector (with components α_0, α_1, α_2, α_3) having the property that $(\boldsymbol{\alpha}\cdot\mathbf{p})^2 = P^2$. ($\boldsymbol{\alpha}\cdot\mathbf{p}$ is the four dimensional scalar product). He then quantized the equation $im_0c = \boldsymbol{\alpha}\cdot\mathbf{p}$. This particle turned out to be the electron. Let us, without giving any a priori reason for doing so, seek a symbolic 4-vector such that

$$[8] \qquad (\boldsymbol{\alpha}\cdot\mathbf{p})^3 = P^2(\boldsymbol{\alpha}\cdot\mathbf{p}).$$

Needless to say, the Dirac α's satisfy this equation, but there may be other α's which do so also. If [8] is to hold the α's must have the following properties:

$$\alpha_\mu^3 = \alpha_\mu \quad (\mu = 0, 1, 2, 3),$$

$$[9] \qquad \alpha_\mu^2\alpha_\nu+\alpha_\mu\alpha_\nu\alpha_\mu+\alpha_\nu\alpha_\mu^2 = \alpha_\nu \quad (\mu \neq \nu),$$

$$(\alpha_\lambda\alpha_\mu\alpha_\nu+\alpha_\nu\alpha_\mu\alpha_\lambda)+(\alpha_\mu\alpha_\lambda\alpha_\nu+\alpha_\nu\alpha_\lambda\alpha_\mu)+(\alpha_\mu\alpha_\nu\alpha_\lambda+\alpha_\lambda\alpha_\nu\alpha_\mu) = 0 \quad (\lambda, \mu, \nu \text{ different}).$$

While these equations are satisfied by the Dirac operators, they can also be met by the following scheme:

$$[10] \qquad \begin{aligned} \alpha_\mu^3 &= \alpha_\mu \quad (\mu = 0, 1, 2, 3), \\ \alpha_\mu^2\alpha_\nu+\alpha_\nu\alpha_\mu^2 &= \alpha_\nu \quad (\mu \neq \nu), \\ \alpha_\mu\alpha_\nu\alpha_\mu &= 0 \quad (\mu \neq \nu), \\ \alpha_\lambda\alpha_\mu\alpha_\nu+\alpha_\nu\alpha_\mu\alpha_\lambda &= 0 \quad (\lambda, \mu, \nu \text{ different}). \end{aligned}$$

The algebra defined by [10] has been studied by Kemmer (1) and he has shown that α's which are 10 by 10 matrices can be found which obey these equations.

It is not impossibly difficult to find four such α's. Since $\alpha_\mu{}^3 = \alpha_\mu$ is the simplest equation which each α obeys, each α has the eigenvalues 1, 0, and -1, and if a representation is chosen in which α_0 is diagonal it seems reasonable to have the numbers 1, 1, 1, 0, 0, 0, 0, -1, -1, -1 along the diagonal. With this start it is possible, but tedious, to find three other α's, and only the results will be recorded. Once the α's are obtained it is easy to show that they have the required properties.

Following Dirac, by analogy, we obtain

$$[11] \qquad im_0c = \alpha_0p_0+\alpha_1p_1+\alpha_2p_2+\alpha_3p_3,$$

and combining the four matrices on the right of [11]

$$[12] \qquad im_0c = \begin{vmatrix} p_0 & A & 0 \\ A^* & 0 & B^* \\ 0 & B & -p_0 \end{vmatrix},$$

where (*a*) each p_0 is a diagonal 3 by 3 matrix,

(*b*) the central zero is a 4 by 4 null matrix,

(*c*) the other zeros are 3 by 3 null matrices,

(*d*) A and B are 4 by 3 matrices and A^* and B^* their complex conjugates, with

$$[13] \quad A = \frac{1}{\sqrt{2}} \begin{vmatrix} -p_y & -p_z & 0 & -p_x \\ p_x & 0 & -p_z & -p_y \\ 0 & p_x & p_y & -p_z \end{vmatrix}, \quad B = \frac{1}{\sqrt{2}} \begin{vmatrix} p_y & p_z & 0 & -p_x \\ -p_x & 0 & p_z & -p_y \\ 0 & -p_x & -p_y & -p_z \end{vmatrix}.$$

Equation [12] becomes an operator equation by replacing p_0 by $-(\hbar/c)\partial/\partial t$, p_x by $-i\hbar\,\partial/\partial x$, etc. In this treatment it is not possible to have p_0 multiplied by a unit matrix (as is the case for a Dirac particle) since α_0 has no reciprocal.

The matrices A and B have the following simple properties:

$$[14] \qquad \begin{aligned} AA^* &= BB^* = \tfrac{1}{2}p^2\,1(3), \\ AB^*B &= \tfrac{1}{2}p^2A, \\ BA^*A &= \tfrac{1}{2}p^2B, \end{aligned}$$

where 1(3) is the unit 3 by 3 matrix and $p^2 = p_x{}^2+p_y{}^2+p_z{}^2$.

It is important to remember that the matrix in [12] is put forward in the present instance only because it has the mathematical property that when it is cubed it produces itself multiplied by P^2. This is certainly not a sufficient reason for studying it, but a brief examination discloses interesting properties which may have value. Let [12] act on a 10 element column matrix

$$\begin{vmatrix} \psi_1 \\ \chi \\ \psi_2 \end{vmatrix},$$

where ψ_1, ψ_2, and χ are three and four element column matrices respectively.

Then

$$\begin{aligned}(im_0c-p_0)\psi_1 &= A\chi,\\ im_0c\chi &= A^*\psi_1+B^*\psi_2,\\ (im_0c+p_0)\psi_2 &= B\chi.\end{aligned} \tag{15}$$

It is difficult to sense the properties of these equations in their present form. However it is possible by elimination of the ψ's to obtain a second-order differential equation for χ, which is

$$-(m_0^2c^2+p_0^2)\chi = (A^*A+B^*B)\chi. \tag{16}$$

To display all the features of this equation it is necessary to write it out in full as

$$-(m_0^2c^2+p_0^2)\begin{vmatrix}\chi_1\\ \chi_2\\ \chi_3\\ \chi_4\end{vmatrix} = \begin{vmatrix} p_x^2+p_y^2 & p_yp_z & -p_xp_z & 0\\ p_yp_z & p_x^2+p_z^2 & p_xp_y & 0\\ -p_xp_z & p_xp_y & p_y^2+p_z^2 & 0\\ 0 & 0 & 0 & p^2\end{vmatrix}\begin{vmatrix}\chi_1\\ \chi_2\\ \chi_3\\ \chi_4\end{vmatrix}. \tag{17}$$

Thus χ_4 obeys

$$\Box\chi_4 = \mu^2\chi_4 \quad (\mu = m_0c/\hbar)\,. \tag{18}$$

It is clear that χ_1, χ_2, and χ_3, which will be renamed S_z, $-S_y$, and S_x respectively, are the components of a 3-vector. From [17], by simple factoring,

$$\begin{aligned}(p_0^2+m_0^2c^2)\begin{vmatrix}S_z\\ -S_y\\ S_x\end{vmatrix} &= \begin{vmatrix} 0 & ip_x & ip_y\\ -ip_x & 0 & ip_z\\ -ip_y & -ip_z & 0\end{vmatrix}\begin{vmatrix} 0 & -ip_x & -ip_y\\ ip_x & 0 & -ip_z\\ ip_y & ip_z & 0\end{vmatrix}\begin{vmatrix}S_z\\ -S_y\\ S_x\end{vmatrix}\\ &= \hbar\begin{vmatrix} 0 & ip_x & ip_y\\ -ip_x & 0 & ip_z\\ -ip_y & -ip_z & 0\end{vmatrix}\begin{vmatrix}(\nabla\times\mathbf{S})_z\\ -(\nabla\times\mathbf{S})_y\\ (\nabla\times\mathbf{S})_x\end{vmatrix},\end{aligned}$$

so that finally

$$(p_0^2+m_0^2c^2)\mathbf{S} = -\hbar^2\nabla\times(\nabla\times\mathbf{S})\,,$$

or

$$\frac{1}{c^2}\frac{\partial^2\mathbf{S}}{\partial t^2}+\nabla\times(\nabla\times\mathbf{S}) = -\mu^2\mathbf{S}. \tag{19}$$

In the light of [18] and [19] it is clear that the four components of χ are the potentials (scalar and vector) associated with a field arising from a particle of rest mass m_0. The first-order equations have been lost sight of but they must be some sort of field equations in an unfamiliar form.

Returning again to equations [15] we next eliminate χ, obtaining

$$\begin{aligned}i\hbar\frac{\partial\psi_1}{\partial t} &= \left(E_0+\frac{AA^*}{m_0}\right)\psi_1+\frac{AB^*}{m_0}\psi_2,\\ i\hbar\frac{\partial\psi_2}{\partial t} &= -\left(E_0+\frac{BB^*}{m_0}\right)\psi_2-\frac{BA^*}{m_0}\psi_1.\end{aligned} \tag{20}$$

It is to be observed that these equations are of the first order in the time derivative and second order in the space derivatives reminding one of Schroedinger's equation. They may be written as

$$[21] \qquad i\hbar \frac{\partial}{\partial t} = \begin{vmatrix} E_0+\dfrac{AA^*}{m_0} & \dfrac{AB^*}{m_0} \\ -\dfrac{BA^*}{m_0} & -E_0-\dfrac{BB^*}{m_0} \end{vmatrix},$$

where only the operator part has been recorded. This certainly looks like the Hamiltonian of a particle with both positive and negative energy states: in fact, except for the second-order derivatives, it reminds one very much of Dirac's equation. (It is necessary to remember that each element in [21] is a 3 by 3 matrix.) The operator in [21] is not Hermitian but the original 10 by 10 operator is.

The operator on the right of [21] when squared gives $E_0^2+c^2p^2$, just as the Dirac Hamiltonian for a free particle does. The 10 by 10 matrix does not have this property at all. The fact that [21] behaves like the Dirac Hamiltonian strengthens the conviction that this equation describes the genuine particle aspect of the reality which [12] represents (if any such reality exists). Let us treat [20] as the equations for a particle, i.e assume that both ψ_1 and ψ_2 contain the factor $\exp(-iEt/\hbar)$. If E is positive and the momentum small, $\psi_2 \ll \psi_1$, and the first approximation for the large component (with time dependence factored out) is obtained by solving

$$[22] \qquad E = E_0+AA^*/m_0 = E_0+p^2/2m_0,$$

where only the operator has been written down. It is hardly necessary to point out that beyond all doubt [21] describes a particle.

Since we have a particle to deal with, let us imagine it to be charged and in a magnetic field. The right thing to do seems to be to write A as $\mathbf{a}\cdot\mathbf{p}$ and A^* as $\mathbf{a}^*\cdot\mathbf{p}$ (refer to [13] to see the meaning of $\mathbf{a}$) and then to subtract $(e/c)\mathbf{A}$ from each $\mathbf{p}$, where $\mathbf{A}$ is the vector potential of the magnetic field. Then [22] becomes

$$[23] \qquad E = E_0+\frac{1}{m_0}\left[\mathbf{a}\cdot\left(\mathbf{p}-\frac{e}{c}\mathbf{A}\right)\right]\left[\mathbf{a}^*\cdot\left(\mathbf{p}-\frac{e}{c}\mathbf{A}\right)\right].$$

For simplicity choose $A_x = -\frac{1}{2}H_y$, $A_y = \frac{1}{2}H_x$, which provides a steady field H in the z direction. The reduction of [23] is easily carried out by using the following relations between the a's:

$$a_xa_x^* = a_ya_y^* = a_za_z^* = \tfrac{1}{2},$$

$$a_xa_y^*+a_ya_x^* = a_xa_z^*+a_za_x^* = a_ya_z^*+a_za_y^* = 0.$$

(A striking similarity with the Pauli matrices for a particle of spin $\frac{1}{2}$ is displayed.) The final result is

$$[24] \qquad E = E_0+\frac{p^2}{2m_0}-\frac{e}{2m_0c}HM_z+\frac{e^2H^2}{8m_0c^2}(x^2+y^2)-\mu_0H(2ia_ya_z^*),$$

where $\mu_0 = e\hbar/2m_0c$ = one Bohr magneton, and

$$[25] \qquad 2ia_y a_x^* = \begin{vmatrix} 0 & -i & 0 \\ i & 0 & 0 \\ 0 & 0 & 0 \end{vmatrix}.$$

This matrix has the eigenvalues 1, 0, and -1, so that the particle behaves as if it had unit spin and a magnetic moment of one Bohr magneton.

Without pursuing our study any further it seems clear that [12] is an operator which unites in a very suggestive manner the particle and field aspects of what seems to be an entity of unit spin. There are numerous representations other than [12], and one additional representation which completely suppresses the particle aspect will now be presented. We subject [12] to a transformation by means of the matrix S, where

$$[26] \qquad S = S^{-1} = \frac{1}{\sqrt{2}} \begin{vmatrix} 1 & 0 & 1 \\ 0 & \sqrt{2} & 0 \\ 1 & 0 & -1 \end{vmatrix}.$$

It is necessary to remember that S must be compatible with [12] so that, for example, each 1 is a 3 by 3 diagonal matrix, the $\sqrt{2}$ is a 4 by 4 diagonal matrix, etc. The transformed matrix is

$$[27] \qquad im_0c = \begin{vmatrix} 0 & M & p_0 \\ M^* & 0 & N^* \\ p_0 & N & 0 \end{vmatrix},$$

where

$$[28] \qquad M = \begin{vmatrix} 0 & 0 & 0 & -p_x \\ 0 & 0 & 0 & -p_y \\ 0 & 0 & 0 & -p_z \end{vmatrix}, \qquad N = \begin{vmatrix} -p_y & -p_z & 0 & 0 \\ p_x & 0 & -p_z & 0 \\ 0 & p_x & p_y & 0 \end{vmatrix},$$

and p_0 is a diagonal 3 by 3 matrix. The 10 elements of the column matrix upon which [27] operates will be called, in order starting at the top, as follows:

$$E_x/i\mu,\ E_y/i\mu,\ E_z/i\mu,\ -H_x/\mu,\ H_y/\mu,\ -H_z/\mu,\ i\phi,\ A_x,\ A_y,\ A_z.$$

This leads to 10 simultaneous, first-order differential equations, which combine very naturally to give the four which follow:

$$[29] \qquad \begin{aligned} \mathbf{E} &= -\nabla\phi - \dot{\mathbf{A}}/c, \\ \mathbf{H} &= \nabla \times \mathbf{A}, \\ \nabla \cdot \mathbf{E} &= -\mu^2\phi, \\ \nabla \times \mathbf{H} &= \dot{\mathbf{E}}/c - \mu^2\mathbf{A}. \end{aligned}$$

These are the equations of the field generated by a particle of spin unity and rest mass m_0.

MESON FIELD (ALTERNATIVE TREATMENT)

It is interesting to recall that all the results achieved above stem from the properties of the 4-vector $\boldsymbol{\alpha}$ which obeys $(\boldsymbol{\alpha} \cdot \mathbf{p})^3 = P^2(\boldsymbol{\alpha} \cdot \mathbf{p})$. A similar

equation holds in three dimensions for the components of the spin vector of a particle of unit spin. Let $\boldsymbol{\tau} = \mathbf{i}\tau_x + \mathbf{j}\tau_y + \mathbf{k}\tau_z$ be a vector with components given by [6] and let $\mathbf{T}$ be any ordinary vector. Then

$$(\boldsymbol{\tau} \cdot \mathbf{T})^3 = T^2(\boldsymbol{\tau} \cdot \mathbf{T}). \tag{30}$$

The expression $\boldsymbol{\tau} \cdot \mathbf{T}$ means $| \boldsymbol{\tau} || \mathbf{T} | \cos\theta$ where θ is the "angle" between $\boldsymbol{\tau}$ and $\mathbf{T}$. Therefore one interprets [30] to mean

$$| \boldsymbol{\tau} |^2 \cos^3\theta = \cos\theta. \tag{31}$$

But $| \boldsymbol{\tau} |^2 = 2$ so that $\cos\theta = 0$ or $\pm 1/\sqrt{2}$. $\boldsymbol{\tau}$ then makes one or other of these angles with any vector at all. Apparently the vector $\boldsymbol{\alpha}$ has somewhat analogous properties in four dimensions. In three dimensions it is possible to have a particle of unit spin which is really two particles of spin $\frac{1}{2}$ bound together in some manner. If $\boldsymbol{\tau}$ is the vector associated with the total spin of this system, then

$$(\boldsymbol{\tau} \cdot \mathbf{T})^4 = T^2(\boldsymbol{\tau} \cdot \mathbf{T})^2, \tag{32}$$

as can easily be verified. Each component of $\boldsymbol{\tau}$ has the eigenvalues 1, 0, 0, -1 (the singlet state introduces the second zero). $\boldsymbol{\tau}$ in this case is a 4 by 4 matrix. One is tempted to wonder if it would be worth looking for a 4-vector $\boldsymbol{\alpha}$ with the property that

$$(\boldsymbol{\alpha} \cdot \mathbf{p})^4 = P^2(\boldsymbol{\alpha} \cdot \mathbf{p})^2. \tag{33}$$

The algebra of these α's is probably very complicated and to approach the problem by a study of this algebra would be an arduous task. However, a 16 by 16 matrix which obeys [33] will be written down. It has been obtained chiefly by guessing so the method of derivation will not be presented. That it has the desired property is easily verified. It is

$$im_0c = \begin{vmatrix} 0 & 0 & \delta & p_0 \\ 0 & 0 & 0 & \eta \\ \delta & 0 & 0 & 0 \\ p_0 & \eta & 0 & 0 \end{vmatrix}. \tag{34}$$

Each element of [34] is a 4 by 4 matrix and

$$\delta = \begin{vmatrix} 0 & 0 & p_x & p_z \\ 0 & 0 & 0 & 0 \\ p_x & 0 & 0 & ip_y \\ p_z & 0 & -ip_y & 0 \end{vmatrix}, \qquad \eta = \begin{vmatrix} 0 & -ip_y & 0 & 0 \\ ip_y & 0 & -p_x & p_z \\ 0 & -p_z & 0 & 0 \\ 0 & p_x & 0 & 0 \end{vmatrix}. \tag{35}$$

If M is the matrix in [34], then $M^4 = P^2M^2$, and this is the simplest equation which M obeys.

It is not easy to see, with a casual glance, that [34] leads to field equations but this would become obvious if one were to write down the 16 equations to which it gives rise. However it can be subjected to a transformation which puts it in a most interesting form. (The transformation matrix will not be given, as it is easier to check that the result satisfies $M^4 = P^2M^2$ than it is to perform the transformation.) The result is

[36] $$im_0c = \begin{vmatrix} U & 0 \\ 0 & V \end{vmatrix},$$

where U is exactly the 10 by 10 matrix given in equation [27], the small zero is a single zero in the 11th row and 11th column, and

[37] $$V = -\begin{vmatrix} 0 & p_0 & p_x & p_y & p_z \\ p_0 & 0 & 0 & 0 & 0 \\ p_x & 0 & 0 & 0 & 0 \\ p_y & 0 & 0 & 0 & 0 \\ p_z & 0 & 0 & 0 & 0 \end{vmatrix}.$$

In the representation given by [36] the 16 functions of the column matrix on which [36] acts divide into three mutually exclusive groups. One function is zero; there is a group of 10 functions which lead once again to the set of equations [29]; and a group of five functions on which the operator V acts. It seems logical to assume that the 10 functions describe the field arising from particles in the triplet state and the five functions the field from the particles in the singlet state with zero spin.

If the five functions on which V operates are called (in order) $-\chi$, T_0, T_1, T_2, and T_3, and if p_x, p_y, p_z are written as p_1, p_2, p_3 and ict, x, y, z, as x_0, x_1, x_2, x_3, then

[38] $$\sum_{\nu=0}^{3} \frac{\partial T_\nu}{\partial x_\nu} = -\mu\chi,$$

and

[39] $$\frac{\partial \chi}{\partial x_\nu} = -\mu T_\nu, \quad (\nu = 0, 1, 2, 3).$$

The author wishes to express his gratitude to the Physics Department of the University of Virginia for a Post Doctoral Fellowship and for kind hospitality.

REFERENCES

1. KEMMER, N. Proc. Cambridge Phil. Soc. 39: 189. 1943.

NOTE

THE EMISSION SPECTRUM OF AlF IN THE REGION 1700-2000 Å

By S. M. Naudé and T. J. Hugo

In previous papers (1) the emission spectrum of AlF in the region 2000–8600 Å has been described. Using the same excitation conditions, the emission spectrum in the region 1700–2000 Å was photographed in the first order of a two-meter vacuum spectrograph with a reciprocal dispersion of 8.6 Å/mm.

The $B^1\Sigma$–$X^1\Sigma$ and $C^1\Sigma$–$X^1\Sigma$ systems were both emitted strongly. The bands in both systems are degraded to shorter wavelengths. In the more intense $B^1\Sigma$–$X^1\Sigma$ system, 40 bands were observed whereas in the $C^1\Sigma$–$X^1\Sigma$ system only 10 were observed. These band-heads with their vibrational assignments are listed in Tables I and II.

TABLE I

Band-heads of the $B^1\Sigma$–$X^1\Sigma$ system

$v'v''$	ν_h (cm.$^{-1}$)	$v'v''$	ν_h (cm.$^{-1}$)	$v'v''$	ν_h (cm.$^{-1}$)	$v'v''$	ν_h (cm.$^{-1}$)
0,3	51941.3	1,3	52790.4	2,3	53624.3	4,4	54481.2
1,4	52027.5	2,4	52862.5	3,4	53681.7	1,0	55128.7
2,5	52110.2	3,5	52928.2	4,5	53731.7	2,1	55171.1
3,6	52188.8	4,6	52988.9	5,6	53775.6	3,2	55210.5
4,7	52254.5	5,7	53040.7	6,7	53808.2	4,3	55240.0
5,8	52316.1	6,8	53083.4	7,8	53828.6	5,4	55266.1
6,9	52368.1	7,9	53113.4	0,0	54282.7	6,5	55280.3
7,10	52407.9	8,10	53131.9	1,1	54341.2	2,0	55956.6
8,11	52431.8	0,1	53492.8	2,2	54393.0	3,1	55984.5
0,2	52711.7	1,2	53561.1	3,3	54441.7	4,2	56021.3

TABLE II

Band-heads of the $C^1\Sigma$–$X^1\Sigma$ system

$v'v''$	ν_h (cm.$^{-1}$)	$v'v''$	ν_h (cm.$^{-1}$)
1,4	55571.9	0,1	56960.2
2,5	55732.4	1,2	57104.7
0,2	56179.4	2,3	57247.2
1,3	56331.7	0,0	57749.8
2,4	56482.8	1,1	57884.6

The band-heads can be represented by the following equations:

$B^1\Sigma$–$X^1\Sigma$ bands:

$$\nu_h = 54249.6+[864.8(v'+\tfrac{1}{2})-7.23(v'+\tfrac{1}{2})^2+0.009(v'+\tfrac{1}{2})^3] -[799.2(v''+\tfrac{1}{2})-4.74(v''+\tfrac{1}{2})^2+0.015(v''+\tfrac{1}{2})^3] .$$

$C^1\Sigma - X^1\Sigma$ bands:

$$\nu_h = 57682.2 + [934.3(v' + \tfrac{1}{2}) - 5.18(v' + \tfrac{1}{2})^2] - [799.0(v'' + \tfrac{1}{2}) - 4.74(v'' + \tfrac{1}{2})^2] .$$

1. NAUDÉ, S. M. AND HUGO, T. J. Can. J. Phys. 31: 1106. 1953; 32: 246. 1954.

RECEIVED MAY 27, 1955.
COUNCIL FOR SCIENTIFIC AND INDUSTRIAL RESEARCH,
P.O. BOX 395,
PRETORIA, SOUTH AFRICA.

Under this heading brief reports of important discoveries in physics may be published. These reports should not exceed 600 words and, for any issue, should be submitted not later than six weeks previous to the first day of the month of issue. No proof will be sent to the authors.

On the Interpretation of Nuclear Resonance Fluorescence Experiments

In recent years a number of observations have been made of resonance fluorescence in nuclei (2, 6, 7, 8, 9, 10, 11, 12). The results have been interpreted in terms of the basic resonance formula relating an absorption cross section σ to a transition probability (times $\hbar$) Γ:

$$\sigma = g\frac{\lambda^2}{8\pi}\frac{\Gamma^2}{(E-E_0)^2+(\Gamma/2)^2}. \tag{1}$$

It has been assumed that the data so interpreted yield directly the partial mean life of the transition for gamma radiation ($\tau = \hbar/\Gamma$) even in the presence of appreciable branching and/or internal conversion.

It is the purpose of the present note to point out that this interpretation is not valid. In the presence of branching or internal conversion, the absorption cross section for the resonant absorption and subsequent re-emission of a *gamma ray* is:

$$\sigma = g\frac{\lambda^2}{8\pi}\frac{\gamma_1^2}{(E-E_0)^2+(\gamma/2)^2} \tag{2}$$

where γ_1 is the gamma ray transition probability for the absorption (and re-emission) transition, while $\gamma = \sum_i \gamma_i + \sum_i \alpha_i$ is the total width of the upper level including all possible modes of de-excitation to all lower levels. γ_i is the gamma transition probability for the ith gamma ray originating from the upper level, while α_i is the corresponding internal conversion transition probability.

In the resonance fluorescence experiments it is the integral of the cross section over energy that matters. Therefore from Equation [1] we find $\int \sigma\, dE \sim \Gamma$, while from Equation [2] we obtain $\int \sigma\, dE \sim \gamma_1^2/\gamma$. If we denote the "gamma ray partial mean life" of the upper level as obtained in the past from Equation [1] as $(\tau_\gamma)_1$, it follows that the correct gamma ray partial mean life is given by

$$\tau_\gamma = (\gamma_1/\gamma)(\tau_\gamma)_1. \tag{3}$$

In the simple case where the upper level is the first excited state then $(\gamma_1/\gamma) = 1/(1+\alpha_{\text{total}})$ where α_{total} is the total internal conversion coefficient. If the mean life of the level (including conversion) is desired, τ_γ given by Equation [3] must be multiplied again by (γ_1/γ). If the upper level is not the first excited state the ratio (γ_1/γ) will involve branching ratios as well as conversion coefficients but the analysis will be the same.

The experimental data available at present are not very precise, but the modification implied by Equations [2] and [3] tends to improve the agreement between the τ_γ values obtained from resonance fluorescence and those obtained from delayed coincidence experiments (1, 3, 4). An example is the 209 kev. transition in Hg^{199}. Metzger (8) quotes a "mean life" based on Equation [1] of $(\tau_\gamma)_1 = (3\pm1)\times10^{-10}$ sec. The de-excitation of the 209 kev. level involves both branching and conversion (13). The experimental value for (γ_1/γ) is approximately 0.5. Thus the correct gamma ray partial mean life is $\tau_\gamma = (1.5\pm0.5)\times10^{-10}$ sec., and the mean life of the 209 kev. level is $\tau = (7.5\pm2.5)\times10^{-11}$ sec. This can be compared with Graham's delayed coincidence measurement (5), $\tau = (10\pm6)\times10^{-11}$ sec. It is evident that the large experimental uncertainties in this and other cases preclude accurate comparisons. As the data become more accurate, however, the difference between the "lifetime" obtained from Equation [1] and the correct τ_γ obtained from Equation [2] will be significant for those transitions in which branching and/or conversion are appreciable.

The author wishes to thank Dr. R. E. Bell for drawing his attention to this problem and for helpful discussion about it.

1. Bell, R. E. Beta- and gamma-ray spectroscopy. *Edited by* K. Siegbahn. North-Holland Publishing Co., Amsterdam. 1955. p. 494.
2. Davey, W. G. and Moon, P. B. Proc. Phys. Soc. (London), A, 66: 956. 1953.
3. Graham, R. L. and Bell, R. E. Phys. Rev. 84: 380. 1951.
4. Graham, R. L. and Bell, R. E. Can. J. Phys. 31: 377. 1953.
5. Graham, R. L. *et al.* Bull. Am. Phys. Soc. 30 (No. 4): 20. 1955.
6. Malmfors, K. G. Arkiv Fysik, 6: 49. 1952.

7. MALMFORS, K. G. Beta- and gamma-ray spectroscopy. *Edited by* K. Siegbahn. North-Holland Publishing Co., Amsterdam. 1955. p. 521.
8. METZGER, F. R. Proceedings of the 1954 Glasgow Conference on Nuclear and Meson Physics. Pergamon Press, London. 1955. p. 201.
9. METZGER, F. R. Phys. Rev. 98: 200. 1955.
10. METZGER, F. R. and TODD, W. B. Phys. Rev. 95: 853. 1954.
11. MOON, P. B. Proc. Phys. Soc. (London), A, 64: 76. 1951.
12. MOON, P. B. and STORRUSTE, A. Proc. Phys. Soc. (London), A, 66: 585. 1953.
13. SHERK, P. M. and HILL, R. D. Phys. Rev. 83: 1097. 1951.

RECEIVED JUNE 22, 1955.
J. DAVID JACKSON
RADIATION LABORATORY,
MCGILL UNIVERSITY,
MONTREAL, QUEBEC.

THE PHYSICAL SOCIETY

MEMBERSHIP of the Society is open to all who are interested in Physics.

FELLOWS pay an Entrance fee of £1 1*s*. ($3.00) and an Annual Subscription of £2 2*s*. ($6.00).

STUDENTS: A candidate for Studentship must be between the ages of 18 and 26, and pays an Annual Subscription of 7*s*. 6*d*. ($1.10).

MEETINGS: Fellows and Students may attend all Meetings of the Society including the annual Exhibition of Scientific Instruments and Apparatus.

PUBLICATIONS include the *Proceedings of the Physical Society*, published monthly in two sections, and *Reports on Progress in Physics*, published annually. Volume XVII, 1954, is now available (price 50*s*. ($7.15)). Members are entitled to receive many of the Publications at a reduced rate.

Further information can be obtained from:

THE PHYSICAL SOCIETY

1, LOWTHER GARDENS, PRINCE CONSORT ROAD

LONDON, S.W.7, ENGLAND

CANADIAN JOURNAL OF PHYSICS

Notes to Contributors

Manuscripts

(i) ***General.*** Manuscripts, in English or French, should be typewritten, double spaced, on paper 8½×11 in. **The original and one copy are to be submitted.** Tables and captions for the figures should be placed at the end of the manuscript. Every sheet of the manuscript should be numbered.

Style, arrangement, spelling, and abbreviations should conform to the usage of this journal. Names of all simple compounds, rather than their formulas, should be used in the text. Greek letters or unusual signs should be written plainly or explained by marginal notes. Superscripts and subscripts must be legible and carefully placed.

Manuscripts and illustrations should be carefully checked before they are submitted. Authors will be charged for unnecessary deviations from the usual format and for changes made in the proof that are considered excessive or unnecessary.

(ii) ***Abstract.*** An abstract of not more than about 200 words, indicating the scope of the work and the principal findings, is required, except in Notes.

(iii) ***References.*** References should be listed **alphabetically by authors' names,** numbered, and typed after the text. The form of the citations should be that used in this journal; in references to papers in periodicals, titles should not be given and only initial page numbers are required. All citations should be checked with the original articles and each one referred to in the text by the key number.

(iv) ***Tables.*** Tables should be numbered in roman numerals and each table referred to in the text. Titles should always be given but should be brief; column headings should be brief and descriptive matter in the tables confined to a minimum. Vertical rules should be used only when they are essential. Numerous small tables should be avoided.

Illustrations

(i) ***General.*** All figures (including each figure of the plates) should be numbered consecutively from 1 up, in arabic numerals, and each figure referred to in the text. The author's name, title of the paper, and figure number should be written in the lower left corner of the sheets on which the illustrations appear. Captions should not be written on the illustrations (see Manuscripts (i)).

(ii) ***Line Drawings.*** Drawings should be carefully made with India ink on white drawing paper, blue tracing linen, or co-ordinate paper ruled in blue only; any co-ordinate lines that are to appear in the reproduction should be ruled in black ink. Paper ruled in green, yellow, or red should not be used unless it is desired to have all the co-ordinate lines show. All lines should be of sufficient thickness to reproduce well. Decimal points, periods, and stippled dots should be solid black circles large enough to be reduced if necessary. Letters and numerals should be neatly made, preferably with a stencil (**do NOT use typewriting**) and be of such size that the smallest lettering will be not less than 1 mm. high when reproduced in a cut 3 in. wide.

Many drawings are made too large; originals should not be more than 2 or 3 times the size of the desired reproduction. In large drawings or groups of drawings the ratio of height to width should conform to that of a journal page but the height should be adjusted to make allowance for the caption.

The original drawings and one set of clear copies (e.g. small photographs) are to be submitted.

(iii) ***Photographs.*** Prints should be made on glossy paper, with strong contrasts. They should be trimmed so that essential features only are shown and mounted carefully, with rubber cement, on white cardboard with no space or only a **very** small space (less than 1 mm.) between them. In mounting, full use of the space available should be made (to reduce the number of cuts required) and the ratio of height to width should correspond to that of a journal page (4¼×7½ in.); however, allowance must be made for the captions. Photographs or groups of photographs should not be more than 2 or 3 times the size of the desired reproduction.

Photographs are to be submitted in duplicate; if they are to be reproduced in groups one set should be mounted, the duplicate set unmounted.

Reprints

A total of 50 reprints of each paper, without covers, are supplied free. Additional reprints, with or without covers, may be purchased.

Charges for reprints are based on the number of printed pages, which may be calculated approximately by multiplying by 0.6 the number of manuscript pages (double-spaced typewritten sheets, 8½×11 in.) and including the space occupied by illustrations. An additional charge is made for illustrations that appear as coated inserts. The cost per page is given on the reprint requisition which accompanies the galley.

Any reprints required in addition to those requested on the author's reprint requisition form must be ordered officially as soon as the paper has been accepted for publication.

Contents

Page

Diurnal Variations in the Number of Shower Meteors Detected by the Forward-scattering of Radio Waves. Part I. Theory—*C. O. Hines* - 493

On the Determination of Electromechanical Coupling Coefficients in a Polyresonant Piezoelectric Vibrator—*E. A. G. Shaw* - - 504

The Effect of a Random Noise Background upon the Detection of a Sinusoidal Signal—*H. S. Heaps* - - - - - - - - - - - - - 509

International Comparisons of the Canadian Primary Radium Standard—*W. S. Michel and G. N. Whyte* - - - - - - - - 521

A Method for the Evaluation of Some Lattice Sums Occurring in Calculations of Physical Properties of Crystals. II—*G. C. Benson and H. P. Schreiber* - - - - - - - - - - - - - - 529

Edge Energies of Alkali Halide Crystals—*H. P. Schreiber and G. C. Benson* - 534

The Fission Yields of Isotopes of Xenon and Krypton in the Neutron Fission of U^{235} and U^{238}—*R. K. Wanless and H. G. Thode* - - 541

The Proton Component of Cosmic Rays at Aircraft Altitudes—*K. W. Ogilvie* - 555

Field Equations from Particle Equations—*W. J. Archibald* - - - 565

The Emission Spectrum of AlF in the Region 1700–2000 Å—*S. M. Naudé and T. J. Hugo* - - - - - - - - - - - - - - - - 573

Letter to the Editor:

On the Interpretation of Nuclear Resonance Fluorescence Experiments—*J. David Jackson* - - - - - - - - - - - - 575

Printed in Canada *by* University of Toronto Press